

# **Consolidation Behavior of Metal Powder in Additive Manufacturing**

**Mohd Rizal Bin Alkahari**

**March 2014**

**Dissertation**

**Consolidation Behavior of Metal Powder in  
Additive Manufacturing**

**Graduate School of Natural Science & Technology**

**Kanazawa University**

**Division of Innovative Technology and Science**

**System Design and Planning**

**School registration no. : 1123122209**

**Name : Mohd Rizal Bin Alkahari**

**Chief advisor : Prof. Takashi Ueda**

## TABLE OF CONTENT

CHAPTER 1 : INTRODUCTION.....	1
1.1 BACKGROUND.....	1
1.2 PROBLEM STATEMENT .....	6
1.3 RESEARCH OBJECTIVES .....	8
1.4 THESIS OUTLINE.....	9
REFERENCES .....	10
CHAPTER 2 : OVERVIEW OF ADDITIVE MANUFACTURING .....	12
2.1 INTRODUCTION.....	12
2.2 RAPID PRODUCT DESIGN AND DEVELOPMENT .....	13
2.3 BASIC PRINCIPLES AND TYPES OF ADDITIVE MANUFACTURING .....	15
2.3.1 Liquid-based AM.....	17
2.3.2 Solid-based AM .....	18
2.3.3 Powder-based AM .....	19
2.4 SELECTIVE LASER SINTERING/SELECTIVE LASER MELTING.....	21
2.4.1 Machining-SLS/SLM Hybrid System .....	22
2.5 CONCLUSIONS .....	24
REFERENCES .....	25
CHAPTER 3 : THERMAL CONDUCTIVITY OF METAL POWDER AND CONSOLIDATED STRUCTURE .....	27
3.1 INTRODUCTION.....	27
3.1.1 Thermal Conductivity of Metal Powder .....	29
3.1.2 Thermal Conductivity of Consolidated Solid Material.....	30
3.2 EXPERIMENTAL SETUP.....	31
3.2.1 Metal Powder Material .....	31
3.2.2 Thermal Conductivity of Metal Powder .....	33
3.2.3 Thermal Conductivity of Consolidated Metal .....	35
3.3 EXPERIMENTAL RESULTS AND DISCUSSION.....	35
3.3.1 Effect of Particle Diameter on Thermal Conductivity of Metal Powder.....	35
3.3.2 Effect of Bulk Density on Thermal Conductivity of Metal Powder.....	37

## TABLE OF CONTENT

---

3.3.3	Effect of Porosity on Thermal Conductivity of Consolidated Structure.....	39
3.3.3.1	Porosity Evaluation and Influence of Laser Processing Parameter.....	39
3.3.3.2	Influence of Porosity on Thermal Conductivity.....	41
3.4	CONCLUSIONS.....	45
	REFERENCES.....	45
CHAPTER 4 : TEMPERATURE DURING CONSOLIDATION PROCESS.....		47
4.1	INTRODUCTION.....	47
4.2	METHODOLOGY.....	49
4.2.1	Pyrometer System Configuration.....	49
4.2.2	Pyrometer Calibration.....	54
4.3	EXPERIMENTAL SETUP.....	59
4.4	EXPERIMENTAL RESULTS AND DISCUSSION.....	61
4.4.1	Pyrometer Signal Profile and Temperature Behavior.....	61
4.4.2	Effect of Process Parameters on Temperature.....	65
4.5	CONCLUSIONS.....	70
	REFERENCES.....	71
CHAPTER 5 : CONSOLIDATION OF METAL POWDER.....		74
5.1	INTRODUCTION.....	74
5.2	EXPERIMENTAL SETUP.....	79
5.3	EXPERIMENTAL RESULTS AND DISCUSSION.....	84
5.3.1	Line Consolidation.....	84
5.3.1.1	Line Consolidation Mechanism.....	85
5.3.1.2	Influence of Laser Power.....	100
5.3.1.3	Influence of Scan Speed.....	103
5.3.1.4	Influence of Surface Condition.....	111
5.3.1.5	Influence of Layer Thickness.....	113
5.3.2	Area Consolidation.....	117
5.3.2.1	Area Consolidation Mechanism.....	118
5.3.2.2	Influence of Processing Parameters.....	123
5.4	CONCLUSIONS.....	126
	REFERENCES.....	128
CHAPTER 6 : PROPERTIES OF CONSOLIDATED STRUCTURE.....		130
6.1	INTRODUCTION.....	130

## TABLE OF CONTENT

---

6.2	EXPERIMENTAL SETUP .....	133
6.2.1	Surface Quality Observation.....	133
6.2.2	Roughness .....	135
6.2.3	Permeability .....	136
6.2.4	Hardness.....	140
6.2.5	Strength.....	141
6.3	EXPERIMENTAL RESULTS AND DISCUSSION.....	143
6.3.1	Surface Quality Observation.....	143
6.3.1.1	Influence of Laser Power.....	144
6.3.1.2	Influence of Scan Speed .....	144
6.3.1.3	Influence of Laser Spot Size.....	145
6.3.2	Surface Roughness.....	146
6.3.3	Permeability .....	151
6.3.3.1	Influence of Porosity on Permeability .....	153
6.3.3.2	Influence of Orientation Strategy on Permeability.....	154
6.3.3.3	Influence of Thickness on Permeability .....	157
6.3.4	Hardness.....	158
6.3.5	Strength.....	159
6.3.6	Characteristics of Consolidated Structures .....	160
6.4	CONCLUSIONS .....	164
	REFERENCES .....	165
	CHAPTER 7 : CONCLUSIONS AND FUTURE WORKS .....	168
7.1	CONCLUSIONS.....	168
7.2	RECOMMENDATION AND FUTURE WORKS.....	173
	ACKNOWLEDGEMENT .....	175
	LIST OF PUBLICATIONS .....	176

## NOMENCLATURE

$K$	Thermal conductivity	W/(m·K)
$K_{powder}$	Thermal conductivity of metal powder	W/(m·K)
$z$	Distance to thermocouple junction	mm
$\rho_{powder}$	Bulk density of metal powder	kg/m <sup>3</sup>
$C_p$	Specific heat of metal powder	J/(g·K)
$T_{max}$	Measured time to maximum voltage point	s
$\Delta t$	Irradiation time	s
$t_{cp}$	Heat transfer time from heat source	s
$a$	Heat source radius	mm
$t$	Time	s
$K_{consolidated}$	Thermal conductivity of consolidated material	W/(m·K)
$\rho_{consolidated}$	Density of consolidated material	kg/m <sup>3</sup>
$C_c$	Specific heat of consolidated material	J/(g·K)
$\alpha$	Thermal diffusivity of consolidated specimen	m <sup>2</sup> /s
$t_{0.5}$	Time of heat pulse reaches to ½ of max temperature	s
$L_{consolidated}$	Thickness of consolidated material	mm
$K_{solid}$	Thermal conductivity of solid material	W/(m·K)
$D$	Average particle diameter	μm
$A_r$	Absorption ratio	%
$t$	Layer thickness	μm

## TABLE OF CONTENT

---

$P$	Laser power	W
$V$	Scan speed	mm/s
$H$	Hatching size	mm
$E$	Energy density	J/mm <sup>2</sup>
$d$	Spot size diameter	mm
$\emptyset$	Porosity	%
$\lambda$	Wavelength	mm
$J$	Scan length	mm
$f$	Shutter speed	fps
$d_c$	Core diameter	$\mu\text{m}$
$\xi_m$	Acceptance angle	°
$e(\lambda, T)$	Emissivity of the object	
$w$	Constant	
$F(\lambda)$	Spectral transmittance of optical fiber	
$L(\lambda)$	Spectral transmittance of condenser	
$D(\lambda)$	Spectral transmittance of detector cell	
$G(\lambda)$	Spectral transmittance of filter	
$T_{Line}$	Temperature during line consolidation	°C
$T_{Area}$	Temperature during area consolidation	°C

# CHAPTER 1 : INTRODUCTION

## 1.1 BACKGROUND

Additive manufacturing (AM) is a relatively new and emerging manufacturing technology that may revolutionize the manufacturing industry. The initial development of the technology dates back approximately 30 years with the introduction by Kodama of a new method for manufacturing three-dimensional models [1]. This was followed by the first commercialized stereolithography-based AM, produced by 3D Systems [2]. Various types of materials are used in AM including metallic materials [3]. Therefore, it has been speculated that AM is the third industrial revolution after mechanization in the 18<sup>th</sup> century and the introduction of the assembly line in the 20<sup>th</sup> century [4].

The growth of the global market for the AM industry is indicated in Fig. 1.1. The growth was surveyed by Wohler Associates Inc., a leading consultancy on AM. It reported on the growth of the AM industry from 1988 to 2012 and revealed there to have been a high level of growth with only a slight decrease in 2009 [5]. They also showed a significant increase in the revenue of AM, which indicates a relatively strong demand for AM. In addition, it is reported that the metal-based AM system has been gaining in popularity in the industry in recent years.

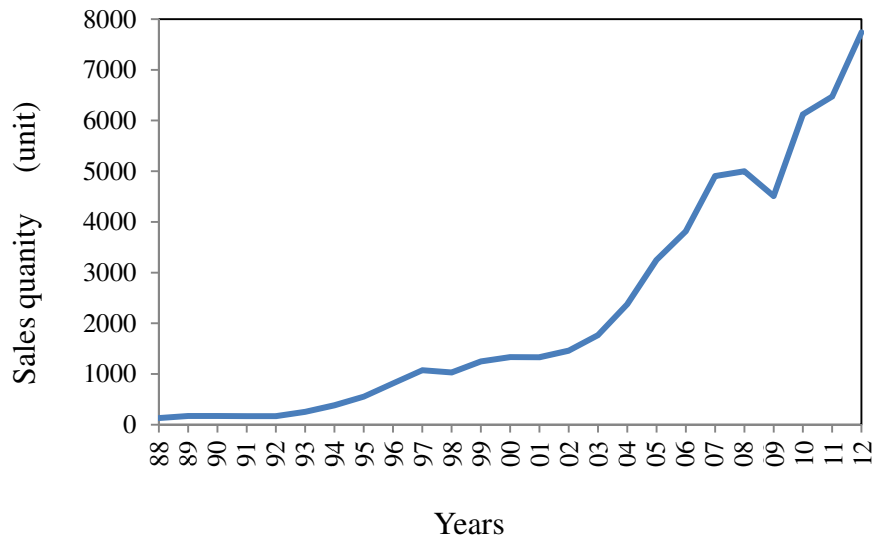


Fig. 1.1 Growth in the additive manufacturing industry [5]

With the realization of the potential of AM in generating revenue and its economic impact, the installation of AM systems is increasing worldwide. The installation of AM systems is presented in the pie chart in Fig. 1.2. The percentage of AM use by the country shows that the US (38%), Japan (9.7%) and Germany (9.4%) have the highest number of AM systems installed.

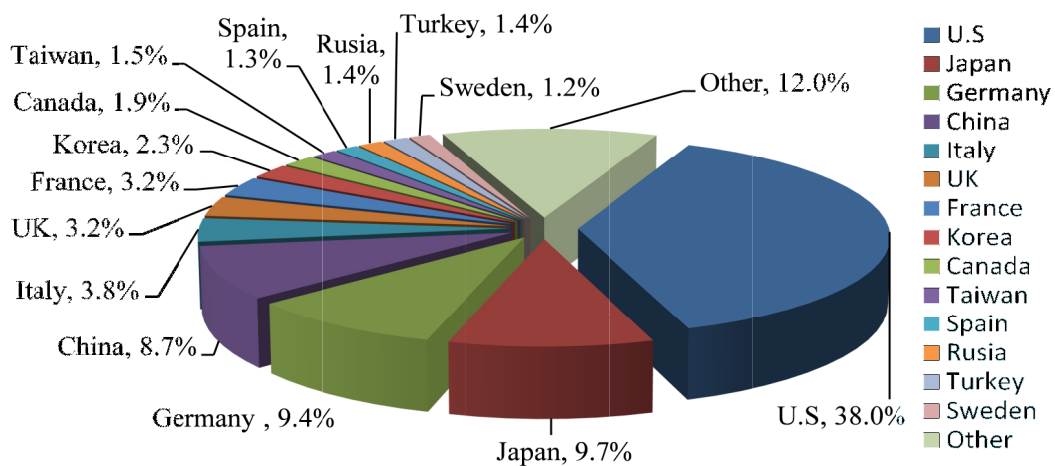


Fig. 1.2 Percentage of industrial AM-systems installed by country [5]

In May 2013, the US government, the country with the highest amount of AM technologies, launched manufacturing hubs and announced the creation of a manufacturing innovation institute. This institute is the National Additive Manufacturing Innovation Institute (NAMII), which focuses on the use of AM to spearhead the development of the manufacturing industry and encourage research throughout the country [6]. Whilst in Japan, the Japanese Economy, Trade and Industry Ministry has started promoting AM and plans to launch new research and development initiatives for the development of AM systems capable of producing metal products in order to ensure its manufacturing competitiveness globally [7][8]. These initiatives taken by the economic giants, are believed to be driven by the immense benefits of AM. Some of the advantages of AM are

- Rapid product introduction into the market
- Customized design and mass customization
- Low cost, in the long term, due to reduced inventory
- Increased design complexity of what can be manufactured
- Less wastage

Despite its advantages, as a relatively new manufacturing technology, AM faces stern challenges before it can be adopted for mass production in manufacturing industries. Some of these challenges are exacerbated by technical obstacles [9]. According to the report, the areas that still need further study are material characterization, material development, process understanding (such as deformation problems, balling and porosity), simulation, part strength and dimensional accuracy. The low number of engineer specializing in this new technology means that technical obstacles directly apply to its industrial application. This is because prior training is needed to operate AM systems. For the initial installation of AM systems in any industry, the setup costs are relatively expensive. There is hesitation on the part of investors

who are not aware of the potential of the technology. Other than that, design for manufacturing (DFM) with an emphasis on AM is not a well-developed sector. Since collaboration between industries is crucial, international standards need also to be established [10]. Although there are some preliminary standards produced by the American Society of Mechanical Engineers (ASME), which cover the different aspects of AM, such as terminology (ASTM F2792 - 12a), design (ISO/ASTM52915 – 13), testing methods (ISO/ASTM52921 – 13) and others. Further standard concerning AM will enhance collaborative design and development among AM users as variety of material and processes are being developed. Despite these challenges, AM technologies are currently increasingly gaining in attention from the manufacturing community and academia worldwide. Therefore, the above-mentioned challenges offer a high prospective for opportunities for research and development. However, there are many technical issues that need to be resolved before the technology is mature enough to be adopted for mass production.

There are many variations of AM processes that have existed since its first introduction. Each process has some unique operating principle and application, which offers its own advantages and disadvantages. Among these processes, Selective laser sintering/Selective laser melting (SLS/SLM) shows high potential for the development of functional products. SLS/SLM is a direct fabrication of near net shape products. SLS/SLM is one of the most promising AM techniques and is widely accepted by the industrial community compared to other competing AM technologies. This is due to its high flexibility in processing different types of materials under various conditions with relatively reasonable material properties [10],[11]. Generally, SLS/SLM has improved the lead-time from design to manufacture in comparison to the classical method. However, there is still the same problem as with other AM processes, namely, that the parts produced with SLS/SLM systems still do not meet some

of the stringent quality issues and requirements that are necessary if they are to be adopted as a good alternative to the conventional method. The capability of producing an end product of desirable quality compared to traditional processing techniques, has still not been achieved [12],[13].

In the SLS/SLM process, a thin layer of powder is deposited, and laser irradiates the powder surface successively until the final product is produced. The iterative process of powder deposition, laser irradiation and molten powder solidification mean the powder metals consolidate based on the CAD data. The product is a consolidated material the properties of which are influenced by metal powder and processing parameters. SLS/SLM involves the consolidation of metal powder under the influence of a high heat that is generated from laser irradiation over a very short space of time. As a result, the powder and consolidated structure experience repetitive microstructural and behavioral changes. This is because the sintering/melting and solidification occur alternately during layer-by-layer laser irradiation.

Furthermore, the consolidation characteristics of metals produced using SLS/SLM are relatively important due to its application in mold design and manufacturing. Therefore, outstanding properties and high-accuracy are vital characteristics that need to be improved for its application in mold manufacturing. The very basic element of developing a good-quality product is understanding the transformation process of the metal powder to the consolidated structure. This transformation occurs after the metal powders are irradiated with a reasonable amount of heat. Understanding the consolidation characteristics is the key to developing a good structure. This enables controlling mechanisms and methods to be implemented so that future development is possible. In order to improve these aspects, it is important to understand the consolidation characteristics and mechanisms during SLS/SLM.

A lot of research has been conducted into the consolidation characteristics during SLS/SLM. The consolidation mechanisms of metal powder can be classified into liquid phase sintering, solid-state sintering, full melting and chemical induced binding [13]. The binding mechanism in the full melting is mainly influenced by the fluid behavior. This is related to the surface tension, viscosity, wetting, evaporation and oxidation [3]. The ability of the metal powder to consolidate during SLS/SLM depends on many factors. These factors affect the quality and mechanisms involved in the formation of a consolidated structure. They can be categorized into processing factors and material factors. Material factors include the size of the metal powder, its impurities, particle shapes (dendrite or irregular), mixture, chemical composition, homogeneity, degree of agglomeration and others. Whereas, the factors associated with its processing are the laser parameters, processing environment, pressure, processing temperature, cooling rate, time and others. Elsen mentioned that there are more than 50 factors which affect the SLS process [14]. However, from among these parameters, the most important factors are laser power, laser spot size, powder layer thickness, laser scan speed and hatching size [15],[16],[17]. Therefore, a physical understanding and observation of laser beams and material interaction with respect to these parameters are important in SLS/SLM research.

### **1.2 PROBLEM STATEMENT**

Earlier studies which carried out real time observations of SLS/SLM processes using various imaging systems did not produce clear results. This is partly due to the nature of the SLS/SLM whereby the consolidation occurs at a micron scale at very high temperatures. Furthermore, the latest study also suggested carrying out a detailed study into the

mechanisms formation of a single track formation and the instabilities of the molten pool that are required for the use of a wider range of commercially available powders is feasible [18]. Hence, a clear and real time monitoring of the consolidation process in SLS/SLM is essential.

SLS/SLM is a complex process as it involves a laser–material interaction process before the consolidated structure is fabricated. During laser irradiation on metal powder, phenomena such as absorption, reflection and heat transfers between different mediums occur. This involves conduction, radiation, convection, phase transformation and chemical reactions taking place. As a result, the laser irradiated region experiences heating, sintering/melting and solidification. Therefore, thermal conductivity is an important thermo physical property in SLS/SLM, which needs to be extensively studied. This is because the ability of the metal powder to conduct heat affects the consolidation process.

As a relatively new process, using a wide variety of materials, the behavior and performance of consolidated materials in SLS/SLM are of utmost importance. Furthermore, since the SLS/SLM process is based on the transformation of metal powders at high temperatures, information on the temperature during SLS/SLM is important. During SLS/SLM processing, the continuous heating and solidification of metal powder within a very short period of time takes place. Hence, the evolution and profile of the temperature in SLS/SLM has a significant effect on the final quality of the consolidated products. Temperature measurement enhances better understanding of the interaction between the powder material and the laser beam [10]. However, few studies have been carried out to measure temperature during SLS/SLM.

### 1.3 RESEARCH OBJECTIVES

This research focuses on understanding the consolidation behavior of a product manufactured using the SLS/SLM process. In order to understand this, the thermal conductivity of the metal powder, the consolidation characteristics during laser irradiation and the properties of the structure are essential. Although the SLS/SLM process has already demonstrated its ability to successfully develop a final product, the structure formation and irregularities of droplets known as balling, porosity and surface quality are still not understood. Furthermore, triggering mechanisms that causes the metal powder to consolidate is the main area of interest for SLS/SLM. This enhances understanding of the SLS/SLM process.

The objectives of the research are

- a. To study the influence of powder particle size, bulk density and powder mixture on the thermal conductivity of metal powder.
- b. To analyze the sintering/melting temperature during SLS/SLM process.
- c. To design and develop a methodology that allows for the monitoring of the consolidation process of metal powder during SLS/SLM.
- d. To understand the characteristics and mechanisms of SLS/SLM during laser irradiation on a metal powdered surface.
- e. To investigate the properties of a consolidated material and its potential to develop a permeable structure.

## 1.4 THESIS OUTLINE

The thesis is divided into seven chapters as follows.

Chapter 1 is an introduction to the research, which covers the background, research objectives and scope of the research work.

Chapter 2 provides an overview of trends in additive manufacturing and its application in the manufacturing industry. The basic principles and different types of AM are described with an emphasis on SLS/SLM. After this, a literature review related to the research is discussed.

Chapter 3 describes the thermal conductivity of metal powders and consolidated structures due to their importance in heat transfer.

Chapter 4 discusses temperature measurements taken during the consolidation process. A pyrometer was utilized to measure the temperature and the effect of laser power and scan speed on the temperature is considered.

Chapter 5 presents the consolidation behavior of the metal powder as the laser beam irradiates it. A high-speed camera was utilized in order to monitor the consolidation at a magnified view during the consolidation process. Based on this, consolidation behavior is presented.

Chapter 6 examines the properties of consolidated structures manufactured using SLS/SLM. As these structures are characterized by the existence of porosity, their potential for use as a permeable structure is investigated.

Chapter 7 concludes the study and highlights further work that can be conducted based on the results attained.

## REFERENCES

- [1] H. Kodama, “Automatic method for fabricating a three-dimensional plastic model with photo-hardening polymer,” *Rev. Sci. Instrum.*, vol. 1770, no. 52, 1981.
- [2] T. Wohlers, *Wohler Report 2011*. Wohlers Associates, 2011.
- [3] J. P. Kruth, G. Levy, F. Klocke, and T. H. C. Childs, “Consolidation phenomena in laser and powder-bed based layered manufacturing,” *CIRP Ann. - Manuf. Technol.*, vol. 56, no. 2, pp. 730–759, Jan. 2007.
- [4] The Economist, “A Third Industrial Revolution,” pp. 1–2, Apr-2012.
- [5] T. Wohlers, *Wohlers Report 2013: Additive Manufacturing and 3D Printing State of the Industry*. Wohlers Associates, 2013.
- [6] “Obama Administration Launches Competition for Three New Manufacturing Innovation Institutes,” *The White House, Office of the Press Secretary*, 2013. [Online]. Available: <http://www.whitehouse.gov/the-press-office/2013/05/09/obama-administration-launches-competition-three-new-manufacturing-innova>. [Accessed: 25-Nov-2011].
- [7] “METI Journal : 3D Printer,” *Ministry of Economy, Trade and Industry Japan*, 2013.
- [8] Reno J. Tibke, “Japan’s 3D Printing Industry,” *Akihabara News*, 2013. [Online]. Available: <http://akihabaranews.com/2013/08/26/article-en/japans-3d-printing-industry-leapfrog-not-catch-game-play-41031748>. [Accessed: 20-Nov-2013].
- [9] D. L. Bourell, M. C. Leu, and D. W. Rosen, *Roadmap for Additive Manufacturing: Identifying the Future of Freeform Processing*. The University of Texas at Austin, Laboratory for Freeform Fabrication, Advanced Manufacturing Center, 2009.
- [10] J. P. Kruth, X. Wang, T. Laoui, and L. Froyen, “Lasers and Materials in Selective Laser Sintering,” *Assem. Autom.*, vol. 23, no. 4, pp. 357–371, 2003.
- [11] S. Kumar, “Selective laser sintering: A qualitative and objective approach,” *JOM*, vol. 55, no. 10, pp. 43–47, Oct. 2003.

- [12] E. N. Hopkinson and P. M. Dickens, *An Industrial Revolution for the Digital Age*. John Wiley & Sons, Inc, 2006.
- [13] J. P. Kruth, “Material Incess Manufacturing by Rapid Prototyping Techniques,” *CIRP Ann. - Manuf. Technol.*, vol. 40, no. 2, pp. 603–614, 1991.
- [14] M. Van Elsen, F. Al-Bender, and J. P. Kruth, “Application of dimensional analysis to selective laser melting,” *Rapid Prototyp. J.*, vol. 14, no. 1, pp. 15–22, 2008.
- [15] A. Simchi and H. Pohl, “Effects of laser sintering processing parameters on the microstructure and densification of iron powder,” *Mater. Sci. Eng. A*, vol. 359, no. 1–2, pp. 119–128, Oct. 2003.
- [16] S. Dingal, T. R. Pradhan, J. K. S. Sundar, A. R. Choudhury, and S. K. Roy, “The application of Taguchi’s method in the experimental investigation of the laser sintering process,” *Int. J. Adv. Manuf. Technol.*, vol. 38, no. 9–10, pp. 904–914, Aug. 2007.
- [17] A. N. Chatterjee, S. Kumar, P. Saha, P. K. Mishra, and A. R. Choudhury, “An experimental design approach to selective laser sintering of low carbon steel,” *J. Mater. Process. Technol.*, vol. 136, no. 1–3, pp. 151–157, May 2003.
- [18] I. Yadroitsev and I. Smurov, “Selective laser melting technology: From the single laser melted track stability to 3D parts of complex shape,” *Phys. Procedia*, vol. 5, pp. 551–560, Jan. 2010.

# **CHAPTER 2 : OVERVIEW OF ADDITIVE MANUFACTURING**

## **2.1 INTRODUCTION**

In the current scenario of global, fast-paced and competitive world market, ability to manufacture the high-quality products at reduced cost and achieve customer satisfaction is essential. Other than that, product manufacturers are also trying to shorten new-product development time as a mean to gain competitiveness. Hence, the product development time becomes a key differentiator for success of a product in the consumer market.

AM is seen as one of the future technologies that able to compete against traditional processing techniques with its distinctive capability of fulfilling the design requirement. Initially AM technology was used as part of the product design and development process where the prototype of a product was fabricated during visual inspection and design verification stage. However, with the advent of technology, its application extends from merely prototyping to manufacturing. Currently, a number of manufacturers utilize the AM systems to manufacture the final products, although the technology is still undergoing extensive research and development (R&D) and have not achieved its maturity stage.

## 2.2 RAPID PRODUCT DESIGN AND DEVELOPMENT

AM technology enables transition of computer-aided design (CAD) data to a real product in a shortened time. This leads to significant improvement in the product-development process. Therefore, it is often called as a tool for rapid product design and development. During its early development, AM technology was used to manufacture prototype before its introduction in the market. Later, AM technology was adopted for manufacturing of complex parts and customized design. Fig. 2.1 illustrates product design and development cycle through concurrent engineering approach, which includes the creation of prototypes as one important stage.

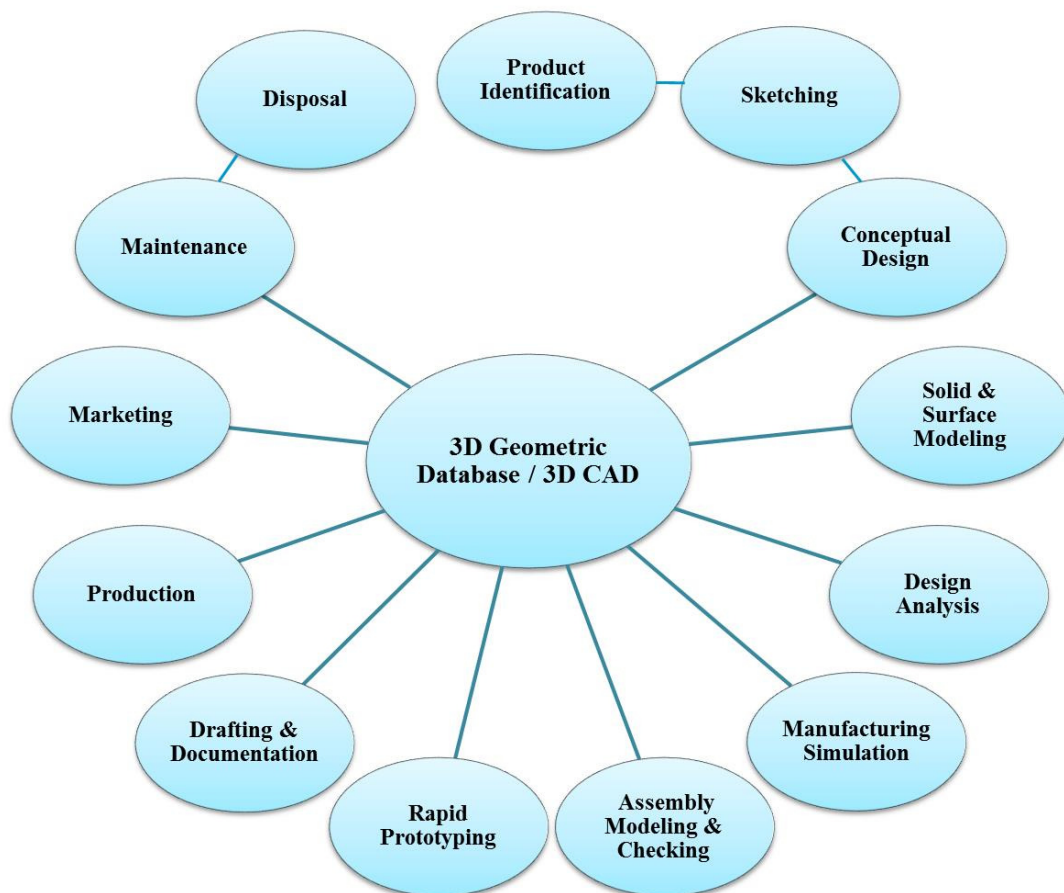


Fig. 2.1 Product design and development cycle through concurrent engineering [1]

There are several terms used to refer the group of AM technologies. Terms used to refer to these technologies are rapid prototyping (RP), layered manufacturing (LM), rapid manufacturing (RM) and 3D printing. Other less common used terms are also used to represent the similar technology; such as solid freeform fabrication (SSF), material addition manufacturing, material in excess manufacturing, desktop manufacturing, additive fabrication, direct digital manufacturing, instant manufacturing, direct CAD manufacturing, and others. These terms evolved since the introduction of the technology. For instance, during early development of AM, the term RP is the most common used since it extensively being in producing prototypes. In fact, RP refers to a group of processes where the manufacturing of three-dimensional part from CAD through additive approach [2].

Later, the term of rapid tooling (RT) was used due to increasing application of AM in the mold design and development. This is also driven by increasing utilization of metal in AM. As a result, the common term RP starts to evolve to RT, which reflects its capability to produce mold and tool in a shortened time compared to the classical subtractive method. Nevertheless, not all AM processes directly start a started as RP. One of the examples is laser cladding. Initially, during its early development, laser cladding was mainly used in corrosion-resistant coating and parts refurbishment [3]. However, its application later extends beyond to cover different applications, including RM.

Hence, RT is a progression from the development of RP technologies. Through RT, tool prototype can be directly produced from the CAD model. One of the principal advantages of employing RT is it capable of shortening the tooling lead time from months to a few days or weeks depending on the complexity of the tooling. Since mold making for both prototype and production component manufacturing currently represents one of the longest and most costly phases in the product-development process, application of RT able to

improve product development time. However, recently, the term AM is more common as to reflect the generic term used to represent the group of this technology and its potential. Application of AM by manufacturing product and tooling directly from digital CAD to a usable product is a significant move towards reducing time to market and product cost. As a result, an increasing number of industries start to employ AM technologies. This trend has a dramatic impact on the product-development process.

### **2.3 BASIC PRINCIPLES AND TYPES OF ADDITIVE MANUFACTURING**

In AM, the basic principle is the model initially generated from three-dimensional (3D) CAD before part manufacturing. After that, the part is fabricated by the addition of the material layer by layer. Generally, AM undergone common stages before a part can be successfully manufactured. Initially, a part is designed using CAD software. The format of the part design is converted to standard triangulation language (STL) file, which is the standard format in AM file conversion. The STL file is transferred to AM machine. Based on the types of AM systems used, proper machine setup to be performed prior to a fabrication process. After that, the fabrication processes start. Once the fabrication process completed, the part is removed from the fabrication chamber. Depending on the AM systems used, post-processing may be required before the part fit enough and ready to be used. Fig. 2.2 illustrates the basic principles and stages of AM in product development.

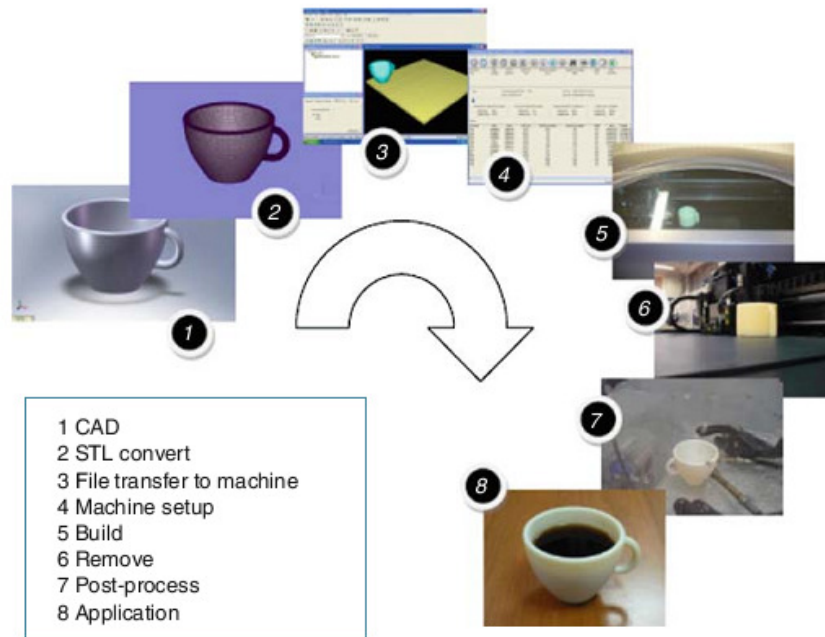


Fig. 2.2 Basic principle and stages in AM [4]

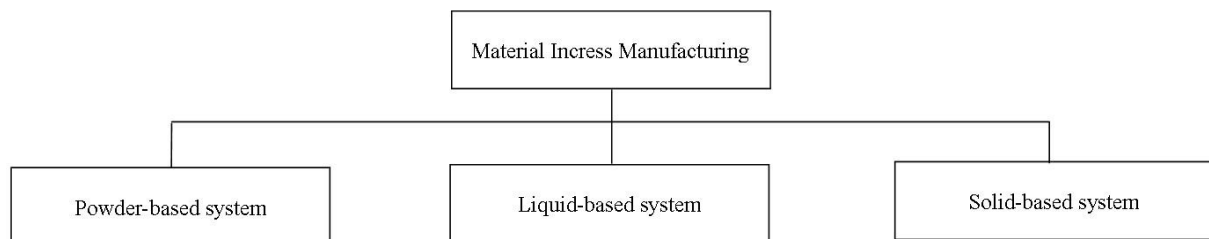


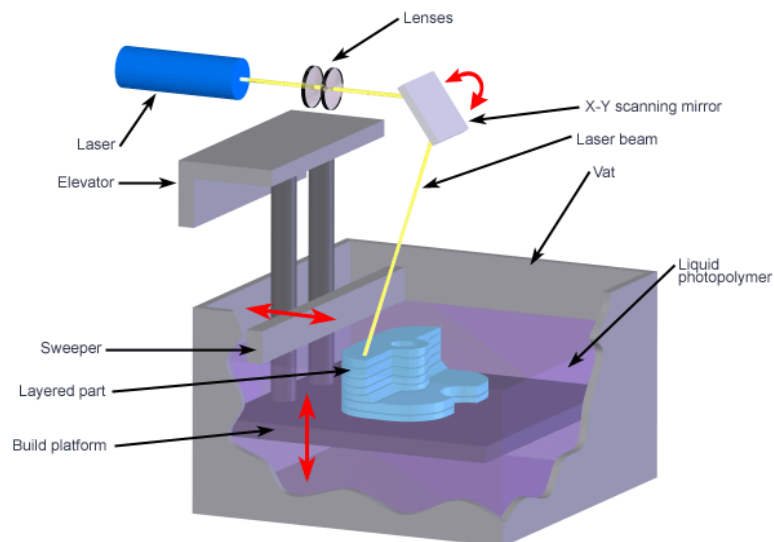
Fig. 2.3 Classification of material incess manufacturing [5]

There are many types of AM processes available. The AM can be classified based on the state of raw material input, baseline technology used and methods of the layer construction [4],[5],[6],[7]. However, among various classifications proposed by AM researchers, the most common classification of AM based on the properties of the initial form of the main material input used during processing. The classification was proposed by Kruth [5] and is shown in the Fig. 2.3. The author used the term material incess manufacturing to

describe relatively similar technology, which then evolve to AM. This classification can be divided into powder-based systems, liquid-based systems and solid-based systems. Each of the systems can be further divided as illustrated in the figure.

### 2.3.1 Liquid-based AM

Liquid-based AM means the initial form of material input to produce the part is in the liquid state. Common materials used are thermoplastic polymers and thermosetting polymers such as polyamide nylons and epoxies respectively. The parts manufactured via the liquid-based systems AM undergone curing process where the liquid is solidified producing 3D solid part. Some of the examples are Stereolithography (SLA), Fused Deposition Modeling (FDM), Solid Ground Curing (SGC), Solid Creation System (SCS) and others [2][8].



Copyright © 2008 CustomPartNet

Fig. 2.4 Liquid-based AM - Stereolithography (SLA)[9]

Fig. 2.4 shows one of the liquid-based AM known as stereolithography (SLA). Most of the liquid-based AM systems build in a liquid resin. The resin later cures or solidifies. As a result, the surface of the hardened layer is produced. Later, the part is lowered for successive layer fabrication. The process is repeated until 3D part based on the STL is completed. Based on the system manufacturers, the techniques may differ slightly in producing the final products.

### **2.3.2 Solid-based AM**

As the name implies, the initial form of the material input prior to part fabrication is in the solid-state. The input material differs in their shape and size. The materials range from polycarbonate, ABS, polymethyl thermoplastic, wax, elastomers, paper (organic fiber) coated proprietary heat-activated epoxy adhesive and other proprietary material of different manufacturers. Common AM systems that classified into this group are Laminated Object Manufacturing (LOM), Paper Lamination Technology (PLT), Multi-Jet Modeling System (MJM) and several other systems [2][8].

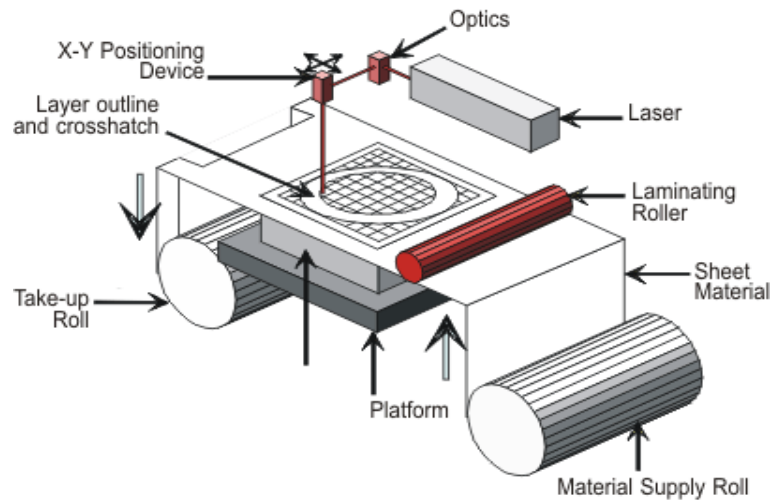


Fig. 2.5 Solid-based AM - Laminated Object Manufacturing (LOM) [10]

### 2.3.3 Powder-based AM

In powder-based AM systems, raw materials used as the main materials are in the powder form. The AM systems and materials vary from a different system developers. Among AM that are classified under powder-based systems are Selective Laser Sintering (SLS), Laser Engineered Net Shape (LENS), 3D Printing (3DP), EOSINT systems, Multiphase Jet Solidification (MJS), laser cladding, Electron Beam Melting (EBM) and others. Examples of the materials are glass filled (GF)/nylon composite, polyamide (nylon), polycarbonate, thermoplastic elastomer and others. Ceramics materials such as aluminum oxide and zirconium oxide also have been used in powder-based AM in development of direct investment casting [2][8].

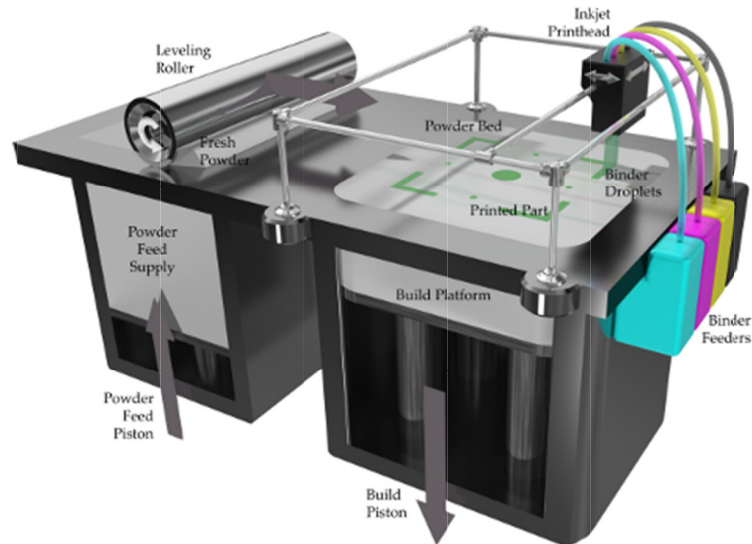


Fig. 2.6 Powder-based AM - 3D Printing, 3DP [11]

Recently, the application of the high-powered laser systems has allowed a wide variety of metal powder to be used in AM. After the laser irradiation on the metal powder, a consolidated structure is formed. The metal powder size varies from 20 to 80 micron. High-energy density causes melting of the metal powder instead of sintering only. Hence, the term SLS and SLM are interchangeably used to describe the same process. This is because the SLS and the SLM are being differentiated by the melting point of the respective materials. Some of the metal powders that have been used are 304, 316, 420 stainless steel, tool steel, gold, bronze, nickel, copper, aluminum and others. However, due to poor consolidability of pure metal, increasing alloy materials have used commercially for application in AM. Some of these examples are titanium alloy (Ti-6Al-4V), austenitic nickel-chromium-based superalloys (Inconel), iron-nickel and others [2][8].

## **2.4 SELECTIVE LASER SINTERING/SELECTIVE LASER MELTING**

Among the processes mentioned above, the SLS/SLM is regarded as the most versatile and potential process. This is due to the capability of the process to deal with a variety of engineering materials range from thermoplastic, composite, ceramics and metallic materials [12]. The SLS/SLM is an emerging technique that seen as a potential future manufacturing approach alternative for product development. A number of advantages that offered by the SLS/SLM process attract injection mold manufacturers to start using SLS/SLM as an alternative process in the mold manufacturing. Among the advantages are shorter time, design freedom, lower cost and reduce waste. Although well known as one of RT application of AM process, credibility of the SLS/SLM in producing high quality, precise and cost effective mold is being challenged by stringent requirement by mold making industry. This is due to some of the drawbacks of part produced via the SLS/SLM. Porosity, lower part strength and poor surface roughness are some of the associated weakness of the consolidated part. However, regardless of the drawbacks, a lot of research has been made on the SLS/SLM.

The SLS/SLM is actually a fabrication of a 3D part, which is accomplished through a layer-by-layer powder deposition. In each layer, the powder is leveled by a roller and sintered by a laser beam. After the successive number of powder deposition and laser sintering, a finished part can be produced via the additive process. Schematic view of the SLS/SLM process is shown in Fig. 2.7.

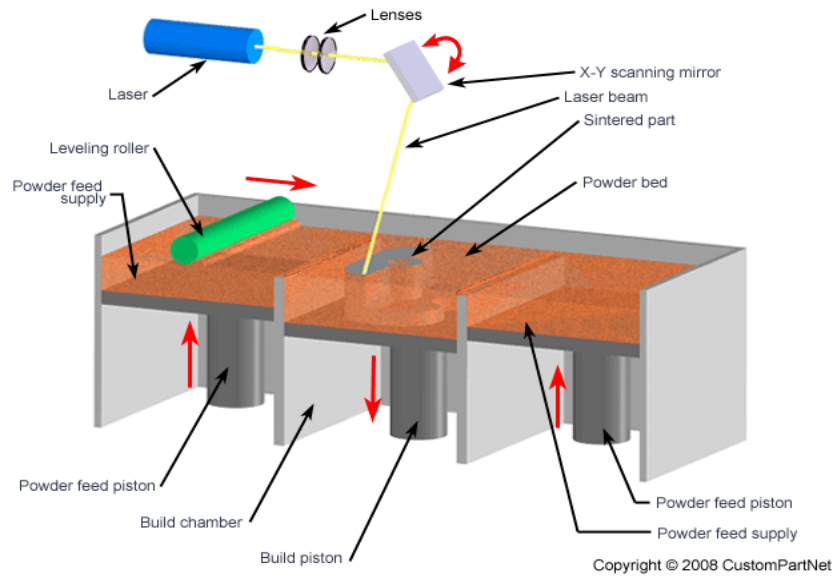


Fig. 2.7 Schematic view of the SLS/SLM [13]

### 2.4.1 Machining-SLS/SLM Hybrid System



Fig. 2.8 Lumex 25C

Development of AM machines is increasing due to high demand and its potential in revolutionizing the manufacturing industry. One of the forefront innovations in AM is the

development of Machining-SLS/SLM Hybrid System. The machine is developed by Matsuura Machinery Corporation Japan. The machine is unique compared to other AM as it is the first multifunction machine, which combines the subtractive and additive processes simultaneously in one setup [14].

Table 2.1 Specification of Lumex 25C

Laser	
Laser type	Yb:fiber (CW)
Wavelength [nm]	1070
Maximum power [W]	500
Scan system	Galvanometer scanner
Maximum scan speed [mm/s]	10 000
Spot diameter [mm]	0.1 – 1.2
Movement	
X-axis [mm]	260
Y-axis [mm]	260
Z-axis [mm]	100
U-axis (forming table) [mm]	185
V-axis (powder table) [mm]	280
W-axis (squeezing blade) [mm]	630
Process area size	
Forming table area [mm]	250 × 250
Maximum work area [mm]	250 × 250 × 150
Feed rate	
X-axis and Y-axis [mm/min]	60 000
Z-axis [mm/min]	30 000
Main spindle	
Revolution speed [rpm]	5 000 - 50 000
Process atmosphere	Inert gas (N <sub>2</sub> )

The machine is capable of performing milling process and SLS/SLM process. As a result, the consolidated structure fabricated via the SLS/SLM can be milled alternately in order to improve part accuracy and roughness issue, which are common shortcomings linked to AM. Hence, it is an ideal machine for the development of injection molding die [15]. The machine is illustrated in Fig. 2.8. The machine is equipped with a laser type Yb: fiber (CW) that has a wavelength of 1070 nm. It has a maximum power 500 W equipped with scan system using galvanometer scanner. The machine is capable of achieving maximum scan speed of 10,000 mm/s. The spot diameter can be varied a range from 0.1 to 1.2 mm. The specification of the machine is tabulated in Table 2.1.

## 2.5 CONCLUSIONS

There are many AM processes and systems available in the market with each of them offers distinctive advantages. These AM can be classified into liquid-based, solid-based and powder-based. One of the emerging technologies in AM is the SLS/SLM. The SLS/SLM is AM method where the powder particles were fused by the laser beam to build up complex 3D object directly from CAD models. The method has revolutionized the way products are manufactured. In Japan, new innovation made in the area of AM with the introduction of Machining-SLS/SLM Hybrid System. The system is the first multifunctional AM system that combines the subtractive processes and additive where the milling process and the laser consolidation process can be made alternately with one setup. As a relatively new machine, there is a high potential for research and study can be performed for further development. In this research, Lumex 25C is extensively being used for the SLS/SLM study.

## REFERENCES

- [1] R. Barr and D. Juricic, “A CAD/CAM Laboratory Experience for a Lower-Division Engineering Design Graphics Course,” in *International Conference on Engineering Education*, 1997.
- [2] R. Nooraini, *Rapid Prototyping: Principles and Applications*. John Wiley & Sons, Inc, 2006.
- [3] E. Toyserkani, A. Khajepour, and S. F. Corbin, *Laser Cladding*. CRC Press, 2004.
- [4] I. Gibson, D. W. Rosen, and B. Stucker, *Additive Manufacturing Technologies*. Springer, 2010.
- [5] J. P. Kruth, “Material Incess Manufacturing by Rapid Prototyping Techniques,” *CIRP Ann. - Manuf. Technol.*, vol. 40, no. 2, pp. 603–614, 1991.
- [6] J. P. Kruth, M. . Leu, and T. Nakagawa, “Progress in Additive Manufacturing and Rapid Prototyping,” *Ann. CIRP- Manuf. Technol.*, vol. 47, no. 2, pp. 525–540, 1988.
- [7] D. T. Pham and R. S. Gault, “A comparison of rapid prototyping technologies,” *Int. J. Mach. Tools Manuf.*, vol. 38, no. 10–11, 1998.
- [8] C. K. Chua, K. F. Leong, and C. . Lim, *Rapid Prototyping - Principles and Applications*, 2nd ed. World Scientific Publishing Co. Pte Ltd, 2003.
- [9] CustomPartNet, “Stereolithography (SLA),” 2013. [Online]. Available: <http://www.custompartnet.com/wu/stereolithography>. [Accessed: 06-Sep-2013].
- [10] AZoNetwork UK Ltd, “Laminated Object Modeling (LOM),” 2013. [Online]. Available: <http://www.azom.com/article.aspx?ArticleID=1650>. [Accessed: 06-Sep-2013].
- [11] V. P. I. and S. University, “Indirect 3D Printing,” 2013. [Online]. Available: <http://www.dreams.me.vt.edu/Facility/Indirect3DP/index.html>. [Accessed: 06-Sep-2013].
- [12] C. K. Chua, K. F. Leong, and L. CS, *Rapid Prototyping: Principles and Applications*. World Scientific Publishing Co. Pte Ltd, 2003.
- [13] CustomPartNet, “Selective Laser Sintering (SLS),” 2013. [Online]. Available: <http://www.custompartnet.com/wu/selective-laser-sintering>. [Accessed: 06-Sep-2013].

- [14] S. Abe, Y. Higashi, H. Togeeyama, I. Fuwa, and N. Yoshida, “Development of milling-combined laser metal sintering method,” *Japan Soc. Precis. Eng.*, vol. 73, no. 8, pp. 912–916, 2007.
  
- [15] S. Abe, Y. Higashi, I. Fuwa, N. Yoshida, and T. Yoneyama, “Milling-Combined Laser Metal Sintering System and Production of Injection Molds with Sophisticated Functions,” in *11th International Conference of Precision and Engineering (ICPE)*, 2006, pp. 288–293.

## **CHAPTER 3 : THERMAL CONDUCTIVITY OF METAL POWDER AND CONSOLIDATED STRUCTURE**

### **3.1 INTRODUCTION**

Understanding of physical properties of the metal powder and the consolidated structure is essential in the SLS/SLM process. Since the process is a direct additive fabrication of part through a layer-by-layer powder deposition and successive laser beam irradiation, both physical properties of the metal powder and the consolidated material are important. During laser irradiation on the metal powder, heat was generated. The heat was then transferred to the surrounding powder, the structure and the material substrate. Therefore, one of the important properties in the SLS/SLM is the thermal conductivity of the metal powder and the consolidated structure. This is because the ability of the metal powder to conduct heat affects the consolidation process during the SLS/SLM.

The importance of the thermal conductivity in the SLS/SLM process has been highlighted by many researchers who have studied the thermal conductivity of metal powder for SLS/SLM application using various methods [1],[2],[3]. In this chapter, thermal conductivity of metal powders with different particle diameters was evaluated. Then, the metal powders were mixed with specified volume ratios to investigate its effect. Thermal

conductivity of the consolidated materials was also examined, and its relation to porosity is elaborated. In determining the thermal conductivity of metal powder, a theoretically verified method using a thermocouple was performed. Measurement on the thermal conductivity of the consolidated material was made using laser flash technique.

Thermal conductivity is an important thermo physical property in the SLS/SLM since the ability of the metal powder to conduct heat will affect the consolidation process. Thermal conductivity,  $K$  is the rate of heat transfer. During the SLS/SLM, laser beam is irradiated to the powder surface. Before consolidation occurs among the powder particles, heat from irradiated powder is conducted to other adjacent powder particles. Good consolidation among the metal powders particles occur based on the appropriate amount of heat to melt the powder particles so that the metal powders can fuse and form solid with surrounding powder particles. During this consolidation process, heat transfer process occurs through the powder particles and air gap. Therefore, thermal conductivity is an essential element in understanding the consolidation process of the metal powders. However, effects of particle diameter, bulk density, mixed powders on the thermal conductivity are not fully understood. Furthermore, the effects of porosity on the thermal conductivity of the consolidated material are also not well established. According to Danninger, availability of engineering data on thermo physical properties of sintered or consolidated steels are scarce and usually not too reliable [4]. Application of a wide variety of consolidated materials also requires extensive technical information for engineering design.

Thermal conductivity is important thermo physical properties for various design applications. Current development in mold making shows the potential of the consolidated material to be used as injection mold. In mold application, efficient heat transfer allows quality parts to be produced. For instance, effective heat removal from a mold cavity in the

injection molding process can reduce the reject caused by burning, warpage and burn marks in molded part. Current studies show that there is only limited data on the thermal conductivity of the consolidated material despite their increasing application[4].

### 3.1.1 Thermal Conductivity of Metal Powder

In order to determine the thermal conductivity of metal powder, there are various techniques such as photo acoustic [5], modified hot wire [6], transient needle probe [7], crenel heating excitation [8] and photo pyroelectric techniques [2]. This research used a technique, which was developed by the thermocouple principles [9]. The technique is relatively simple, cost-effective and fast but still produced a reliable result. The mathematical expression of thermal conductivity was theoretically derived and verified by using instantaneous point source of heat [10]. In this technique, time taken to reach the maximum voltage when a heat source exists at a specified distance using a thermocouple concept is measured. Based on this, the thermal conductivity of metal powder,  $K_{powder}$  can be determined.

$$K_{powder} = \frac{z^2 \rho_{powder} C_p}{6T_{max}} \quad (3.1)$$

where  $z$  is distance from the powder surface to thermocouple junction,  $\rho_{powder}$  is metal powder bulk density,  $C_p$  is specific heat of metal powder, and  $T_{max}$  is measured time to maximum voltage point. Since  $K_{powder}$  is dependent on metal powder bulk density,  $\rho_{powder}$ , the air gap among the metal powder particles is already taken into account in determination of thermal conductivity. Based on the assumption made and mathematical derivation, Eq. 3.1 is only valid if and only if  $\Delta t/t_{cp} < 0.1$  and  $z/a > 3.87$  are satisfied, where  $\Delta t$  is irradiation time,

$t_{cp}$  is heat transfer time from heat source,  $a$  is heat source radius and  $z$  is distance from the heat source surface. Throughout this experiment, the  $z/a$  value was set equal to 4 whereas of  $\Delta t/t_{cp}$  was less than 0.1.

### 3.1.2 Thermal Conductivity of Consolidated Solid Material

There are many techniques to measure the thermal conductivity of solid material. Each of these techniques offers advantage over others for different applications. Generally, these techniques can be divided into two main methods known as steady-state method and transient method [11]. Steady-state method refers to condition when the temperature of the material measured does not change with time. Transient method on the other hand refers to a group of techniques that perform measurement during the material being heated. Among thermal conductivity techniques that are classified as transient method are transient plane source, transient line source,  $3\omega$ , radial flow, laser flash and others.

In this research, laser flash technique was used to measure the thermal conductivity of the consolidated material from the SLS/SLM process. The laser flash technique measured the thermal conductivity as the laser was irradiated by a short laser pulse for less than 1 ms. The thermal conductivity of consolidated materials,  $K_{consolidated}$  of the specimens was determined from Eq. 3.3 where  $\rho_{consolidated}$  is density,  $C_c$  was specific heat and  $\alpha$  was thermal diffusivity of the consolidated specimen. The thermal diffusivity is calculated based on the temperature rise, which is given by Eq. 3.2 where  $t_{0.5}$  is time from the start of heat pulse reaches to be one-half of its maximum temperature, and  $L_{consolidated}$  is the thickness of the consolidated material. During the laser pulse, the temperature on the opposite side of the consolidated sample was

recorded. The thermal diffusivity and the thermal conductivity of the consolidated material are given by the following equations.

Thermal diffusivity of consolidated materials,

$$\alpha = \frac{1.37L_{consolidated}^2}{\pi^2 t_{0.5}} \quad (3.2)$$

Thermal conductivity of consolidated materials,

$$K_{consolidated} = \rho_{consolidated} C_c \alpha \quad (3.3)$$

## 3.2 EXPERIMENTAL SETUP

### 3.2.1 Metal Powder Material

Metal powder used in the experiment was SUS316L with the particle diameter of 10, 20, 50 and 100  $\mu\text{m}$ . The specification of the metal powder is indicated in Table 3.1. The metal powder particle shape was irregular. The specific heat was recorded at 0.50 J/(g·K).

Table 3.1 Specification of SUS316L metal powder

Metal powder material	Average particle diameter, $D$ ( $\mu\text{m}$ )	Specific heat, $C$ J/(g·K)[9]	Particle shape
SUS 316L	10, 20, 50, 100	0.50	Irregular

Table 3.2 Specification of ferrous based metal powder

Type		Fe, Cu, Ni
Average particle diameter	$D$	25 $\mu\text{m}$
Shape		Irregular
Bulk density	$\rho_{\text{powder}}$	4190 $\text{kg/m}^3$
Absorption ratio (at wavelength 1070 nm)	$A_r$	25%
Layer thickness	$t$	50 $\mu\text{m}$

Another material used in the study was a ferrous-based metal powder. The material is a mixture of chromium molybdenum steel (70%), copper (20%) and nickel (10%) with the average particle diameter of 25  $\mu\text{m}$ . In this research, fabrication of the consolidated material was made by using this ferrous-based metal powder mixture. Detail study on the properties and consolidation characteristics of the material was made in the successive chapter. The powder was prepared through gas atomization method. The specification of the metal powder is tabulated as Table 3.2. The metal powder was deposited on a cold-rolled steel substrate that was sandblasted by #46 grain. This was to improve wettability of molten powder. Similar to any SLS/SLM system, the metal powder was deposited under influence of gravitational force and then was leveled by squeegee blade. Throughout the experiment, the thickness of the metal powder was maintained at 50  $\mu\text{m}$ .

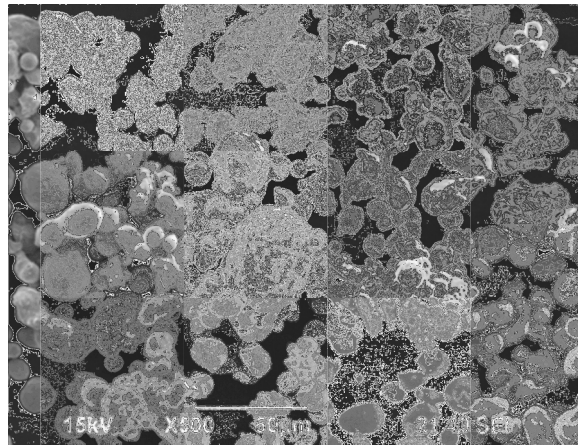


Fig. 3.1 SEM image of ferrous based metal powder

### 3.2.2 Thermal Conductivity of Metal Powder

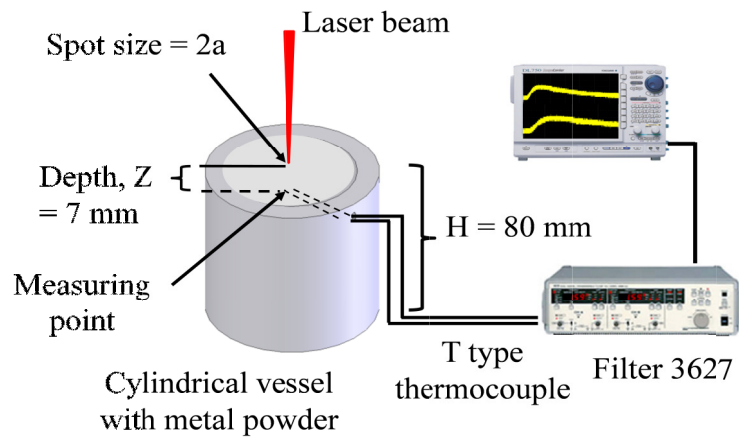


Fig. 3.2 Experimental setup

In this experiment, a continuous type Yb: fiber laser (LP-F10 model) manufactured by SUNX was used to irradiate the laser beam on the metal powder surface. The laser beam diameter on the metal powder was used as a heat source in the thermal conductivity

measurement. The experimental setup is shown in Fig. 3.2. The cylindrical vessel was made from aluminum alloy with an outer diameter of 100 mm, inner diameter 80 mm and depth 60 mm. The thermocouple used in the experiment was T type (copper-constantan) with a wire diameter of 0.1 mm and 7 mm distance from top of powder surface. Other conditions set were laser wavelength,  $\lambda = 1070$  nm, spot size,  $2a = 2$  mm, irradiation time,  $\Delta t = 4$  seconds and irradiation energy,  $E = 40$  J. Fig. 3.3 indicates common output obtained from the thermocouple during the thermal conductivity measurement and their nomenclature.  $T_{\max}$  is measured time to the maximum voltage achieved and used to calculate thermal conductivity based on Eq. 3.1.

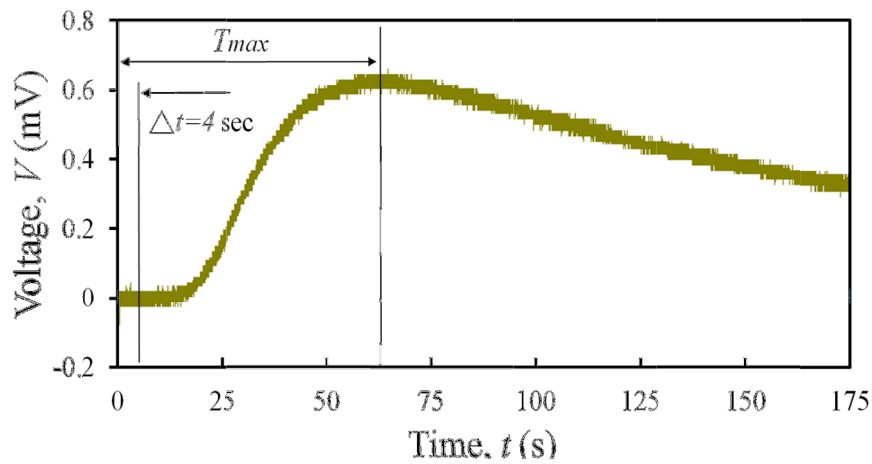


Fig. 3.3 Oscilloscope output

### 3.2.3 Thermal Conductivity of Consolidated Metal

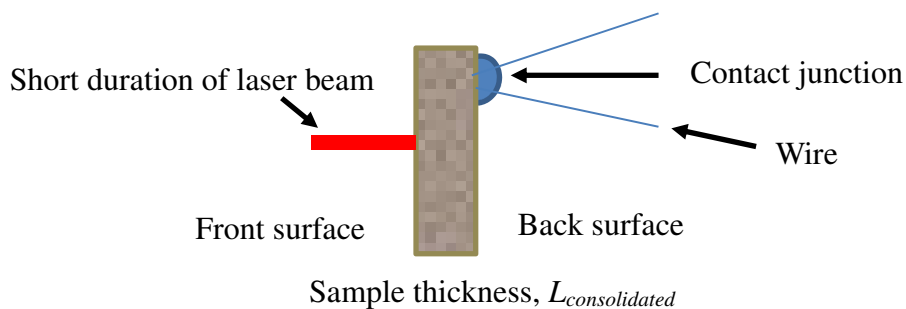


Fig. 3.4 Laser flash method for thermal conductivity measurement

Determination of the thermal conductivity of the consolidated materials was analyzed using laser flash technique as shown in the Fig. 3.4. During the measurement, a short duration of heat pulse was applied on a surface of 1.5 mm thickness specimen with 8 mm width and 8 mm length. Then temperature changes at the opposite surface were recorded. The laser flash measurement was made using Ulvac Riko Laser Flash – Thermal Constant Analyzer TC-7000 machine.

## 3.3 EXPERIMENTAL RESULTS AND DISCUSSION

### 3.3.1 Effect of Particle Diameter on Thermal Conductivity of Metal Powder

$T_{max}$  recorded for 10, 20, 50 and 100  $\mu\text{m}$  SUS 316 L metal powders were 180.0, 110.6, 59.0 and 51.4 seconds respectively. The thermal conductivity of SUS 316 L the metal powders with different particle diameters are shown in Fig. 3.5. The graph shows that the thermal conductivity is increasing with the particle diameter. This behavior was due to the

conductive heat transfer mechanism among the powder particles. Fig. 3.6 shows the comparison of schematic presentation among the small and large powder particles inside the cylindrical vessel. As indicated in the figure, there were points where the particles were in contact with other the powder particles. When the laser beam was irradiated on the powder, heat was transferred through these contact points to the measuring point. Higher thermal conductivity of the larger powder particles from heat source to measuring point was caused by the more prevalent conductive heat transfer mechanism of the greater particle and less resistance during heat transfer. During heat conduction from heat source to the thermocouple measuring point, the small powder particles subjected to more resistance due to repetitive changes between solid and air as a medium of heat transfer. In contrast, for the large particles, the behavior is vice versa. Therefore, heat transfer of the large particle to the measuring point was higher due to less heat loss. As a result, the thermal conductivity of the large particle is higher.

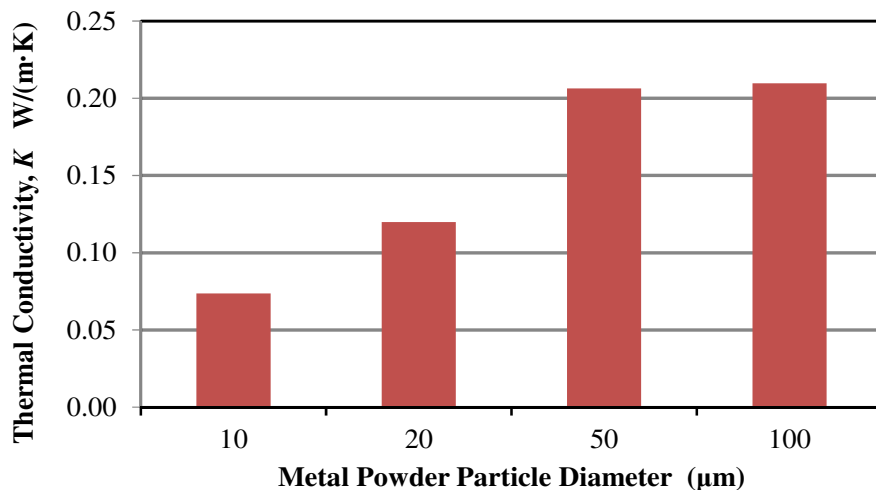


Fig. 3.5 Effect of particle diameter on thermal conductivity

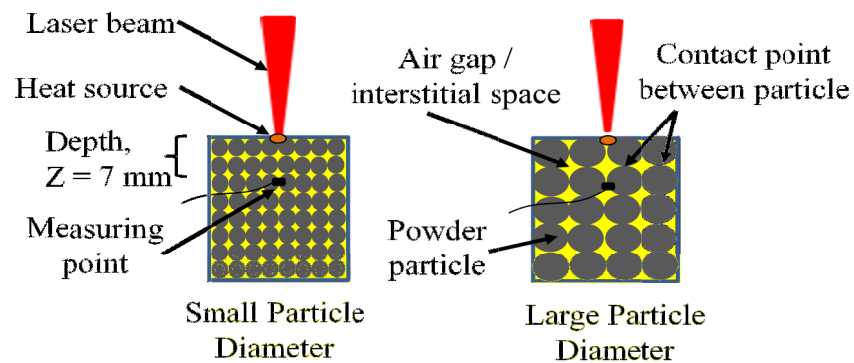


Fig. 3.6 Comparison of schematic presentation of particle arrangement

### 3.3.2 Effect of Bulk Density on Thermal Conductivity of Metal Powder

In order to investigate the effect of bulk density on thermal conductivity, the surface of the metal powder inside the cylindrical vessel was manually compressed and similar experimental setup as shown in Fig. 3.2 was repeated with different bulk density. The result in Fig. 3.7 shows the effect of bulk density of the metal powder on the thermal conductivity. The graph shows that the thermal conductivity of the metal powder is increasing with bulk density. This might be explained by referring to Fig. 3.8, which shows schematic particle arrangement of the powder particle during the experiment. When the metal powder was compressed, the air gaps among the powder particles were displaced due to external force exerted during compression. Thus, more particles can be added to the cylindrical vessel and the bulk density of the metal powder was increased. At high bulk density, contact points among the powder particles increased since more powder particles were physically in contact with their neighboring particles. Therefore, more effective heat transfer from the heat source to the thermocouple measuring point occurred. As a result, conductive heat mechanism among the powder particles was more prevalent in the higher bulk density powder.

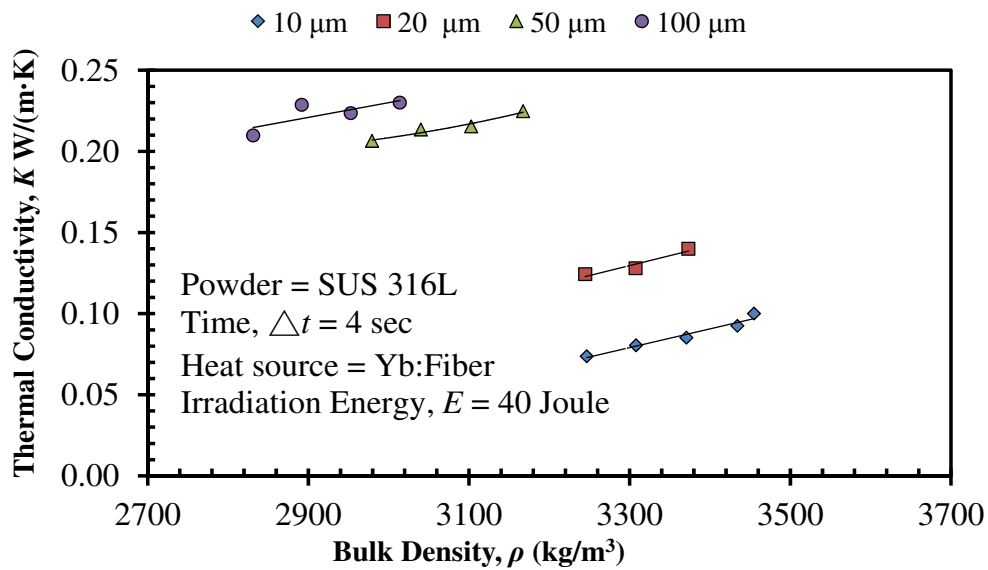


Fig. 3.7 Effect of bulk density on thermal conductivity

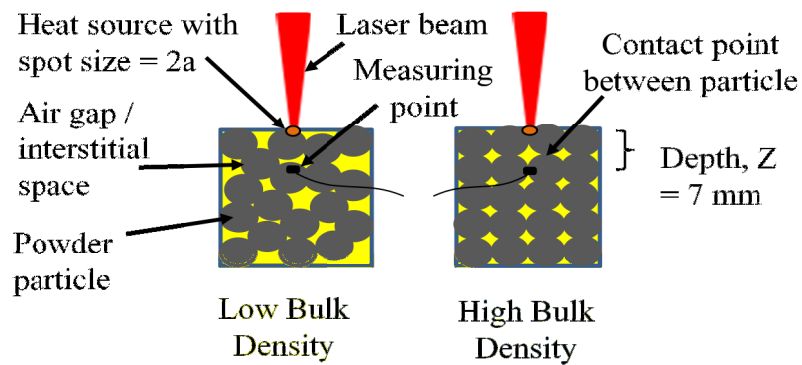


Fig. 3.8 Comparison of schematic presentation of particle arrangement in different bulk density

### 3.3.3 Effect of Porosity on Thermal Conductivity of Consolidated Structure

#### 3.3.3.1 Porosity Evaluation and Influence of Laser Processing Parameter

The consolidated materials were fabricated with the ferrous-based metal powder material using LUMEX 25C SLS/SLM system. Laser processing condition used during the experiment was set at 45  $\mu\text{m}$  hatching size, 50  $\mu\text{m}$  layer thickness and spot diameter of 0.1 mm. The laser power was varied from P=100 W to 500 W whereas the speed was increased from speed of 444 mm/s to 4000 mm/s. The surface quality of the consolidated material was examined for existence of porosity. The specimens were then sectioned using wire cut prior to porosity examination. Before the thermal conductivity measurement, both surfaces were polished with #150 grain size. Percentage of porosity on the consolidated material was analyzed using image-processing software, Scion Image as shown in Fig. 3.9. The images were captured using the Keyence VHX-1000 digital microscope. The ratio of the void area to surface at area of each specimen was determined after the images were binarized. The porosity percentage was calculated based on the following formula.

$$\text{Porosity, } \emptyset = \frac{A_C - A_{\text{Non-pore}}}{A_C} \times 100 \quad (3.4)$$

Where

$\emptyset$  = porosity

$A_C$  = area of consolidated surface

$A_{\text{Non pore}}$  = area of non-pore surface

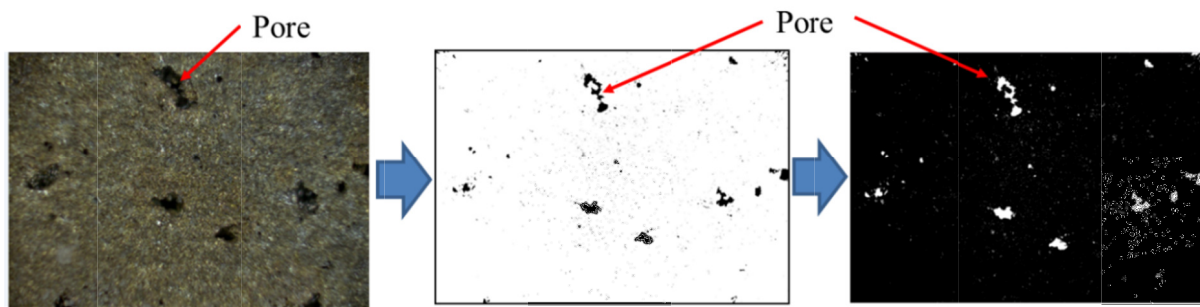


Fig. 3.9 Porosity determination using Scion Image

The influence of scan speed on the porosity was analyzed at two different laser power, 200 W and 300 W. The result is illustrated in Fig. 3.10. The result shows increasing porosity with the rise of the scan speed. Generally, less porosity was obtained when the laser power was set at 300 W compared to when the laser power was 200 W.

The laser power was also varied in order to investigate the influence of laser power on the porosity. The experiment was performed when the scan speed was set at 444 mm/s and 2000 mm/s at various laser power. The result is presented in Fig. 3.11. In contrast to the effect of scan speed, the porosity is decreasing with the increase of laser power. Comparison of the porosity at the scan speed of 444 mm/s and 2000 mm/s at various laser power indicates that the porosity was always lower when laser scan speed was 444 mm/s.

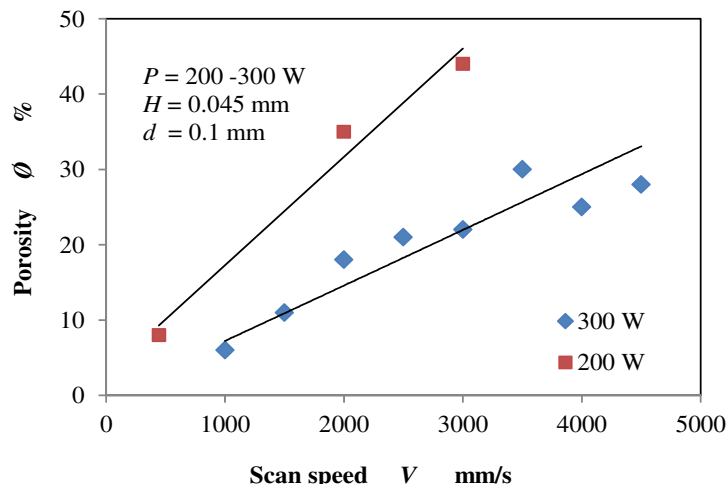


Fig. 3.10 Influence of scan speed on consolidated material porosity

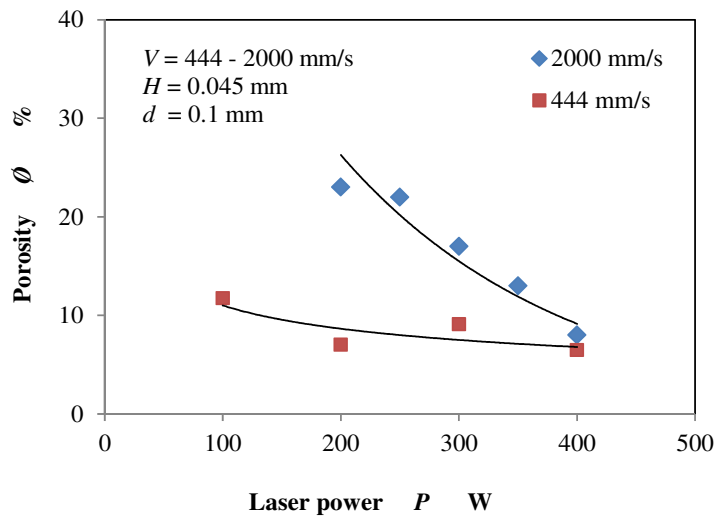


Fig. 3.11 Influence of laser power on porosity

### 3.3.3.2 Influence of Porosity on Thermal Conductivity

The influence of scan speed and laser power can be further illustrated by referring to the single parameter that relates effect of laser power ( $P$ ), scan speed ( $V$ ) and hatching size ( $H$ ) known as energy density ( $E$ ). The relation of energy density to other parameters used in

the SLS/SLM is given by Eq. 3.5 [12][13][14]. Therefore, the porosity of the consolidated material at various energy density values was determined.

$$\text{Energy density, } E = \frac{\text{Laser power}}{\text{Scan speed} \times \text{hatching size}} \quad (3.5)$$

The sectioned surface of the consolidated material with the existence of porosity at various energy density values as depicted in Fig. 3.12. The figure shows decreasing amount of porosity with the increase of energy density. Fig. 3.13 further indicates the relation of energy density on the porosity of the consolidated structure. The graph shows before energy density of 3 J/mm<sup>2</sup>, the porosity is decreasing abruptly corresponds to small change in energy density. However, after 3 J/mm<sup>2</sup>, the porosity does not decrease significantly with the increase of energy density.

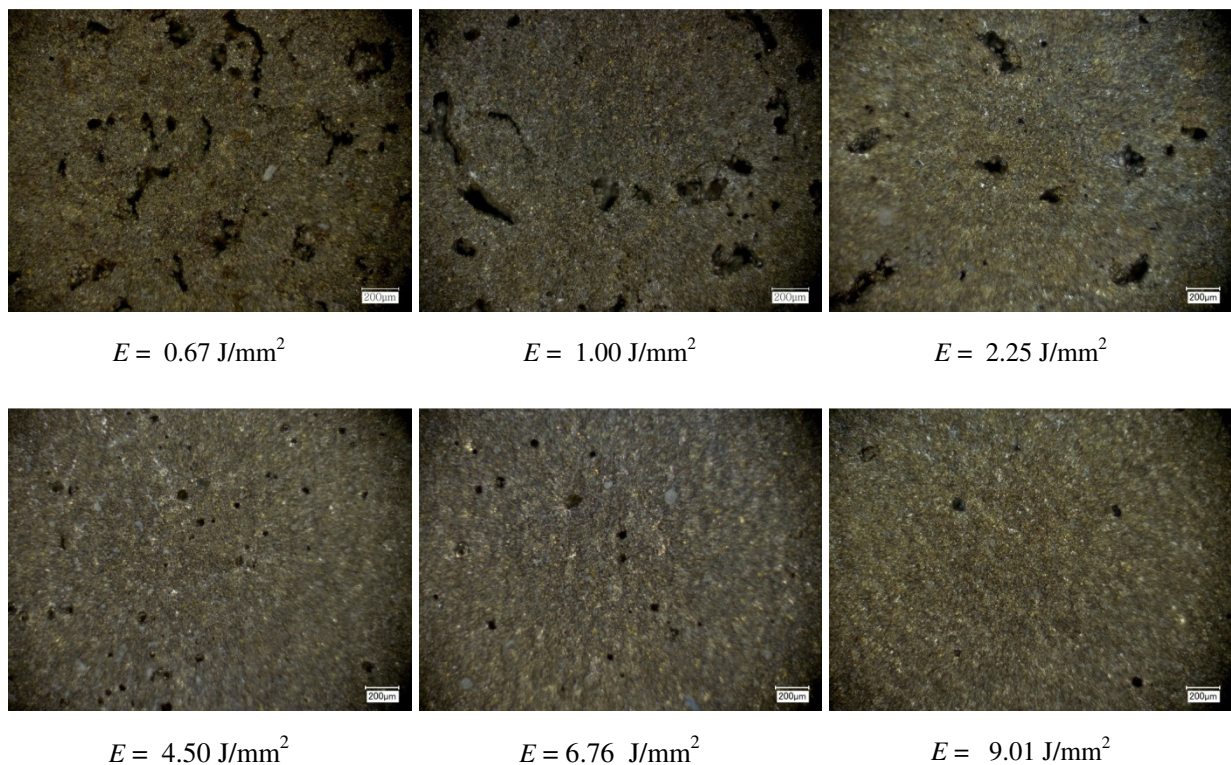


Fig. 3.12 Porosity on consolidated structure

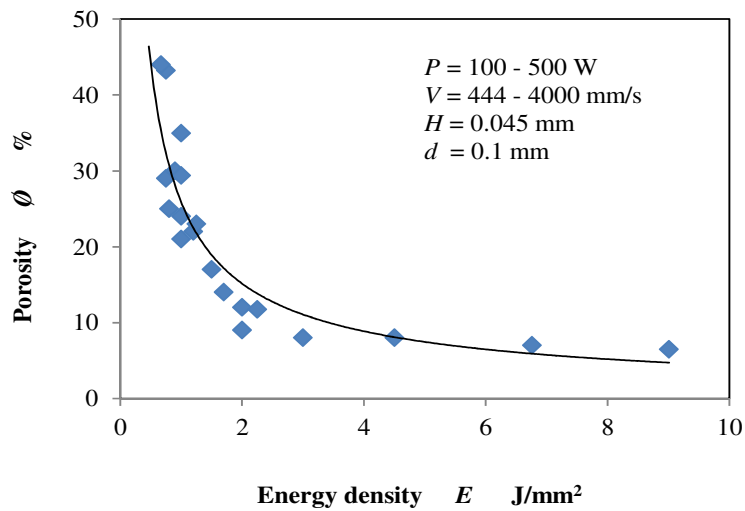


Fig. 3.13 Effect of energy density on porosity of consolidated structure

Fig. 3.14 shows the effect of percentage of the porosity on the thermal conductivity. The result indicated that the thermal conductivity was decreasing with the increase of porosity. This is due to increasing percentage of scattered pores. The pores were subjected to convective heat transfer mechanism, which reduced the overall heat transfer rate to measuring point. This is illustrated in Fig. 3.15. Average thermal conductivity of the consolidated material was compared with a previously obtained result of the metal powder and the same material in the form of solid material. The comparison is shown in Table 3.3.

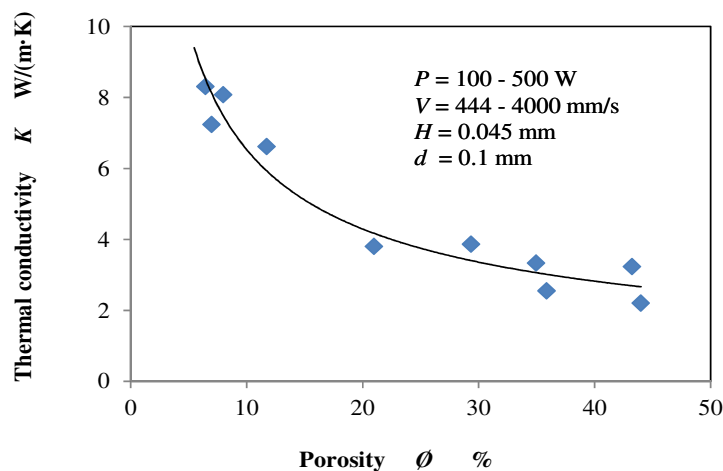


Fig. 3.14 Effect of porosity on thermal conductivity

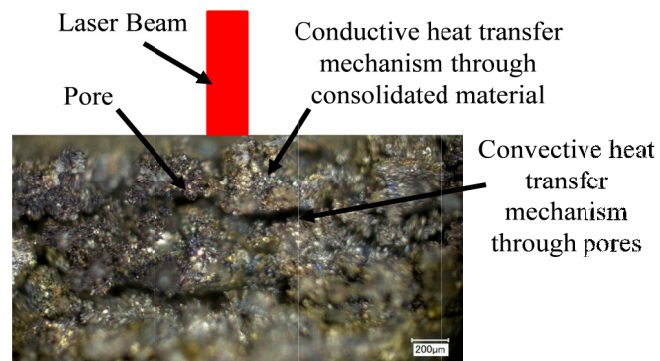


Fig. 3.15 Side view of consolidated material

Significant difference in the values of the thermal conductivity of the same type material in the different state was due to existence of the air gap and loose particle arrangement in the powder material. In the consolidated material, the structure was formed with a considerable amount of porosity. Thus, the thermal conductivity of the consolidated material was in between its corresponding material in powder and solid form.

Table 3.3 Comparison of thermal conductivity

Material	Thermal Conductivity, $K$ W/(m·K)		
	Powder, $K_{powder}$	Consolidated, $K_{consolidated}$	Solid, $K_{solid}$
Ferrous based metal mixture	0.15	2.2 to 8.3	42.60

### 3.4 CONCLUSIONS

Based on the experiment conducted, following conclusions are obtained.

1. The air gap among the metal powders particles contributed to the low thermal conductivity of metal powder. However, the thermal conductivity was increasing with the metal powder density and powder particle diameter.
2. The thermal conductivity of the consolidated material was decreasing with the increase of porosity. This was attributed to the decrease of the conductive heat transfer mechanism due to the increase of pores within the consolidated material.
3. The high difference in thermal conductivity among powder, consolidated and solid material was attributed to the distinctive heat transfer mechanism and the porosity in each material state.

### REFERENCES

- [1] A. V. Gusarov, T. Laoui, L. Froyen, and V. I. Titov, "Contact thermal conductivity of a powder bed in selective laser sintering," *Int. J. Heat Mass Transf.*, vol. 46, no. 6, pp. 1103–1109, Mar. 2003.
- [2] M. Rombouts, L. Froyen, a. V. Gusarov, E. H. Bentefour, and C. Glorieux, "Photopyroelectric measurement of thermal conductivity of metallic powders," *J. Appl. Phys.*, vol. 97, no. 2, p. 024905, 2005.
- [3] M. Rombouts and J. Kruth, "Impact of physical phenomena during selective laser melting of iron powders," in *TMS 2009 138th Annual*, 2009, vol. 1, no. figure 1, pp. 397–404.
- [4] H. Danninger, C. Gierl, M. S. Gonzalez, J. Schmidt, and E. Specht, "Thermal expansion and thermal conductivity of sintered steels," in *International Conference on Advances in Powder metallurgy & Particulate Materials*, 2010, pp. 27–30.

- [5] A. Rossencwaig and A. Gersho, "Theory of the photoacoustic effect with solids," *J. Appl. Phys.*, pp. 64–69, 1976.
- [6] I. H. Tavman, "Effective Thermal Conductivity of Granular Porous Materials," *Int. Commun. Heat Mass Transf.*, vol. 23, pp. 169–176, 1996.
- [7] N. Lockmuller, J. Redgrove, and L. Kubičár, "Measurement of thermal conductivity with the needle probe," *High Temp. - High Press.*, vol. 35/36, no. 2, pp. 127 – 138, 2003.
- [8] F.Albouchi, F.Mzali, and S.B.Nasrallah, "Measurement of the Effective Thermal Conductivity of Powders Using a Three-Layer Structure," *J. Porous Media*, vol. 10, no. 6, pp. 537–550, 2007.
- [9] T.Furumoto, T. Ueda, A. Hosokawa, S. Abe, and T. H. C. Childs, "Study on the Measurement of Physical Properties in the Metal Powder for Rapid Prototyping - Proposal of the Measurement of Thermal Conductivity," *J. Japan Soc. Precis. Eng.*, vol. 73, no. 5, pp. 558–562, 2007.
- [10] J. C. J. H.S Carslaw, *Conduction of Heat in Solids*, 2nd ed. Oxford University Press, Oxford, 1959, pp. 256–261.
- [11] Terry M. Tritt, *Thermal Conductivity: Theory, Properties, and Applications*. Kluwer Academic/Plenum Publishers, 2004.
- [12] N. Kobayashi, T. Ueda, T. Furumoto, A. Hosokawa, and R. Tanaka, "Laser Sintering Characteristics of Metallic Powder with Yb Fiber Laser - Optimization of Processing Conditions about Laser irradiation -," in *Proceedings of International Conference on Leading Edge Manufacturing in 21st century : LEM21 2009 The Japan Society of Mechanical Engineers*, 2009, vol. 2009, no. 5, pp. 593–596.
- [13] S. Abe, Y. Higashi, H. Togeyama, I. Fuwa, and N. Yoshida, "Development of milling-combined laser metal sintering method," *Japan Soc. Precis. Eng.*, vol. 73, no. 8, pp. 912–916, 2007.
- [14] K. Maeda and T. H. . Childs, "Laser sintering (SLS) of hard metal powders for abrasion resistant coatings," *J. Mater. Process. Technol.*, vol. 149, no. 1–3, pp. 609–615, Jun. 2004.

## **CHAPTER 4 : TEMPERATURE DURING CONSOLIDATION PROCESS**

### **4.1 INTRODUCTION**

SLS/SLM involves a layer by layer sintering/melting of metal powder until a complete 3D part is finally fabricated. This involves continuous heating and solidification during its processing. Therefore, temperature behavior is crucial in developing a good consolidated structure. In the SLS/SLM processing, powder metals are sintered/melted and then solidified to form a solid metals part. Usually the metal powder within the range of 20 to 100 micron thickness of is deposited on each layer. Then, the laser is irradiated line by line to the metal powder successively until final part is produced. Since SLS/SLM involves the consolidation of metal powder to be solid under influence of high-energy density from laser source, it is a paramount to investigate how the consolidation process occurs. The process is very much influenced by the amount of heat supplied to the small and localized sintering/melting region. Hence, information on temperature is very useful in understanding the thermal behavior during processing for developing a better part quality.

Consolidation of metal powder is a complex process as there are continuous heating and solidification of metal powder within a very short period. Hence, understanding temperature evolution and behavior in the SLS/SLM has a significant effect on the final quality. Furthermore, temperature measurement enhances better understanding of the

interaction between the laser beam and powder bed [1]. Nevertheless, only few studies were carried out to monitor SLM process [2]. Among the studies that investigated thermal behavior during SLS/SLM as reported from [2] to [16]. Bayle et al. used pyrometer and infrared camera to monitor SLM process on 50 W laser system[2]. Temperature evolution in relation to the brightness temperature and information at higher spatial and temporal resolution was reported. Furumoto et al. utilized two-color pyrometer to measure temperature at laser irradiation area [3],[4]. The author recently has correlated the temperature measurement made to observation made using high speed camera and the consolidation characteristics [5].

Chivel and Smurov developed an optical system and integrate with industrial SLS/SLM machine [6]. The system facilitates monitoring spatial distribution of brightness temperature. They later monitored temperature and overhang the problems [7]. Chivel further the investigation by using pyrometer and CCD camera to control the overhang layers and 3D object melting [8]. Craegh et al. successfully developed a feedback control and monitoring system. The system facilitates the melt pool observation during consolidation process [9][10]. Pavlov et al. reported on interesting research on pyrometric analysis of the thermal process in SLM using 50 W fiber laser [11]. However, the result presented at that time only in arbitrary unit due to calibration complexity. Hence, the actual temperature is unknown. Approximately similar setup with further comprehensive pyrometric analysis was reported by Doubenskaia et al. [12]. Other than that, Islam et al. reported process characteristics of powder bed fusion by comparing measured temperatures and on-line photography [13].

Based on the current research, most of the studies reported temperature measurement at laser power below 200 W. This indicates that there is only limited data on temperature measurement during AM. This is due to difficulty to get accurate measurement of high temperature during SLS/SLM. This is because the small size of laser irradiation point.

Furthermore, the powder consolidation is located within confined and closed processing area. Therefore, this study reports on temperature measurement using the industrial standard AM system at laser power range from 10 W to 500 W. Temperature measurement was performed using the two-color pyrometer system. The pyrometer system was theoretically developed and experimentally verified in previous research [14][15]. The variation of the pyrometer system utilizing different detectors and configuration were previously developed. The pyrometer has been used in various material processing applications. Some of these applications are in grinding [15], turning [16],[17],[18], laser forming [19], milling [20].

Recently, the temperature measurement using the developed pyrometer at low laser power of  $P=40$  W was reported in analyzing line consolidation [3],[4],[5]. However, in industrial application, high laser power over the range of several hundred watts is commonly used. This is to ensure successful development of 3D part directly from metal powder [21]. In this experiment, the temperature analysis was made under various processing conditions in order to investigate the effect of processing conditions on temperature. Based on the result, the consolidation behavior of the metal powder with emphasis on temperature evolution that occurred during SLS/SLM of the consolidated material is investigated.

## **4.2 METHODOLOGY**

### **4.2.1 Pyrometer System Configuration**

The schematic of basic structure of the two-color pyrometer used in the experiment is as illustrated in Fig. 4.1. The technique integrates chalcogenide optical fiber, condenser lens,

germanium (Ge) filter and detectors. The optical fiber is used to transmit signal from target area to the detectors. The two infrared detectors were used for detecting different spectral of wavelength.

The infrared ray emitted during consolidation of metal powder within target area was captured by chalcogenide fiber. The energy was converted to the electric signal after being amplified. The electrical signal, which is the voltage output, was recorded using Yokogawa DL750 oscilloscope. In order to avoid the effect of emissivity, the ratio between InAs and InSb was used in determining the consolidation temperature. The influence of emissivity occurred on the consolidated surface is negligible when the ratio of output signal is used in the measurement [22]. The ratio between the voltage outputs from the detectors can be correlated to the temperature during consolidation with the reference to the calibration curve.

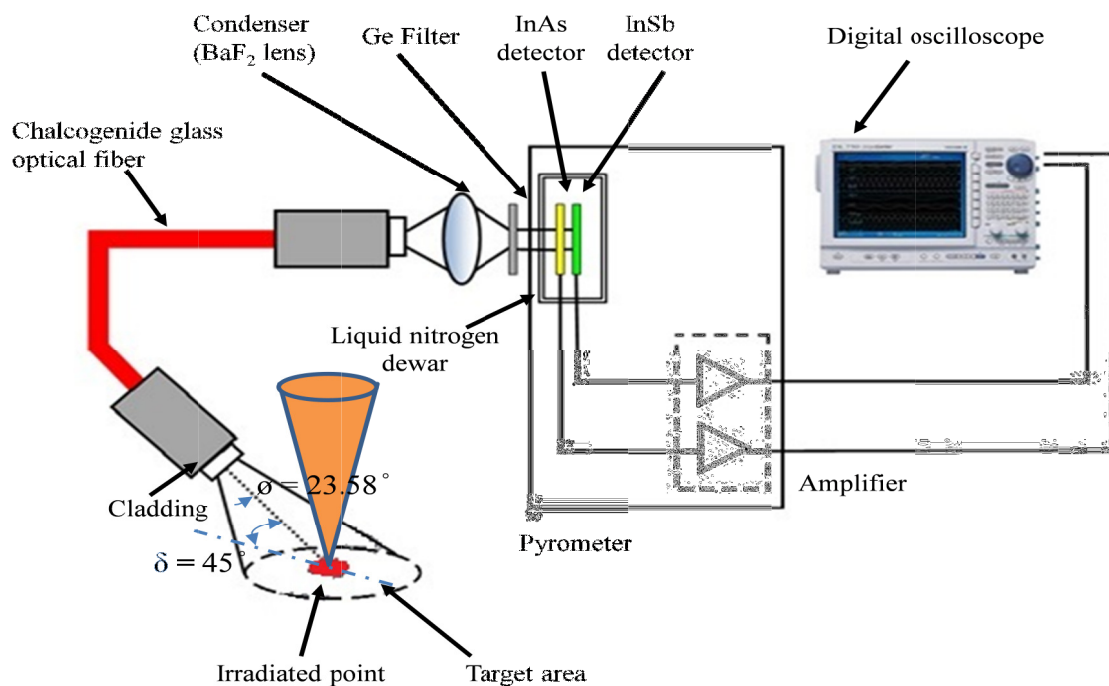


Fig. 4.1 Structure of two-color pyrometer

The chalcogenide optical fiber used in the experiment is a 380  $\mu\text{m}$  diameter. The spectral transmittance of chalcogenide fiber is illustrated in Fig. 4.2. The figure shows that the fiber able to transmit wavelength from 1  $\mu\text{m}$  to 6.6  $\mu\text{m}$ . The detail of the fiber characteristic is tabulated in Table 4.1. Before the signal transmitted to the detectors, the signal was condensed by  $\text{BaF}_2$  condenser lens. Fig. 4.3 illustrates the spectral transmittance of the condenser lens between 0.1  $\mu\text{m}$  to 20  $\mu\text{m}$ . The figure shows the condenser len has constant transmittance between 0.5  $\mu\text{m}$  to 14  $\mu\text{m}$ .

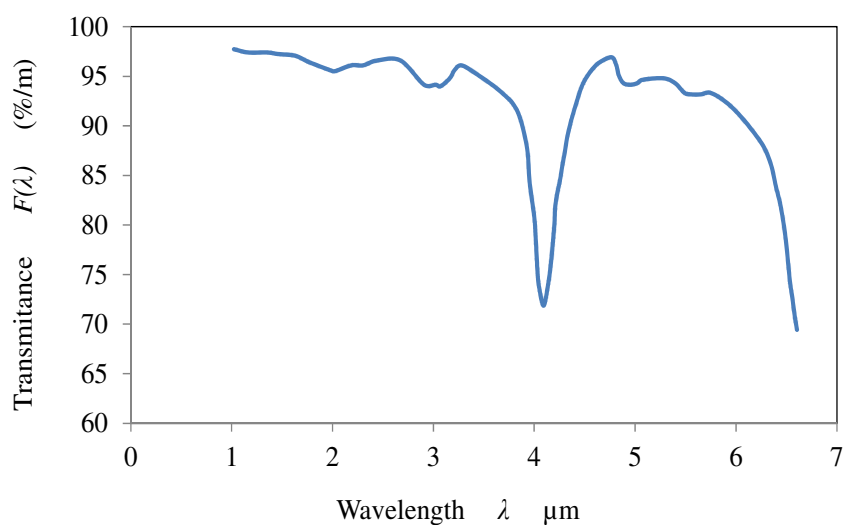


Fig. 4.2 Spectral transmittance of chalcogenide glass fiber

Table 4.1 Specifications of chalcogenide glass fiber

Core diameter [ $\mu\text{m}$ ]	$d_c$	380
Numerical aperture	$NA$	0.4
Refractive index distribution		Step type
Acceptance angle [degree]	$\xi_m$	$23.58^\circ$
Transmission wavelength range [ $\mu\text{m}$ ]		1 to 6.6

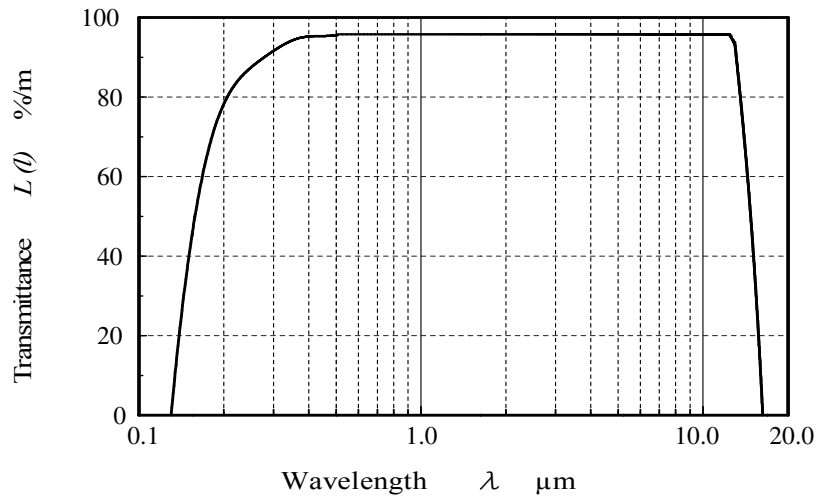


Fig. 4.3 Spectral transmittance of BaF<sub>2</sub> condenser lens

Other than that, Germanium (Ge) filter was added to the pyrometer configuration. This is to ensure the laser beam was not detected by the InAs and InSb detector. This also protected the pyrometer system from laser irradiation [3],[23]. The spectral transmittance of Ge is shown in Fig. 4.4. Since Ge cut off all wavelengths below 1.60 μm, the filter able to cut the wavelength of the Yb: fiber laser which was 1.07 μm. As a result, the pyrometer system was not affected by the radiation from the laser beam.

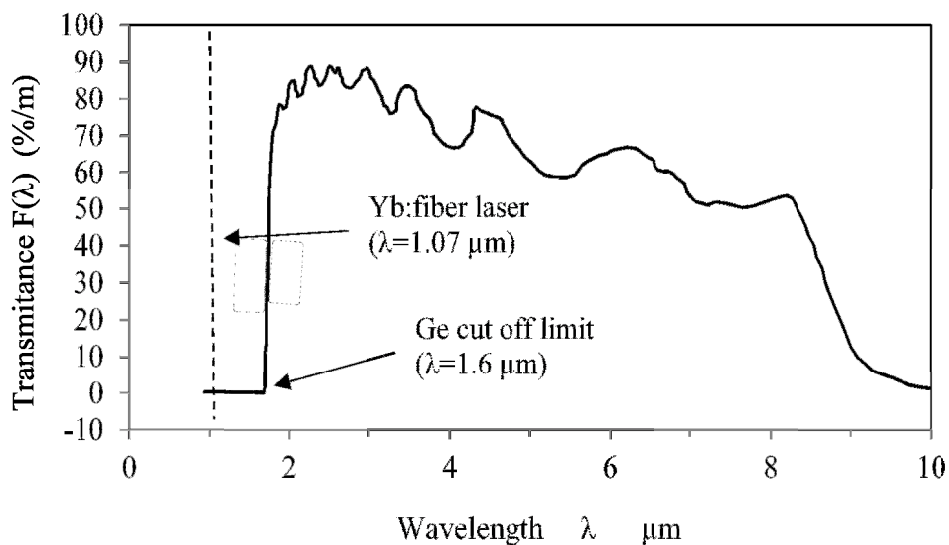


Fig. 4.4 Spectral transmittance of germanium filter

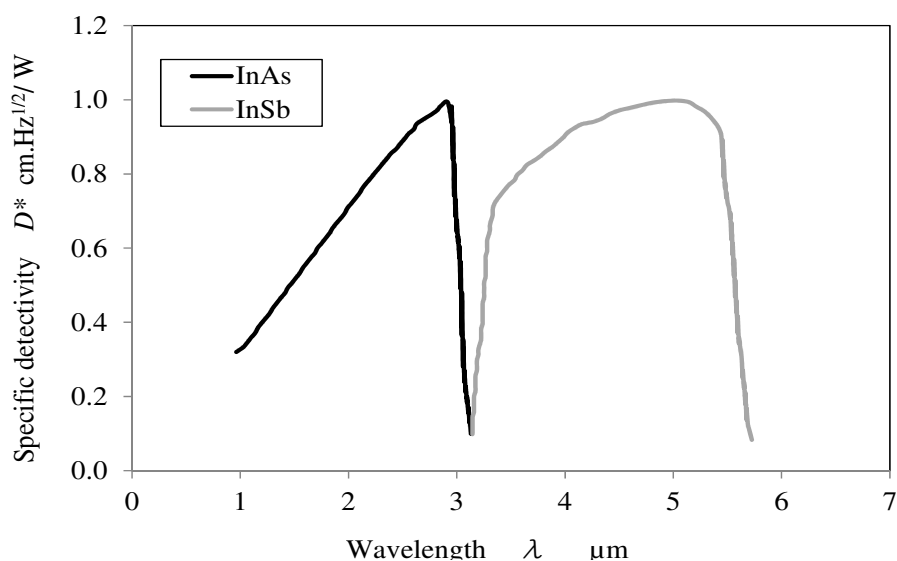


Fig. 4.5 Spectral transmittance of detectors

The infrared detectors used in the experiment were Indium Arsenide (InAs) and Indium Antimonide (InSb). The detectors were mounted in sandwich configuration to cater different range of acceptable wavelengths. InAs was used to detect radiation range from 1  $\mu\text{m}$  to 3  $\mu\text{m}$ . Whereas, InSb captured radiation from 3  $\mu\text{m}$  to 5.5  $\mu\text{m}$ . The spectral transmittance of the detectors is shown in Fig. 4.5. In order to achieve high sensitivity of the detectors, the detectors were kept at 77 K using liquid nitrogen.

Configuration and selection of the fiber, condenser, filter and detectors used for the pyrometer allows signal captured by the chalcogenide fiber to be transmitted effectively from target area to the detectors. This was because the chalcogenide fiber with transmission wavelength from 1 to 6  $\mu\text{m}$  was condensed by  $\text{BaF}_2$  that has constant permeability from 0.5 to 14  $\mu\text{m}$ . The signal was then detected by InAs and InSb at the range of 1 to 3  $\mu\text{m}$  and 3 to 5.5  $\mu\text{m}$  respectively. With the sampling time of 1  $\mu\text{s}$  used in the experiment, the pyrometer is fast enough to capture the signal that converted to the electrical signal.

Theoretically, the pyrometer able to receive the total energy radiated from the surface of the target area. The assumption made in this theoretical calculation was the object has a

blackbody surface at the uniform temperatures with no losses to the surroundings. The calculation was determined based on relative sensitivity of the pyrometer. Then, the calibration curve was verified experimentally and compared to theoretical curve where the values were calculated based on the following formula.

$$\Lambda_{InAs/InSb} = \frac{\Lambda_{InAs}}{\Lambda_{InSb}} = \frac{\int_{\lambda_1}^{\lambda_2} \omega_1 \varepsilon_1(\lambda, T) E_{b\lambda}(\lambda, T) F(\lambda) L(\lambda) G(\lambda) D_{InAs}(\lambda) d\lambda}{\int_{\lambda_1}^{\lambda_2} \omega_2 \varepsilon_2(\lambda, T) E_{b\lambda}(\lambda, T) F(\lambda) L(\lambda) G(\lambda) D_{InSb}(\lambda) d\lambda} \quad (6.1)$$

where,  $\varepsilon_1(\lambda, T)$  and  $\varepsilon_2(\lambda, T)$  are emissivity of the object,  $w_1, w_2$  are constant,  $F(\lambda)$  is spectral transmittance of optical fiber,  $L(\lambda)$  is spectral transmittance of condenser,  $D_{InAs}(\lambda)$ ,  $D_{InSb}(\lambda)$  is spectral transmittance of detector cell and  $G(\lambda)$  is spectral transmittance of filter.

### 4.2.2 Pyrometer Calibration

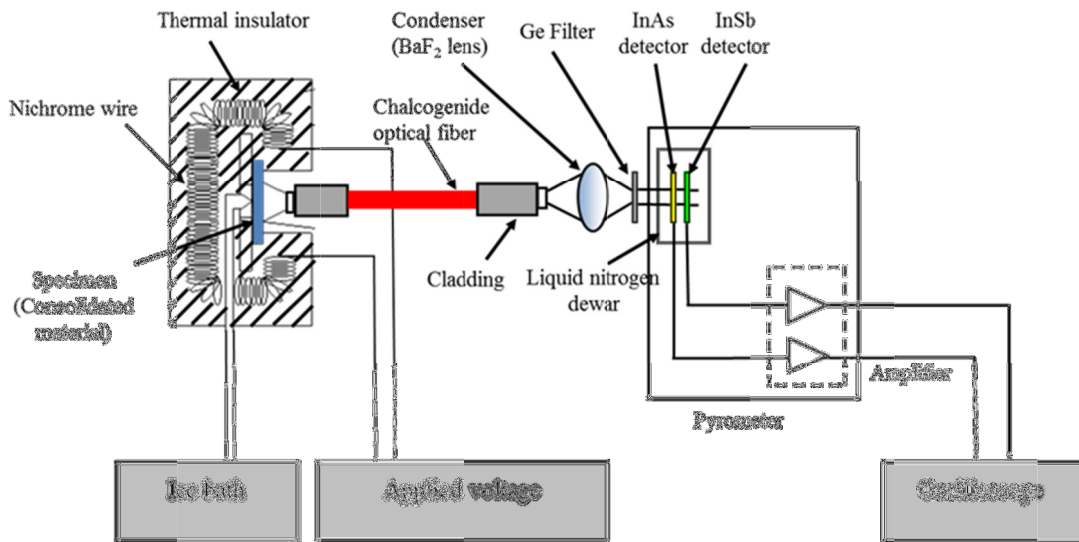


Fig. 4.6 Schematic structure of pyrometer calibration

In order to correlate voltage ratio to any temperature values, calibration of the consolidated material temperature with respect to the voltage ratio of the detectors is essential. Fig. 4.6 depicts the schematic structure of pyrometer calibration. However, temperature in the SLS/SLM relatively high causing common calibration method using a thermocouple is not sufficient. Therefore, two calibration methods were used to cater calibration at the different range of temperature. Two methods were used for calibration purpose that is for temperature below 800°C and above 800°C.

The first calibration method was made for temperature range below 800°C. This was performed using a thermocouple with the consolidated material as the specimen. The material was polished before calibration preparation. The surface roughness was measured at  $R_a = 0.0882 \mu\text{m}$ . Typical signal output captured through the oscilloscope is shown in Fig. 4.7. The upper signal was InAs signal and the bottom signal is the InSb signal. The temperature was plotted with respect to the output signal. Comparison between the theoretical and experimental value is presented in Fig. 4.8. A relatively good result was obtained between the data.

The second method based on surface melting of work material as laser was irradiated on the surface. In this method, laser power was increased incrementally and the ratio at melting started was used as reference for calibration of the pyrometer. Five different materials were used as the specimen in the surface melting calibration of the pyrometer. These materials are titanium, chromium molybdenum steel alloy (SCM440), silicon carbide (SiC), low carbon steel and stainless steel (SUS316L). Specification of these materials as tabulated in the Table 4.2.

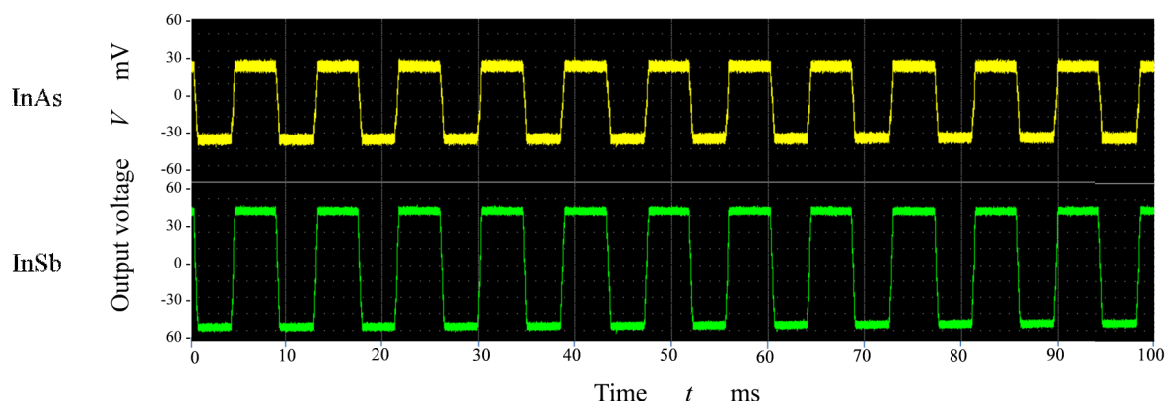


Fig. 4.7 Typical oscilloscope signal output

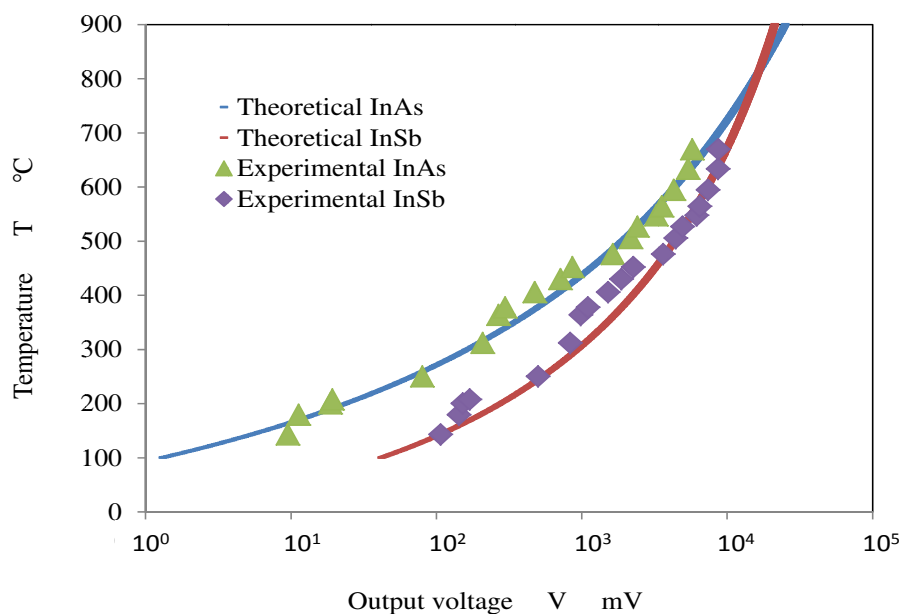
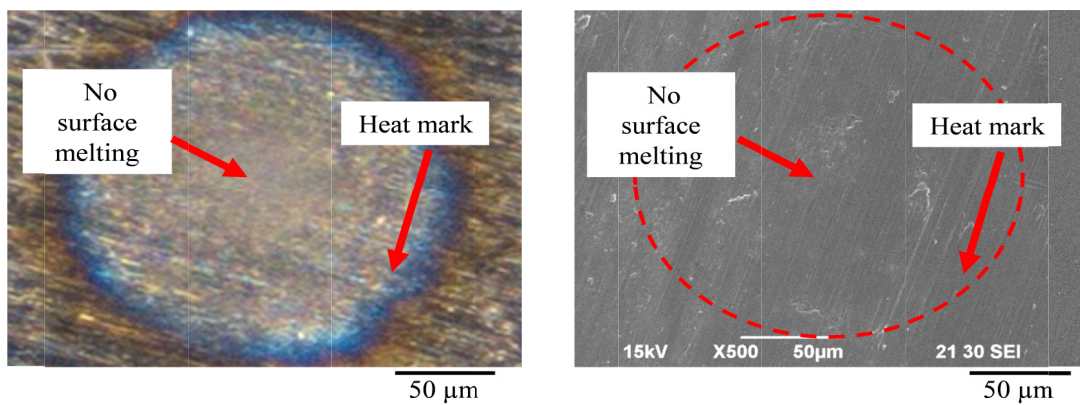


Fig. 4.8 Relation of output voltage with temperature

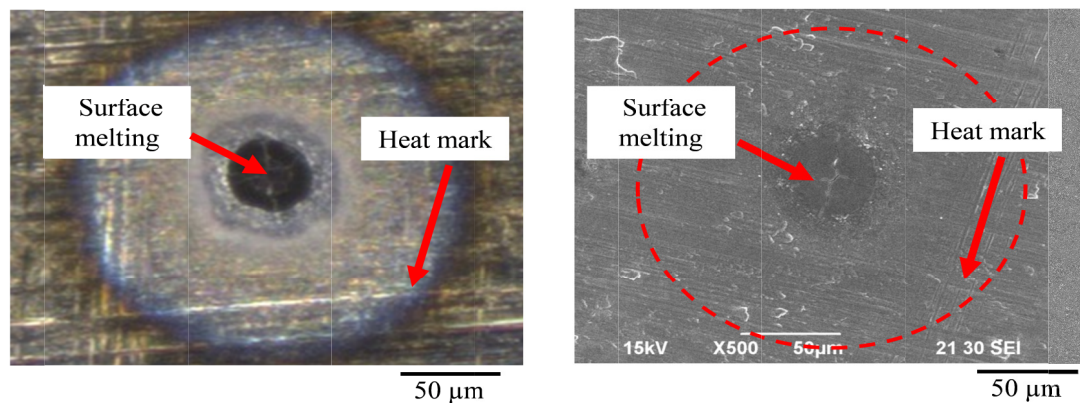
The change on the titanium surface after the laser was irradiated is depicted Fig. 4.9. The SEM image shows the difference between surface structure before melting and after melting. Thermal damage was formed when heat was irradiated on the surface causing a ring-shaped heat mark. With the increase of laser power, sufficient heat caused the surfaces started to melt. This has changed the structures at their respective melting temperature. The ratio of InAs and InSb at these points were calculated and plotted in the calibration curve as shown in Fig. 4.10.

Table 4.2 Melting temperature of materials used in surface melting calibration

No	Material	Melting Temperature (°C)	Reference
1	SUS316L	1375 - 1450	[24]
2	JIS SCM440 (ANSI 4140)	1416 - 1510	[25], [26]
3	Low carbon steel	1480 - 1526	[24]
4	Titanium	1650 - 1670	[27]
5	Silicon carbide	2200	[28]



(a) No surface melting observed using optical microscope and SEM



(b) Surface melting observed using optical microscope and SEM

Fig. 4.9 Changes in the titanium surface as laser is irradiated on surface

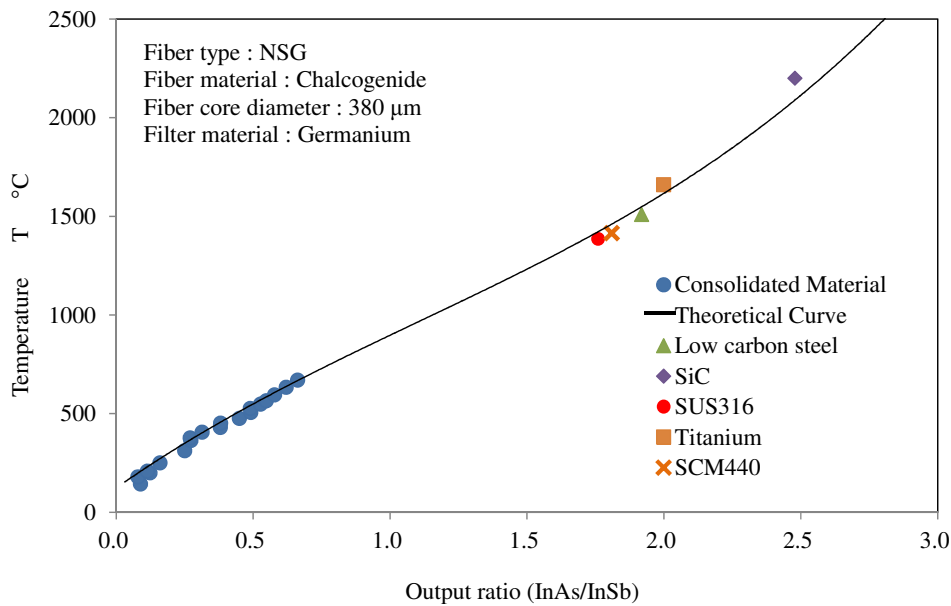


Fig. 4.10 Voltage ratio and temperature calibration curve

The output ratio of InAs to InSb when the minimum laser required to melt the specimen was recorded and used as a reference to the calibration curve. The result obtained from the calibration is illustrated in Fig. 4.10. The figure shows the relationship of the voltage output ratio to the temperature. The line denotes the theoretical curve, which can be calculated based on the sensitivity of various material and parts used in the developed pyrometer system. On the other hand, the points indicate the experimental results. It can be observed that the points approximately fit to theoretical curve. Therefore, throughout the experiment, conversion of ratio output to temperature was made using this calibration curve.

### 4.3 EXPERIMENTAL SETUP

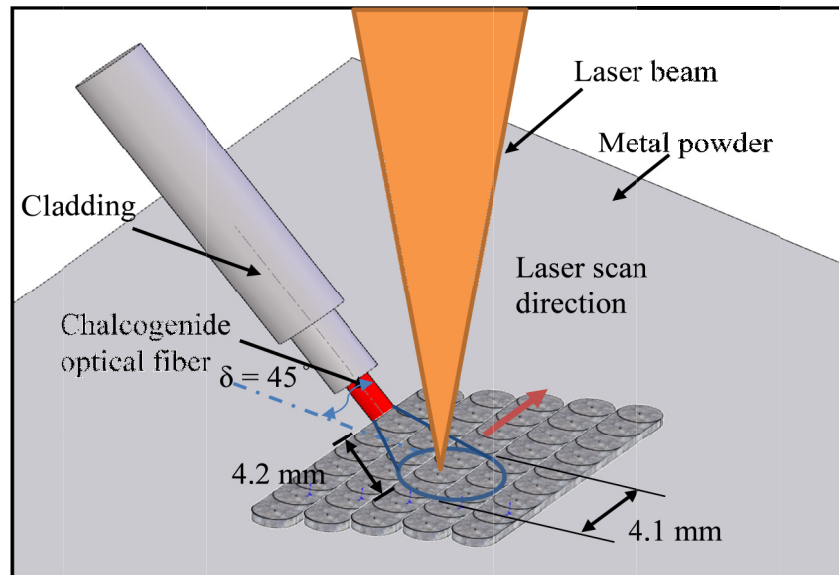


Fig. 4.11 Experimental setup

Schematic of experimental setup is shown in Fig. 4.11. The temperature measurement of the area consolidation was performed on AM facility manufactured by Matsuura Machinery Corporation (Japan) Model 25C. The laser used in the study is Yb: fiber laser. The chalcogenide optical fiber was placed at 45 degrees from the substrate surface. The distance between the optical fiber to consolidated line structure was set at 4 mm. The core diameter of chalcogenide optical fiber was 380  $\mu\text{m}$  with acceptance of 23.58 degree. Experimental condition used is tabulated in Table 4.3.

In the SLS/SLM, metal powder on the same layer is irradiated line-by-line. Repetitive and successive line-by-line consolidations at equal hatching distance formed area consolidation. Temperature measurement of the line consolidation was reported in previous research [3][4]. It is important to note that within the area consolidation, the characteristics of the line consolidation during were also observed. This is because the nature of consecutive

line irradiation in the SLS/SLM. The differences of the line consolidation and the area consolidation is defined and illustrated in the Fig. 4.12 below. The line consolidation refers to a single-track structure that formed a straight line after the metal powder was irradiated by the laser beam. Whereas the area consolidation refers to the successive laser irradiation of the line consolidation at the specified distance known as the hatching size.

Table 4.3 Experimental conditions

Laser type		Yb:fiber
Power [W]	$P$	100 - 500
Scan speed [mm/s]	$V$	444 - 2222
Beam diameter [mm]	$d$	0.1
Scan length [mm]	$J$	10
Hatching size [mm]	$H$	0.045

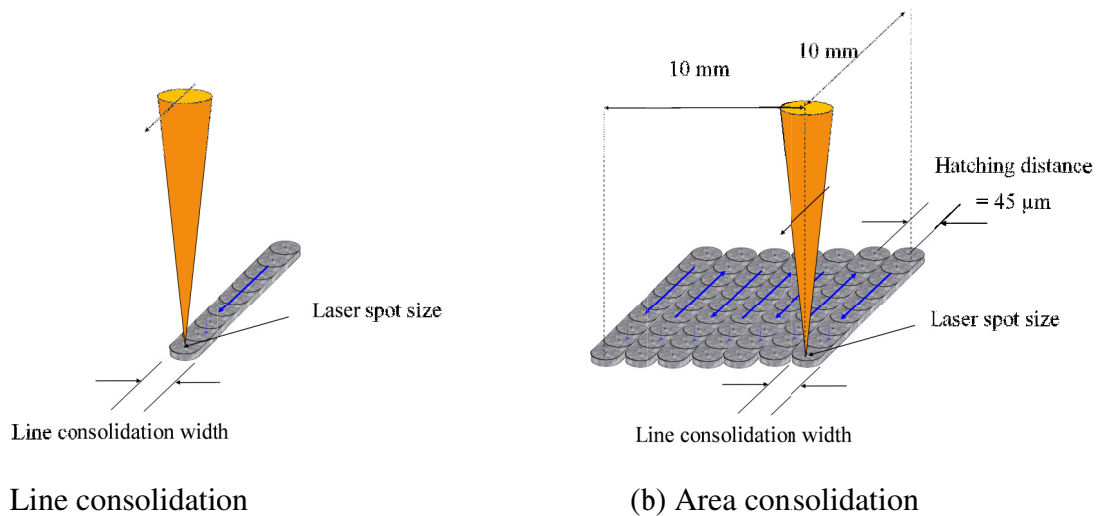


Fig. 4.12 Line consolidation and area consolidation in the SLS/SLM

## 4.4 EXPERIMENTAL RESULTS AND DISCUSSION

### 4.4.1 Pyrometer Signal Profile and Temperature Behavior

Fig. 4.13 shows typical pyrometer signal as a function of time. This was recorded during temperature measurement when the laser power  $P = 200$  W and scan speed  $V = 444$  mm/s. Fig. 4.13(a) shows signal received by the two detectors of the pyrometer over the time. The profile is a fluctuating wave that increases and decreases back. This corresponds to the relative distance of the laser irradiation location to the centerline of target area, X-X and Y-Y. The profile of the temperature shown in Fig. 4.13 can be explained in further detail by referring to the schematic figure shown in Fig. 4.14.

During the temperature measurement, the target area for temperature measurement was fixed and the laser beam was scanned using a galvanometer. Initially, when the laser beam movement was on line the consolidation of  $L_0$ , the laser beam was not irradiated inside the target area. As a result, there was no signal measured by the pyrometer. Successive adjacent line consolidation  $L_{0+1}$  was still not detected because of the same reason. However, when the laser beam passed the border during line consolidation,  $L_s$ , the pyrometer started to detect relatively low infrared energy. This was because line consolidation,  $L_s$  was inside of target area of temperature measurement. Low infrared energy was due to far distance from the center of target area. The energy was then converted to electrical signal. Relatively low infrared energy detected at far distance from the centerline X-X but still inside the target area resulted in low electrical signal. The signal when the laser beam approaching the centerline is shown in Fig. 4.13 and indicated by  $A_s$  and  $B_s$  for InAs and InSb output signal respectively. Whereas its respective location of the line consolidation,  $L_s$  is shown in Fig. 4.14. Later, line-



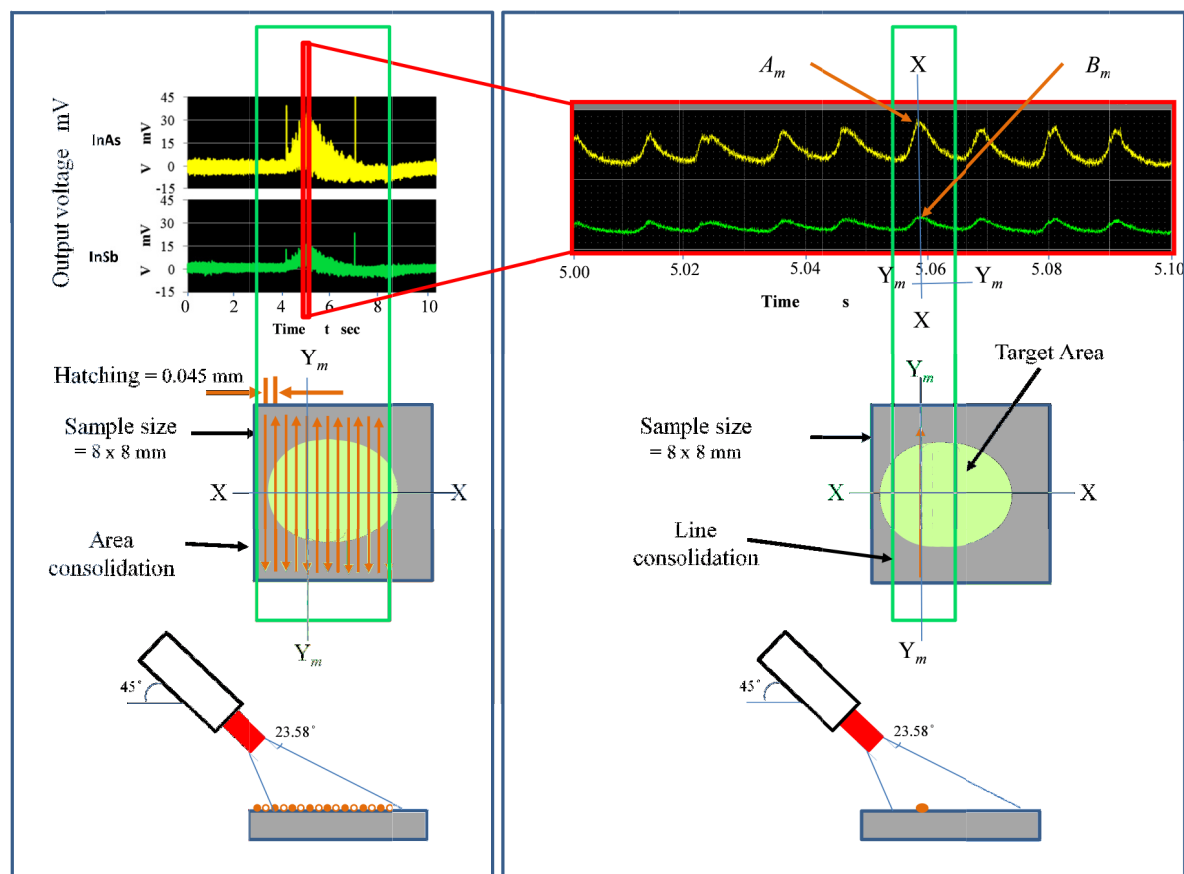
When the laser beam moved along the axis  $Y_m$ - $Y_m$  towards centerline X-X, line consolidation of  $L_m$  was produced. This resulted in an increased of output voltage signals. The signals were maximum as the laser beam reached the centerline X-X. Similarly, these signal decreased abruptly as soon as the laser beam passed the centerline. The position on the signal curve is denoted as  $A_m$  for InAs output and  $B_m$  for InSb output. During laser beam movement along the line consolidation  $L_m$ , maximum InAs and InSb output was recorded. This is due to the shortest distance between the chalcogenide fiber and the target area.

Next, line irradiation on subsequent line consolidation,  $L_{m+1}$  was performed in opposite direction. When the laser beam approached the centerline X-X, similar phenomenon was observed. Again, the signal increased and achieved its maximum voltage as the laser beam reached the centerline X-X. Successive line consolidation followed the same temperature profile when the laser beam approached the centerline. This process was repetitive until line consolidation  $L_e$ . As a result, area consolidation was formed. Similarly, maximum signal was recorded when the laser beam was approaching the centerline. However, due to the position of the chalcogenide fiber was further than previously consolidated line, the maximum signal recorded was decreasing with similar temperature profile.

Therefore, based on experiment, it can be generalized that the signal was not detected when the laser beam was not inside the target area. Once the laser irradiation is inside the target area, the signal was increasing as the laser beam approaching the centerline X-X. The signal decreased back as the laser beam and moved away from the centerline X-X decreased. This is due to cooling of the consolidated structure. Changes in voltage values were captured through radiation by the chalcogenide optical fiber. As the laser beam approached the centerline X-X from  $Y_m$ - $Y_m$  line, maximum voltage recorded due to the shortest distance.

This distance is denoted by  $D_m$  in the figure. The recorded InAs and InSb signal showed a relatively same profile at proportionate voltage value between the captured signals.

Detail explanation on behavior of temperature profile is further illustrated in the 2D image as shown in Fig. 4.15. The behavior simultaneously represents the line consolidation and the area consolidation recorded during the experiment. It is important to note the target area was relatively large compared to the laser beam diameter. Hence, the profile obtained in the Fig. 4.15(a) is actually presenting an area consolidation whereas the Fig. 4.15(b) is presenting each line consolidation at 0.045 mm hatching.



(a) Area consolidation

(b) Line consolidation

Fig. 4.15 Comparison between area consolidation and line consolidation during SLS/SLM

## 4.4.2 Effect of Process Parameters on Temperature

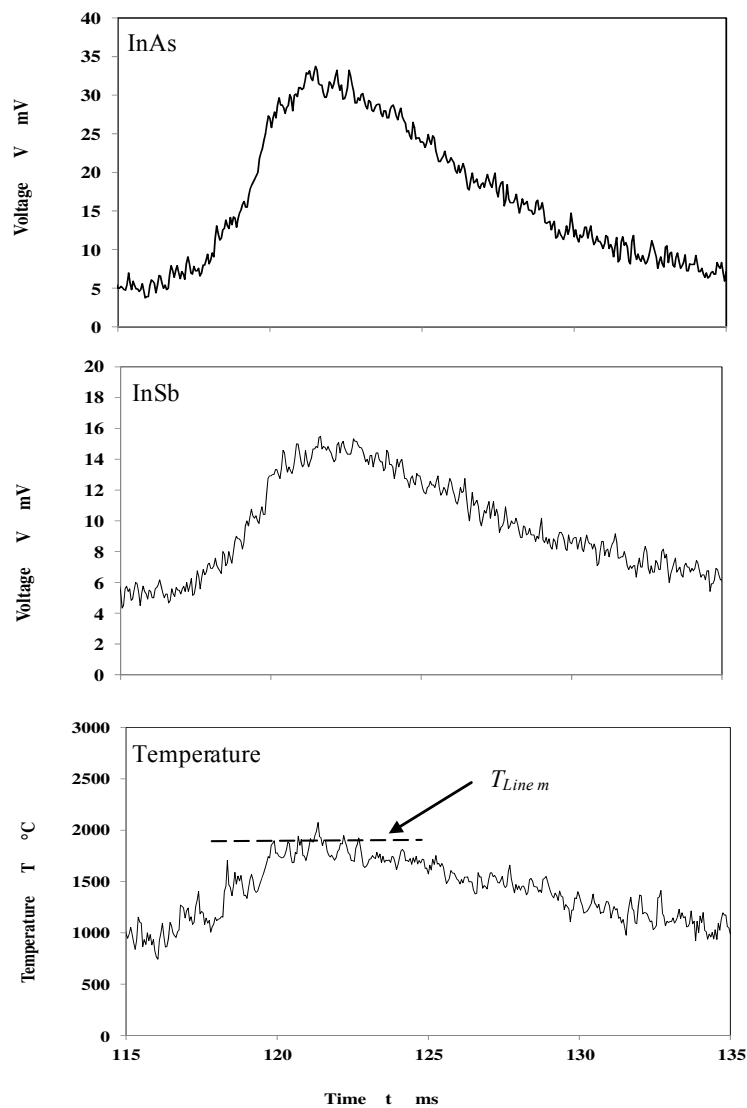


Fig. 4.16 Pyrometer output and temperature profile during line consolidation of  $L_m$

Consolidation temperature can be determined by calculating the ratio of the InAs to InSb recorded output signal. Later, the corresponding temperature value was deduced with respect to calibration curve. In order to observe the signal in detail, the figure only concentrates on one of the repeating curves from area consolidation. The curve is selected based on the curve that shows maximum InAs and InSb output signal, which is line consolidation  $L_m$ . Fig. 4.16 shows the pyrometer output and temperature profile during line consolidation  $L_m$ . The figure

indicates InAs and InSb signal and its corresponding temperature with the function of time. The values of recorded signal were fluctuating over the time. For each time interval, determination of temperature was made by taking the ratio of InAs to InSb and then was correlated to the calibration curve. The profile shows an increasing value until it reached saturated value and started decreasing back. The profile was obtained due to the laser beam approached the centerline X-X. Hence, this resulted in increased in the signals. These signals recorded maximum value as the laser beam reached the centerline X-X. After that, the signal decreased abruptly due to movement of the laser beam away from the center. Small noise and fluctuation in the recorded values were contributed by metal movement and metal powder splattering. Determination of the line consolidation  $L_m$  temperature,  $T_{line\ m}$  is based on saturated value before the temperature started to drop back as shown in Fig. 4.16.

In order to measure the temperature profile of area consolidation, repetitive profile of each line consolidation was analyzed using the same procedure. Since within area consolidation there is successive line consolidation, the average temperature of five lines consolidation before line consolidation  $L_m$  was calculated. Therefore, generally maximum temperature of the area consolidation in this experiment was determined based on the following expression. The figure that illustrates the expression is shown in Fig. 4.17.

$$\text{Temperature of area consolidation, } T_{area} = \frac{\sum_{i=L_{m-4}}^{i=L_m} T_{line\ i}}{5} \quad (6.2)$$

if

$$i = L_{m-4}, L_{m-3}, L_{m-2}, L_{m-1}, L_m$$

where

$L$  = line consolidation number during area consolidation

$L_m$  = line consolidation number that has highest output signal detected by pyrometer during area consolidation

$T_{area}$  = temperature of area consolidation

$T_{line\ i}$  = temperature of line consolidation at during line consolidation number  $i$

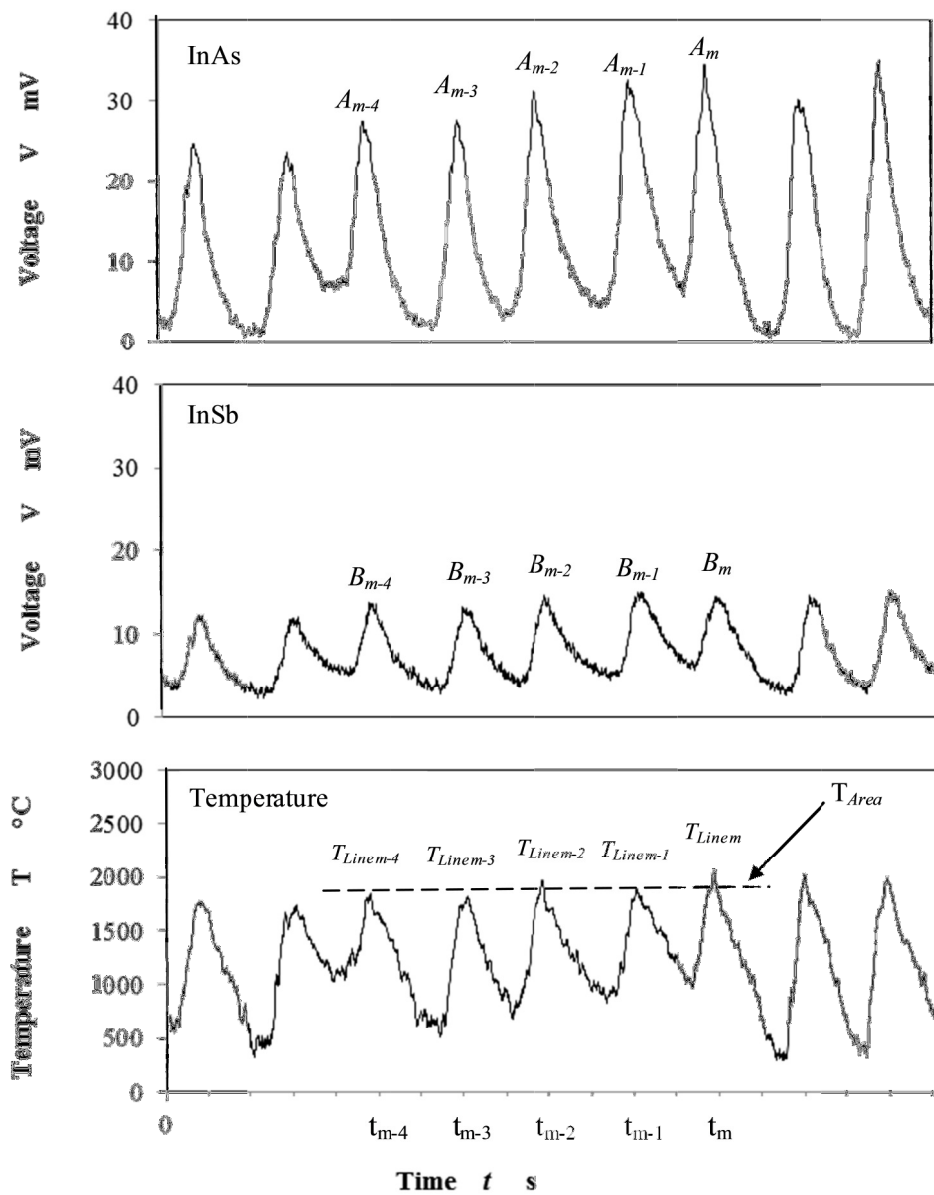


Fig. 4.17 Pyrometer output and temperature profile during area consolidation

It can be seen from the figure that the signal output of InAs and InSb varies based the position from the centerline. Nevertheless, the maximum temperature,  $T_{area}$  was almost constant at approximately 1800 °C. Laser beam that is moving in opposite direction alternately did not affect the temperature result. This is because in both conditions, the laser approached and moved away from the target area. This has produced an increased and decreased of the signal respectively.

Fig. 4.13 to Fig. 4.17 illustrates detail analysis on of pyrometer profile and temperature behavior. The analysis based on when the laser power,  $P = 200$  W and scan speed,  $V = 444$  mm/s. In order to investigate the effect laser parameter, the temperature measurement experiment was repeated at various processing conditions. The result is depicted in Fig. 4.18. The figure shows the temperature rise during area consolidation from approximately 1800 °C to 2200 °C as the laser power was increased from 100 W to 500 W. The maximum temperature was observed when laser power was set at 500 W.

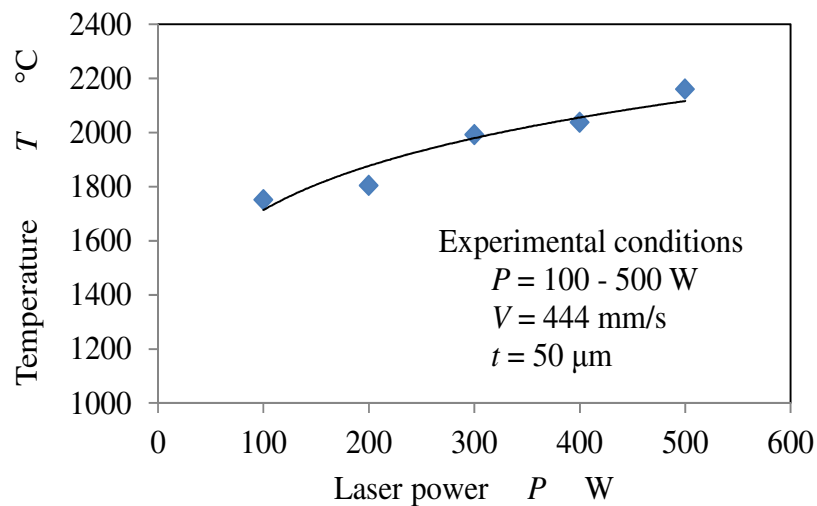


Fig. 4.18 Influence of laser power on temperature

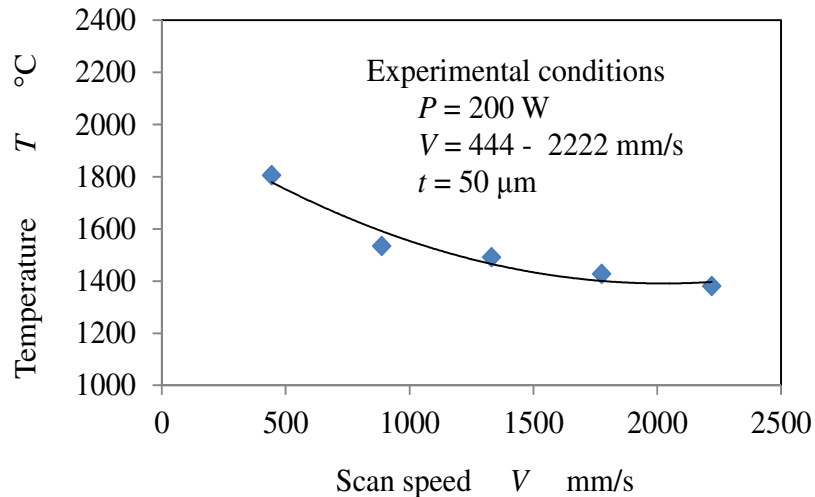


Fig. 4.19 Influence of scan speed on temperature

On the other hand, Fig. 4.19 illustrates the effect of scan speed when the scan speed was increased from 444 mm/s to 2222 mm/s at constant laser power,  $P=200$  W. It can be seen that, as the scan speed is increased, the maximum temperature recorded is decreasing from approximately at 1800 °C to 1400 °C. Therefore, the temperature was declining with the increase of the laser scan speed. This is due to relatively short laser irradiation time on the powdered surface during laser movement. As a result, lower temperature was recorded at high scan speed.

This behavior was contributed by the amount of heat radiated on the powdered surface during consolidation. When energy density was relatively high, the heat that was radiated initially liquefied the outer layer of the metal powder and subsequently melted the metal powder. Due to the very thin layer of metal powder thickness of 50 μm, the heat was also transferred to the substrate surface. The heat was then transferred radially through the substrate material circumferentially mainly through conduction from the laser irradiation spot. This was due to high difference in the thermal conductivity of cold-rolled substrate surface (56 W/(m·K)) in comparison to the metal powder (0.14 W/(m·K)). Higher laser power caused an increase of energy density per unit area around the laser irradiation spot. When the energy

was not fully transferred to its surroundings, increase of the temperature was observed with the increase of laser power.

The result represents the average maximum temperature. It is important to note that during laser irradiation, repetitive heating and cooling of consolidated structure occurred. This is contributed by successive line-by-line laser irradiation on the metal powder due to hatching distance. Furthermore, it is important to note the result obtained in the temperature measurement assumed that the temperature of the target area was uniform.

### **4.5 CONCLUSIONS**

The influence of processing parameter on the temperature of the consolidated structure was analyzed during SLS/SLM process. Based on the experiment, it was found that:

1. The temperature measurement technique used in the study can be applied for temperature monitoring in additive manufacturing.
2. The temperature profile of the line consolidation was due to laser beam scanning as it approached and moved away from the center of the target area.
3. The temperature profile of the area consolidation indicates repetitive line consolidation that occurred on the surface. Generally, the temperature during consolidation was increasing with the rise of laser power and decreasing with the increase of scan speed.

**REFERENCES**

- [1] J. P. Kruth, L. Froyen, M. Rombouts, J. Van Vaerenbergh, and P. Mercelis, “New Ferro Powder for Selective Laser Sintering of Dense Parts,” *CIRP Ann. - Manuf. Technol.*, vol. 52, no. 1, pp. 139–142, 2003.
- [2] F. Bayle and M. Doubenskaia, “Selective Laser Melting process monitoring with high speed infra-red camera and pyrometer,” in *Proc. SPIE*, 2008, vol. 6985, pp. 698505–698505–8.
- [3] T. Furumoto, T. Ueda, N. Kobayashi, A. Yassin, A. Hosokawa, and S. Abe, “Study on Laser Consolidation of Metal Powder with Yb: fiber Laser - Evaluation of Line Consolidation Structure,” *J. Mater. Process. Technol.*, vol. 209, no. 18–19, pp. 5973–5980, Sep. 2009.
- [4] T. Furumoto, T. Ueda, T. Tsukamoto, N. Kobayashi, A. Hosokawa, and S. Abe, “Study on Laser Consolidation of Metal Powder with Yb: fiber laser - Temperature Measurement of Laser Irradiation Area,” *J. Laser Micro/Nanoengineering*, vol. 4, no. 1, pp. 22–27, Apr. 2009.
- [5] T. Furumoto, T. Ueda, M. R. Alkahari, and A. Hosokawa, “Investigation of Laser Consolidation Process for Metal Powder by Two-Color Pyrometer and High-Speed Video Camera,” *CIRP Ann. - Manuf. Technol.*, vol. 62, no. 1, pp. 223–226, Jan. 2013.
- [6] Y. Chivel and I. Smurov, “On-Line Temperature Monitoring in Selective Laser Sintering/Melting,” *Phys. Procedia*, vol. 5, pp. 515–521, Jan. 2010.
- [7] Y. Chivel and I. Smurov, “Temperature Monitoring and Overhang Layers Problem,” *Phys. Procedia*, vol. 12, pp. 691–696, Jan. 2011.
- [8] Y. Chivel, “Optical In-Process Temperature Monitoring of Selective Laser Melting,” *Phys. Procedia*, vol. 41, pp. 897–903, Jan. 2013.
- [9] T. Craeghs, F. Bechmann, S. Berumen, and J. P. Kruth, “Feedback control of Layerwise Laser Melting using Optical Sensors,” *Phys. Procedia*, vol. 5, pp. 505–514, Jan. 2010.
- [10] T. Craeghs, S. Clijsters, E. Yasa, F. Bechmann, S. Berumen, and J. P. Kruth, “Determination of Geometrical Factors in Layerwise Laser Melting using Optical Process Monitoring,” *Opt. Lasers Eng.*, vol. 49, no. 12, pp. 1440–1446, Dec. 2011.
- [11] M. Pavlov, M. Doubenskaia, and I. Smurov, “Pyrometric analysis of thermal processes in SLM technology,” *Phys. Procedia*, vol. 5, pp. 523–531, Jan. 2010.
- [12] M. Doubenskaia, M. Pavlov, S. Grigoriev, E. Tikhonova, and I. Smurov, “Comprehensive Optical Monitoring of Selective Laser Melting,” *J. Laser Micro/Nanoengineering*, vol. 7, no. 3, 2012.

- [13] M. Islam, T. Purtonen, H. Piili, A. Salminen, and O. Nyrhilä, “Temperature Profile and Imaging Analysis of Laser Additive Manufacturing of Stainless Steel,” *Phys. Procedia*, vol. 41, pp. 828–835, Jan. 2013.
- [14] T. Ueda, A. Hosokawa, and A. Yamamoto, “Studies on Temperature of Abrasive Grains in Grinding—Application of Infrared Radiation Pyrometer,” *J. Eng. Ind.*, vol. 107, no. 2, p. 127, 1985.
- [15] T. Ueda, M. Sato, T. Sugita, and K. Nakayama, “Thermal Behaviour of Cutting Grain in Grinding,” *CIRP Ann. - Manuf. Technol.*, vol. 44, no. 1, pp. 325–328, 1995.
- [16] T. Ueda, K. Yamada, and K. Nakayama, “Temperature of Work Materials Irradiated with CO<sub>2</sub> Laser,” *CIRP Ann. - Manuf. Technol.*, vol. 46, no. 1, pp. 117–122, Jan. 1997.
- [17] T. Ueda, M. Sato, and K. Nakayama, “The Temperature of a Single Crystal Diamond Tool in Turning,” *CIRP Ann. - Manuf. Technol.*, vol. 47, no. 1, pp. 2–5, 1998.
- [18] T. Ueda, M. Al Huda, K. Yamada, and K. Nakayama, “Temperature measurement of CBN tool in turning of high hardness steel,” *CIRP Ann. - Manuf. Technol.*, vol. 48, no. 1, pp. 63–66, 1999.
- [19] T. Ueda, E. Sentoku, K. Yamada, and A. Hosokawa, “Temperature Measurement in Laser Forming of Sheet Metal,” *CIRP Ann. - Manuf. Technol.*, vol. 54, no. 1, pp. 179–182, Jan. 2005.
- [20] T. Ueda, M. Sato, A. Hosokawa, and M. Ozawa, “Development of Infrared Radiation Pyrometer with Optical Fibers—Two-Color Pyrometer with Non-Contact Fiber Coupler,” *CIRP Ann. - Manuf. Technol.*, vol. 57, no. 1, pp. 69–72, Jan. 2008.
- [21] J. P. Kruth, X. Wang, T. Laoui, and L. Froyen, “Lasers and Materials in Selective Laser Sintering,” *Assem. Autom.*, vol. 23, no. 4, pp. 357–371, 2003.
- [22] M. A. Davies, T. Ueda, R. M’Saoubi, B. Mullany, and A. L. Cooke, “On The Measurement of Temperature in Material Removal Processes,” *CIRP Ann. - Manuf. Technol.*, vol. 56, no. 2, pp. 581–604, Jan. 2007.
- [23] M. Al Huda, K. Yamada, A. Hosokawa, and T. Ueda, “Investigation of Temperature at Tool-Chip Interface in Turning Using Two-Color Pyrometer,” *J. Manuf. Sci. Eng.*, vol. 124, no. 2, p. 200, 2002.
- [24] M. F. Ashby, *Materials Selection in Mechanical Design*, 3rd ed. Butterworth Heinemann, 2005.
- [25] U. AZoNetwork Ltd, Cheshire, “AISI 4140 Alloy Steel.” [Online]. Available: <http://www.azom.com/article.aspx?ArticleID=6769>. [Accessed: 09-Dec-2013].
- [26] U. G.L. Huyett Ltd, Minneapolis, “Engineering Handbook,” *G.L. Huyett Ltd*, 2004. .
- [27] E. Oberg, F. D. Jones, H. L. Horton, and H. H. Ryffel, *Machinery Handbook*, 27th ed. Industrial Press Inc, 2004.

- [28] D. W. Richerson, *Modern Ceramic Engineering, Properties, Processing, and Use in Design*. Marcel Dekker Inc., 1985, p. 35.

# **CHAPTER 5 : CONSOLIDATION OF METAL POWDER**

## **5.1 INTRODUCTION**

SLS/SLM is one of the most promising AM techniques that are widely accepted by the industrial community. This is due to its high flexibility in processing different types of material under various conditions. However, the capability of the product to have a desirable quality comparable to traditional processing techniques is still not achievable. Consolidation characteristics and the influence of processing parameters are important in determining the SLS/SLM part quality. Many studies reported the final consolidated structure quality with respect processing parameters, but limited studies address the transformation of the metal powder to the consolidated structure in detail. Nevertheless, it is essential to understand the consolidation behavior of metal powder. During SLS/SLM, the laser-irradiated area is relatively small and the process is executed within a confined closed chamber at a very high temperature. This has caused direct observation on the transformation of metal powder to the consolidated material during laser irradiation on the powdered surface is a challenging task.

In this chapter, consolidation process on different surfaces of ferrous metal powder is examined. The monitoring of the real time consolidation process was performed using a high-speed camera with telescopic lenses. Hence, interaction of laser and material and transformation of metal powder to consolidated structure within a powder fusion zone (FZ)

was observed. The line consolidation characteristics were analyzed according to the line consolidation width, FZ and metal particle splattering behavior. The influences of laser power and scan speed on these characteristics were analyzed. Utilization of high-speed videography also allows analysis on the evolution of melt pool. Processing parameters were varied in order to study the influences on the consolidation of metal powder during SLS/SLM. Based on this, the consolidation characteristics during SLS/SLM are reported and the line consolidation is classified.

Understanding of the consolidation process is a key in improving the part fabricated via SLS/SLM. Therefore, a number of researches try to understand the consolidation behaviour through visualization of the process. However, only limited studies are available and some of the images were not clear enough. Hence, observation on the transformation process of the metal powder particle to the consolidated structure was insufficient. Monitoring of SLS/SLM is crucial as it allows observation on the thermo-fluid behavior of the melt pool region and its surroundings during the powder consolidation. The movement of the laser beam in the SLS/SLM can be relatively fast at the maximum speed of 5000 mm/s. Utilization of the high-speed camera is essential so that the evolution of the melt pool and the consolidated structure formation can be closely observed.

Process visualization of SLS/SLM with high-speed imaging using various methods has been made by many researchers. Study made on visualization of SLS/SLM was made by Hauser to view track formation revealed a periodic melting of powder ahead of the main track [1]. It is reported that the tracks do not grow in length steadily but as a series of steps. The experiment was recorded by video filming through a MIG welding glass filter. The series of images recorded is as indicated in Fig. 5.1.

Series of images was also recorded using the high-speed infrared camera by Bayle. Based on the research, the temperature during interaction between the laser and the metal powder was measured. Other than that, the dynamics of emitted droplets from the molten pool was reported. The author suggested it is important to study SLM in more detail by applying very precise temporal and spatial scales. Some of these high-speed infrared series of images obtained by Bayle as shown in the Fig. 5.2.

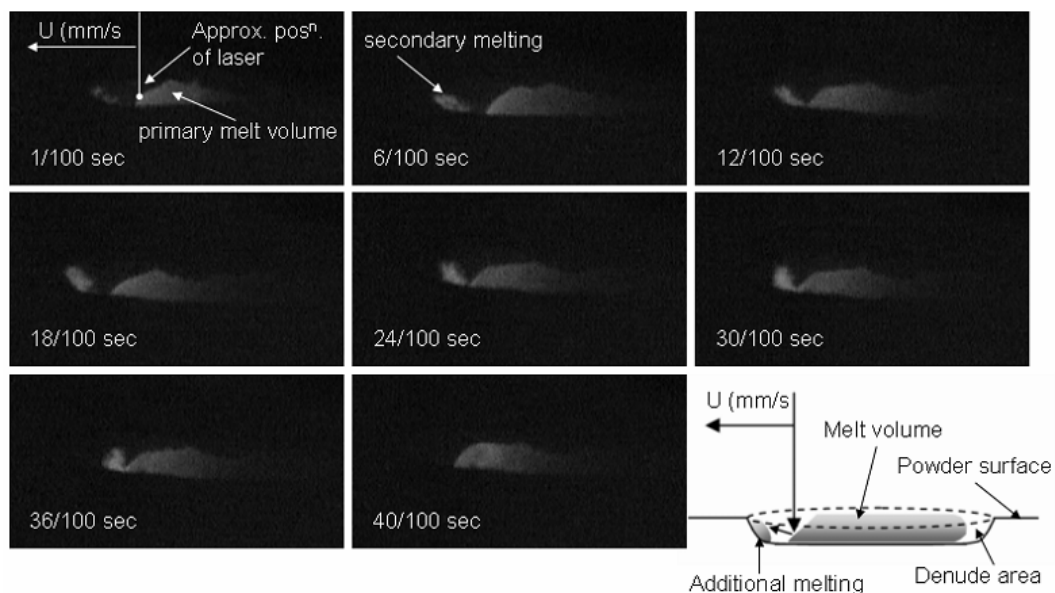


Fig. 5.1 High-speed image of track formation [1],[2]

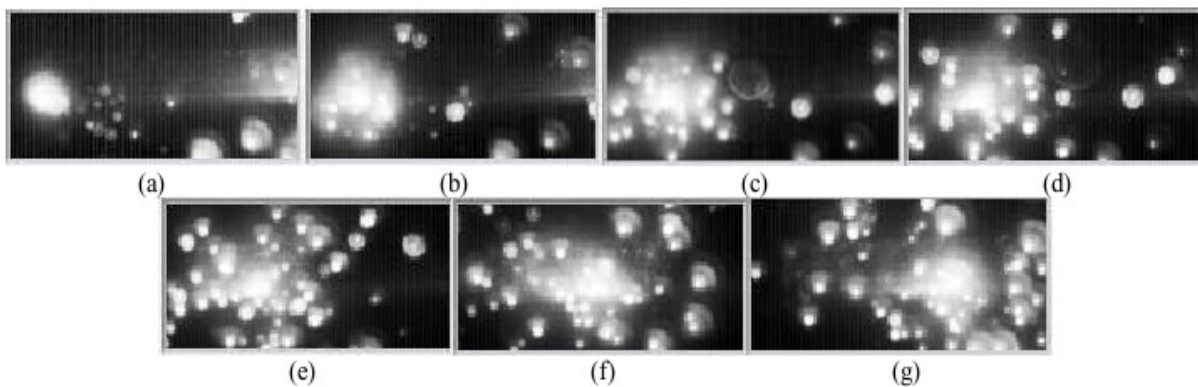


Fig. 5.2 Sequence of dynamic of droplets emitted from molten pool [3]

Melt pool observation during SLM was also reported by Kruth [4]. In the study, melt color level from the recorded images was extracted. Based on the color, assumption was made at certain pixel color in order to identify the molten material and to calculate the melt pool geometry. Typical image of the melt pool obtained and analyzed from the experiment is shown in Fig. 5.3.

Other than that, Kruth also proposed a monitoring system that used CMOS camera and a photodiode for image recording [5]. Through the developed monitoring system, the problem of overhang structure could be improved. The correlation of the melt pool size can be obtained from the system. However, the system has insufficient illumination for high resolved picture [6]. Therefore, Lott proposed a design of an optical system for monitoring of SLM process [6]. The proposed design enables high scanning speed during the laser irradiation and the melt pool to be monitored. Nevertheless, the system still needs to be improved in order to obtain clearer images of the melt pool dynamics. The screenshot of high-speed recording of 750 mm/s obtained from the preliminary results of the proposed design is shown Fig. 5.4.



Fig. 5.3 Typical image of SLM melt pool from high-speed camera [5]

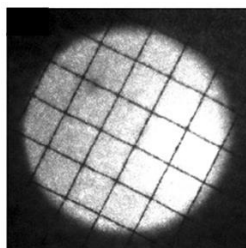


Fig. 5.4 Screenshot of high-speed recording [6]

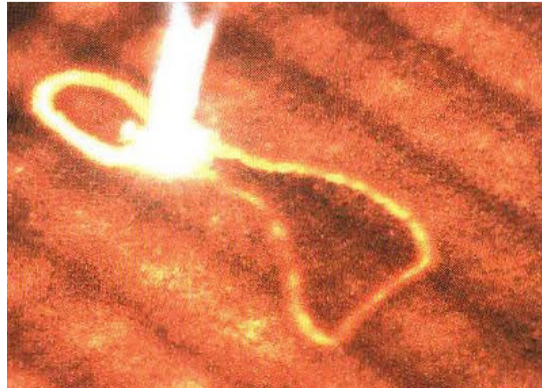


Fig. 5.5 High-speed image of melt pool [7]

Hagedorn also reported the evolution of the melt pool by observing the SLS/SLM process through the high-speed camera [7]. However, radiation and reflection from the fusion zone relatively high and do not allow clear observation on the laser beam - metal powder interaction region and within the melt pool region. Another approach used to monitor the melt pool is through a novel method so called mapping approach. The system monitors the melt pool with integration of a data processing algorithm [8]. To date, the recent report on SLS/SLM visualization was made by Chivel [9]. The author reported monitoring during SLM of overhang layers. Based on the study, the melt penetration into the powder bed and its mechanisms have been explained. Fig. 5.6 depicts the observation made by Chivel with the arrow indicating the melting front area.

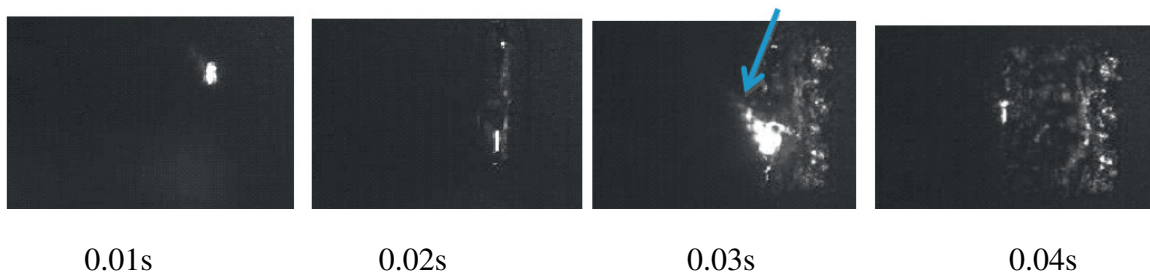


Fig. 5.6 Monitoring of overhang layer melting using high-speed imaging [9]

Based on the review on process visualization of SLS/SLM process, it can be summarized that since the development of AM especially SLS/SLM process, significant effort has been made in understanding the process behavior through process visualization and monitoring. However, the observation was not apparent due to difficulty in accessing the processing area. This is due to temperatures within the range of 1000°C to 2200°C, micron sized of the melted/sintered powder, and the very high scanning speeds during the sintering/melting process. Current research demonstrated the visualization of the process behavior could be achieved by self-developed vessel design and proper experimental setup. As a result, detail analysis can be made on the series of high-speed image obtained. Based on this, consolidation mechanism and characteristics as the laser irradiated on the metal powder are reported.

## 5.2 EXPERIMENTAL SETUP

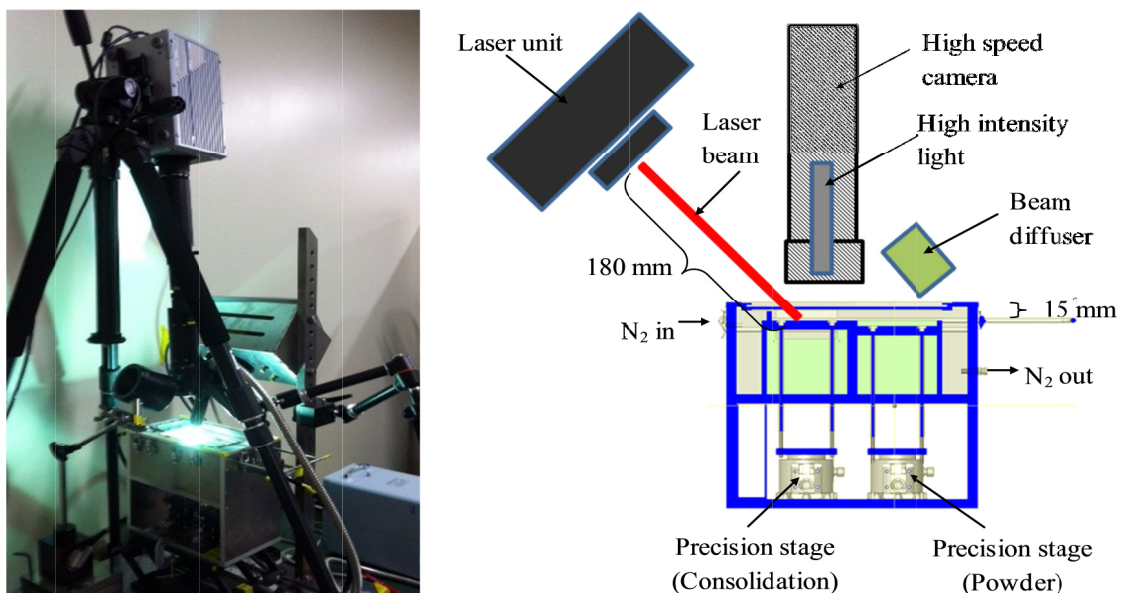


Fig. 5.7 Setup of consolidation monitoring apparatus

In order to monitor the consolidation characteristics of metal in the SLS/SLM, a special small-scaled SLS/SLM machine was designed and fabricated. The experimental setup is shown in Fig. 5.7. The Yb: fiber laser beam was placed at a 45-degree angle from the surface so as to improve the visibility of the consolidation that occurred on the powdered surface. To avoid harmful laser beam, a beam diffuser was used to reduce the reflected beam. A metal halide lamp was used in order to ensure sufficient lighting to the laser irradiation region and its surroundings. The consolidation process was carried out in a closed test chamber with a nitrogen-controlled atmosphere. This was to improve the quality of the consolidated part since oxidation was avoided during the process.

In this experiment, two types of laser equipment were used. For laser power of 1 W to 40 W, the laser equipment was LP-10 manufactured by SUNX Ltd. The laser beam was a continuous Yb: fiber. The beam was a Gaussian shape with the focal diameter of 45  $\mu\text{m}$ . The laser power was varied from 1 to 40 W. The scan speed used was set from 1 to 250 mm/s. For laser power of 40 W to 150 W, the laser equipment used was manufactured by IPG Photonics (Model YLR-3000-AC-Y11). The laser beam was also a continuous 1070 nm wavelength Yb: fiber with a beam diameter of 50  $\mu\text{m}$ . The laser power was increased to the maximum of 150 W. The scan speed was varied to from 100 mm/s to 500 mm/s.

High-speed camera used was a FASTCAM SA5 with shutter speed of 10,000 fps. In order to protect the camera from the scattered laser beam and enhance the visibility of the consolidation process within fusion zone, a filter was used. The filter was a laser protective shield manufactured by Sigma Koki, YL-500P-Y1 with dimensions of 50 mm x 50 mm and a thickness of 3.5 mm. The filter was made from polymethyl methacrylate and was able to absorb the wavelength of 1064 nm. This enhanced the visibility of the consolidation of metal powder through the high-speed camera during laser irradiation. The condition used in the

experiment is tabulated in Table 5.2 and Table 5.2. The optical density of the filter is shown in Fig. 5.8.

Table 5.1 Experimental conditions of laser power source

	Laser 1	Laser 2
Model	SUNX Ltd. (Model LP-F10)	IPG Photonics (Model YLR-3000-AC-Y11)
Type	Yb:fiber	Yb:fiber
Wavelength [nm] $\lambda$	1070	1070
Beam diameter at focal spot [ $\mu\text{m}$ ]	45	50
Power [W] $P$	1 - 40	50 - 150
Scan speed [mm/s] $V$	1 - 200	100 - 500

Table 5.2 Experimental conditions of high-speed camera and filter

High-speed camera	
Model	FASTCAM SA5
Shutter speed [fps] $f$	10,000
Resolution	768 x 648
Light source	Metal halide lamp
Filter	
Model	Sigma Koki (YL-500P-Y1)
Material	Polymethyl metaacrylate
Thickness [mm]	3.5
Size [mm]	50 x 50

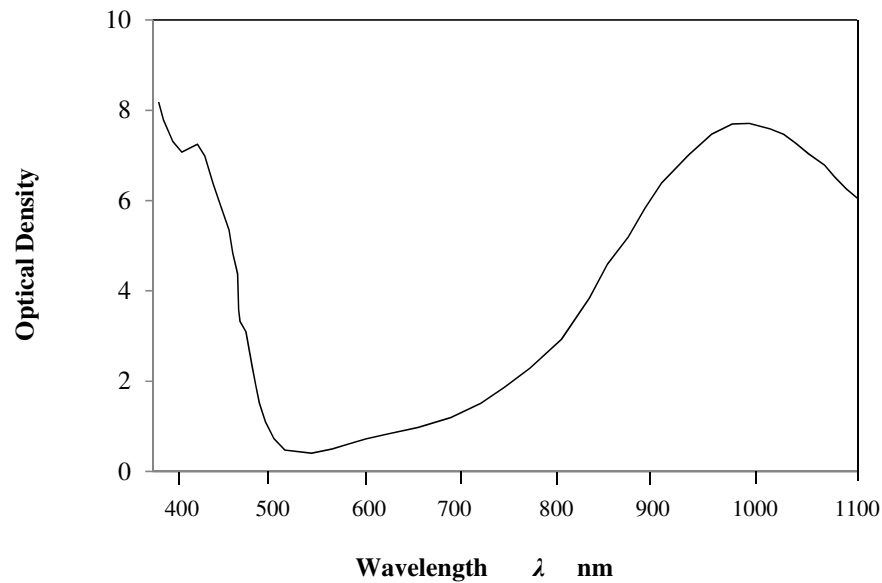


Fig. 5.8 Optical density of the filter

The influences of laser power and scan speed on line consolidation characteristics were analyzed. The analysis was made with respect to characteristics defined in the study. These characteristics are consolidation width, melt pool, powder fusion zone (FZ) region, splattering behavior and consolidation mechanism. The consolidation characteristics nomenclature used in the study is illustrated in Fig. 5.9. During laser irradiation, metal powder was heated. This produced single-track formation referred as line consolidation before solidification. After the molten powder solidified, movement and shrinkage occurred. As a result, a smaller consolidated structure was produced. This is referred to as line consolidation width after solidification. The solidification has created a powder-free area between the consolidated structure and the metal powder that is not fused by laser irradiation.

Consolidated agglomerate refers to a group of metal powder particles that coalesce, forming molten powder, which then solidifies together producing a ball-shaped agglomerate with various diameters at different processing parameters. Melt pool is the region where the metal powder completely in the liquid state due to high temperature after laser irradiation on

the powdered surface. Another line consolidation characteristic observed was the powder fusion zone (FZ). The FZ in the SLS/SLM process is defined as the area that is being fused as the laser beam moves forward during laser irradiation. Throughout the experiment, the observation was made twice: that is, without filter and with filter. Measurement of the FZ was made using the series of images from the high-speed camera without the filter. The boundary zone of the FZ is defined by the existence of an elliptical brighter region. Hence, the area was determined based on the major diameter and minor diameter of the ellipse. The measurement was made using the high-speed camera software, Photron FASTCAM Viewer. It is important to note that the FZ observed throughout the experiment is approximately elliptical shaped due to the laser orientation being at 45 degrees from the laser substrate surface.

The material used in the study was a ferrous-based metal powder material with the particle mean diameter of 25  $\mu\text{m}$ . The material was a mixture of steel, copper-phosphorous alloy and nickel with a weight percentage of 70%, 20% and 10% respectively. The detail specification of the metal powder and SEM image is as previously illustrated in Table 3.1 and Fig. 3.1 of Chapter 3.

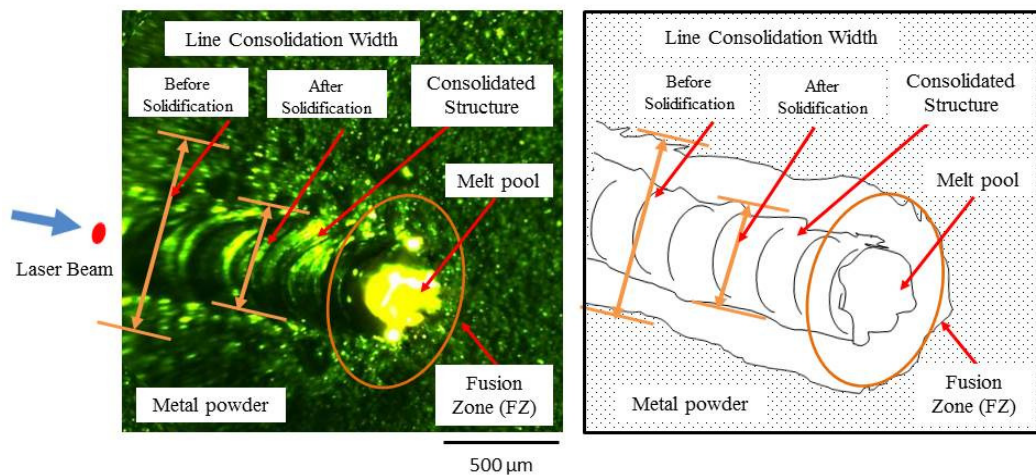


Fig. 5.9 Line consolidation characteristics nomenclature

### 5.3 EXPERIMENTAL RESULTS AND DISCUSSION

#### 5.3.1 Line Consolidation

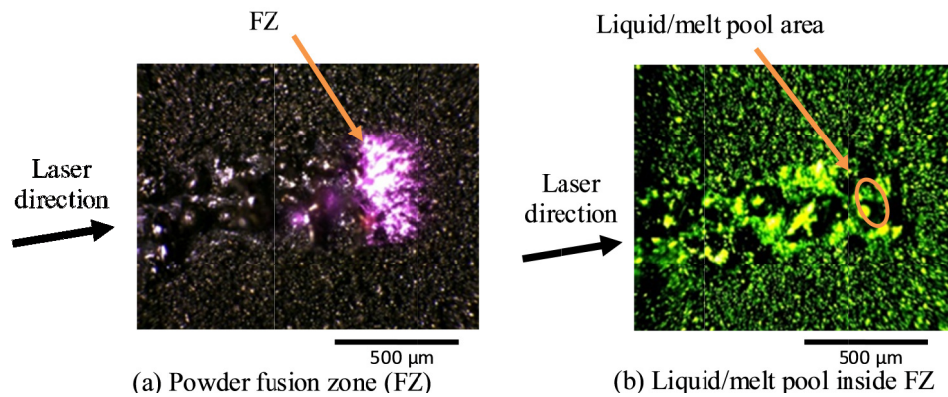


Fig. 5.10 Line consolidation during laser irradiation

Understanding line consolidation characteristics is important because during the SLS/SLM process, the laser beam is irradiated line by line on the powdered surface. As the laser beam is continuously irradiated in a straight line, a line consolidation is formed. Still images obtained from the high-speed camera are shown in Fig. 5.10. Fig. 5.10(a) shows the powder FZ on line consolidation, which can be seen on the high-speed camera when there is no filter used during laser irradiation. The figure clearly shows an elliptical shape of the FZ caused by the irradiated laser beam on the metal powder. Fig. 5.10(b) on the other hand, depicts the line consolidation under same setting when a filter was used. When there was no filter, consolidation within the FZ was not clear due to very high brightness intensity. In contrast, with the application of the filter, the consolidation behavior and transformation of the metal powder that occurred within the liquid/melt pool region can be observed clearly. The liquid/melt pool is located inside the FZ. The figures also show a direct relationship between the major diameter of the FZ and the line consolidation width. The major diameter

of the FZ was found to be approximately the same as the line consolidation width before solidification. Observation on the metal powder when the filter was used allowed the mechanism to be monitored.

5.3.1.1 Line Consolidation Mechanism

Understanding the consolidation process and mechanism of metal powder are of utmost importance in the SLS/SLM. This is because the consolidation of the metal powder is the essence of development of 3D structures. An examination of the consolidation mechanism that occurred in the study revealed that the metal powder particles experienced changes in their shape and structure as consolidated agglomerates were formed. Based on the high-speed camera image obtained under various processing conditions, similar behavior and consolidation mechanisms were revealed. Based on the observation, the consolidation process of metal powder during the SLS/SLM process can be divided into stages. These stages correspond to the different region on line consolidation. The metal powder underwent several stages of transformation due to high-localized temperature during laser beam irradiation on the metal powder and the substrate interaction process.

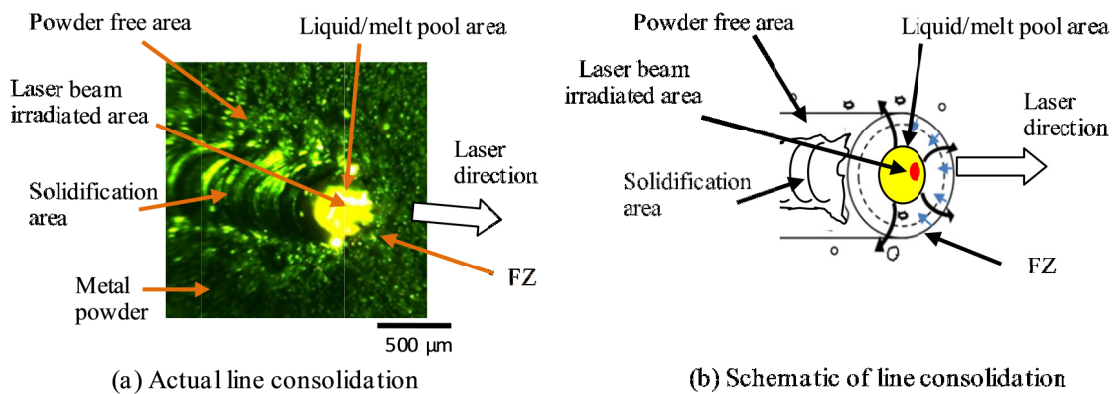


Fig. 5.11 Main area in line consolidation structure

Fig. 5.11(a) shows the actual line consolidation with FZ. Existence of the different regions within line consolidation, which reflect stages that occurred during SLS/SLM can be schematically illustrated in Fig. 5.11(b). Since the nature of SLS/SLM processes where the movement of the laser beam was continuously travels and irradiates on the new powder surface. The schematic figure may represent the line consolidation region at any instantaneous position. The region can be divided into five different regions,

- Region 1 : Laser beam irradiated region
- Region 2 : FZ
- Region 3 : Liquid/melt pool region
- Region 4 : Solidification region
- Region 5 : Powder free region

Region 1 is the laser beam irradiated region. The region is the actual size of the laser beam diameter as it was irradiated from the laser source. The region is the main region that received irradiated heat from laser source. Therefore, this region has the highest temperature compared to other regions. Based on the moving of heat source theory, the peak temperature location may be slightly nearer the rear end, depending on the speed [10].

Region 2 termed as powder FZ is the area where the heat from the laser beam irradiated region was transferred radially to its surroundings. As a result, the metal powder on the surrounding was also fused together. The FZ was surrounded by more glittering circumference. The glittering was caused by reflection of the semi-solid of the metal powder particles as they started to melt, or as they started to solidify. It is important to note that the temperature near the edge of the FZ was lower compared to the temperature in the center due to temperature distribution.

Region 3 is the liquid/melt pool area. During laser irradiation, liquid pool developed and flowing of molten powder occurred. When the melting was achieved, the region formed a melt pool. The flowing of the molten powder depends on its viscosity at that time. Hence, there was less glittering observed in the center of the FZ or inside the liquid/melt pool region. Within the liquid/melt pool region also, it was observed that fast movement occurred of the metal powder particles toward the center with the increase of scan speed. During these movements, collisions between metal powder particles were observed. Collisions between metal powder particles contributed to the splattering of the metal powder. An increasing amount of splattered molten powder and particles occurred in a circumferential direction as the scan speed was increased. As a result, the amount of splattering that occurred in the vicinity of the line consolidation increased where they tended to be displaced further from the line consolidation structure.

The region 4 was formed after the laser beam moved away from the irradiated spot. Hence, the line consolidation structure cooled down, and solidification process started. Solidification of the molten powder caused shrinkage due to transformation from liquid to solid occurred.

As a result, region 5, which is the powder-free region, was formed. Most of the powder that was previously deposited on this surface was transformed to consolidated material after laser irradiation, leaving irregularities on the surface. The size of the region differs with processing parameter used. When the area is big enough, it may contribute towards the formation porous area within the consolidated material after successive laser irradiation was made.

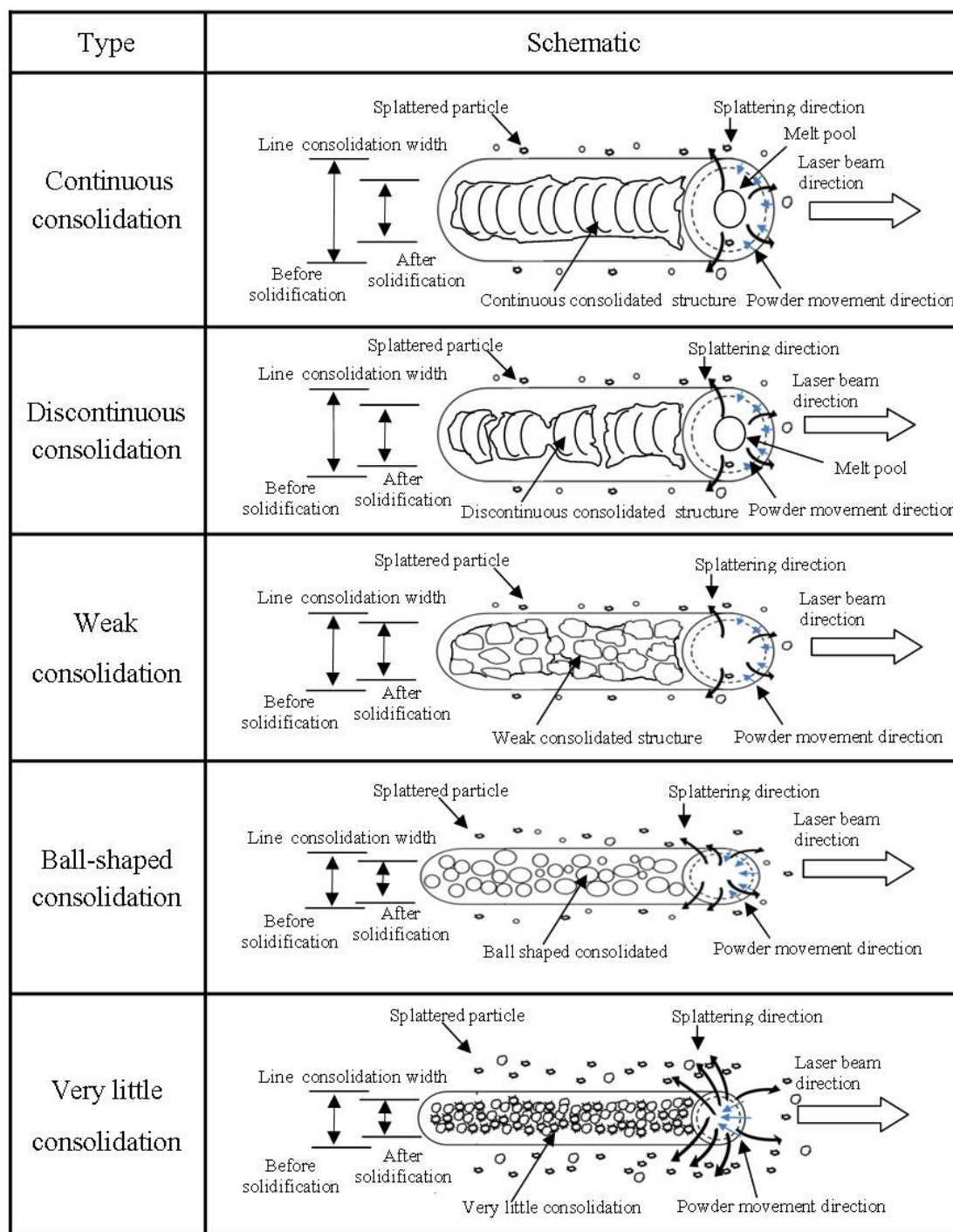


Fig. 5.12 Schematic presentation of line consolidation characteristics

Generally, the quality of the line consolidation and types can be summarized schematically by Fig. 5.12. Changes of laser power and scan speed resulted in variations in the line consolidation characteristics. As shown in the figure, changes in line consolidation

characteristics were observed in terms of line consolidation width, FZ, structure quality and splattering behavior. Hence, the consolidation can be classified as continuous consolidation, discontinuous consolidation, ball-shaped consolidation, weak consolidation and very little consolidation. The characteristics of the consolidation observed can be generalized as follows.

a. Continuous consolidation - is characterized by the formation of a connected and uniform shaped track. This form of consolidation is considered as good because the structures are connected to each other in a straight line coherently. As a result, a relatively dense surface was produced.

b. Discontinuous consolidation - is characterized by an uneven shape structure. The structures are relatively dense but most of them are not continuously connected. At low laser power, the discontinuity was more prominent. However, the discontinuity was improving with the increase of laser power. At high laser power, the discontinuous consolidated structure produced characterized by long and cylindrical shaped with highly coarsened surface.

c. Ball-shaped consolidation - is characterized by the existence of a high number of ball shaped structures that are scattered randomly on the line consolidation track. The circular structure was discontinuous and not connected to each other resulting rougher surface. Some of these structures coalesced with the substrate surface, forming hemisphere shapes.

d. Weak consolidation - is characterized by scattering and a small amount of sintered the metal powder, which can be easily broken. The shape is relatively irregular due to the shape of metal powder. Sintering between metal powder particles only occurs between the surfaces of the metal powder and occasionally coalesces with the substrate surface.

e. Very little consolidation - is characterized by most of the metal powder particles unconnected, except to the neighboring particles. Changes of the individual metal powder shape were observed due to the small amount of heat. Nevertheless, the energy density was not enough to cause coalescence with a large amount of metal powder particles.

Application of various materials leads to complexity in determining the optimum parameter that could produce a relatively good consolidated structure. The mechanism and phenomenological analysis indicated that it is apparent that the quality of the structure is affected by the laser parameters. The consolidation of metal powder exhibits different properties due to the energy irradiated to the metal powder, which is related to the viscosity, surface tension, laser absorption, surface tension, wettability, roughness of the substrate, viscosity, and others.

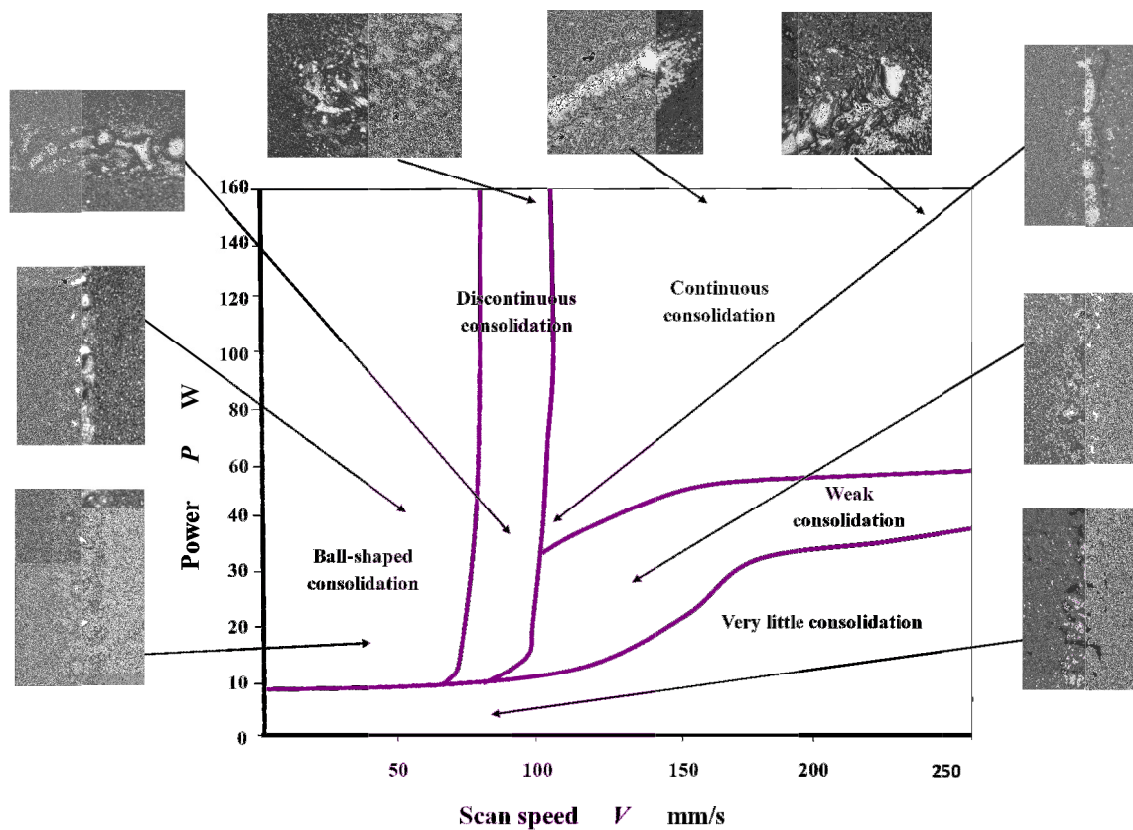


Fig. 5.13 Process map

Generally, effective molten metal flow within the FZ allows relatively smoother surface structure. Therefore, observation of the melt pool and optimization of processing parameters is crucial in determining the best conditions to ensure the continuous consolidated structures can be manufactured. Kruth et al suggested that for each new material, a process map needs to be developed experimentally [11]. This is due to different property changes of the materials used during SLS/SLM processing. Variations of line consolidation quality was reported by many authors using various materials [12],[13],[14].

Therefore, in this research, the process map of the metal powder mixture was also determined. The laser was varied from 1 W to 150 W, and the laser scan speed range was from 1 to 250 mm/s. The line consolidation quality and its relation to these parameters is shown in Fig. 5.13. The process map represents the general consolidation characteristics that can be attained from the SLS/SLM process. The value of the energy density and temperature is shown below the respective image. Other parameters such as powder thickness and beam diameter were kept constant.

Hence, based on the observation, it can be deduced that higher temperature is required to melt the metal powder to form a good and continuous structure. However, too high temperature caused overheating of the laser irradiation area. The heat was transferred radially at the rate where it affected the surrounding metal powder. As a result, a poor consolidated structure was produced. These are reflected by the formation of ball shaped and discontinuous structures.

Based on the study also, it can be summarized that the transformation process of metal from the powder state to the consolidated structure occurred as the laser was irradiated powder surface. The process was highly influenced by the amount of heat on the irradiation spot, which then affected the surface tension and flowability of the molten powder. During

the heat transfer process, initially the heat was radiated on the metal powder and substrate material with the size of the laser beam. The heat was then transferred to the surrounding. However, due to the high thermal conductivity differences between the substrate and the metal powder, the radial direction of heat transfer mainly occurred from the substrate through conduction. As a result, the metal powder on the surface of the substrate and surrounding the laser spot area was heated through the substrate material. A localized high temperature occurred on the irradiation spot within a very short time. Sufficient thermal energy liquefied outer layer of the metal powder first. Further heating then liquefied the successive layer and eventually changed the powder to molten state.

Rapid increase in the temperature has caused high-temperature gradient in the consolidated region. The high temperature stimulated physical changes and chemical reaction. The differences in the temperature between the edge and center of the liquid/melt pool also contributed to the consolidation characteristics where the flow molten powder was observed. It is generally accepted that the surface tension is dependent on the temperature. As a result, the high-temperature gradient has induced the surface tension on the irradiated surface.

Since a number of groups of molten powder spread and coexisted simultaneously on the FZ, gradient of the surface tension had initiated the powder movement within the FZ. Movement of the metal powder has induced collision between metal powders, which contributed to metal powder splattering. Melt pool was formed as a significant amount of the metal powder fully melt. Chaotic movement of the powder particle and the laser beam on the melt pool has also caused sudden momentum on the melt pool. Furthermore, the entrapped gases between the powder particles were under the influence of the high temperature. As a result, small explosions occurred that contributed to the splattering of the molten metal.

When the laser beam moved forward in laser direction, the melt pool cooled down. Hence, semi-molten metal formed and then solidified to a consolidated structure.

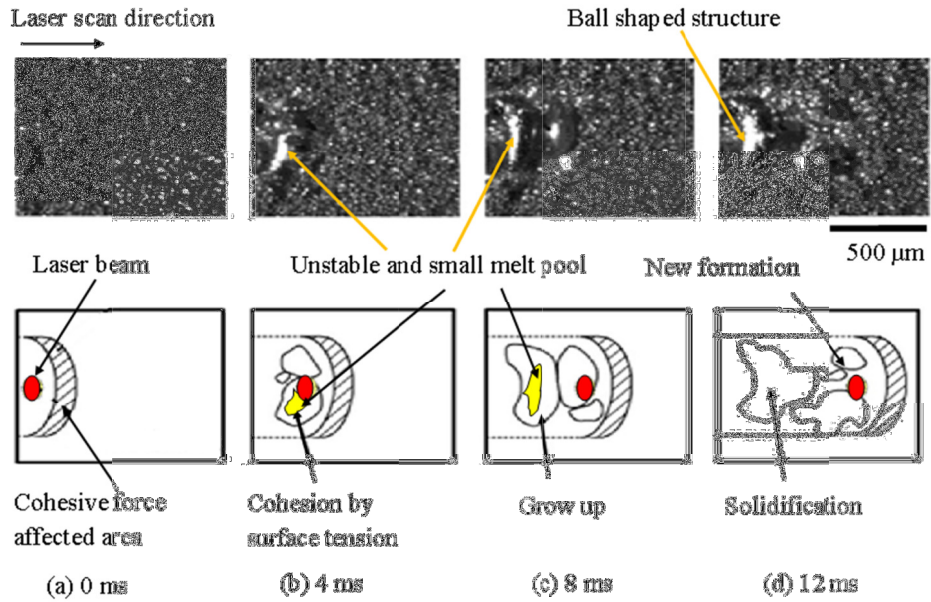


Fig. 5.14 Ball shaped type consolidation at  $P = 40 \text{ W}$ ,  $V = 50 \text{ mm/s}$

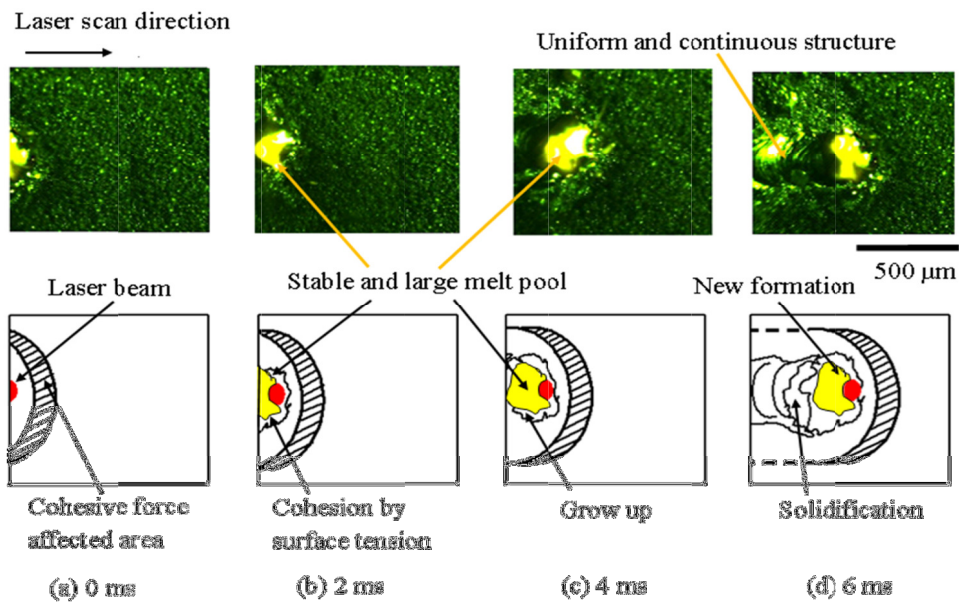


Fig. 5.15 Continuous type consolidation at  $P = 150 \text{ W}$ ,  $V = 250 \text{ mm/s}$

The consolidation process can also be schematically illustrated in the Fig. 5.14 and Fig. 5.15. The figure shows the top view of the consolidation process of the ball type consolidation and continuously type consolidation respectively. The laser was set at 40 W whereas the scan speed was 50 mm/s. As the laser beam was irradiated powder surface, the powder was heated. When the energy was a sufficiently high, molten area was formed as indicated in Fig. 5.14(a). The surface tension caused movement of the powder from the circumferential area toward the center of the laser beam as illustrated in Fig. 5.14(b). Further heating caused the melt pool to grow up gradually. This is depicted in Fig. 5.14(c). However, the melt pool was relatively very small. As a result, the melt pool transformed to the ball shaped directly. When the laser beam moved away, heat was dissipated from the melt pool to the surroundings. This caused solidification of the molten powder. In contrast, in continuous type consolidation, bigger melt pool was formed. This is indicated in Fig. 5.15. Bigger melt pool enhanced stability of the liquid cylinder. Hence, mixing of metal at a high temperature occurred, which allowed the formation of continuous consolidated structure.

The main composition of the powder mixture was steel, which the melting temperature was 1540 °C. Therefore, when the temperature is below than the melting temperature, only sintering of the metal powder occurred. Fig. 5.16 shows the schematic of the sintered metal powder which occurred at laser power of 10 W. The steel powder was partially melted. The recorded temperature was 1520 °C [15]. Hence, the shape of the ball-shaped structure formed was relatively rough. In contrast, at high laser power, the melting of metal powder was achieved. Therefore, a spherical shaped consolidated structure that wet to substrate was formed. This was obtained under the influence of the surface tension that acted on the molten powder. The image of the molten powder at melting condition is depicted in Fig. 5.17 and Fig. 5.18 when the laser power was 150 W.

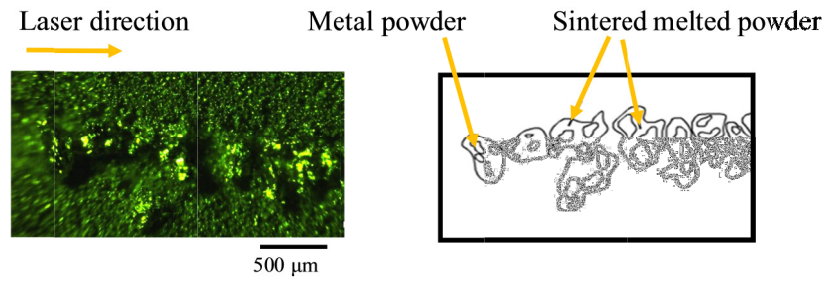


Fig. 5.16 Consolidation of metal powder when  $P = 10$  W,  $V = 88$  mm/s

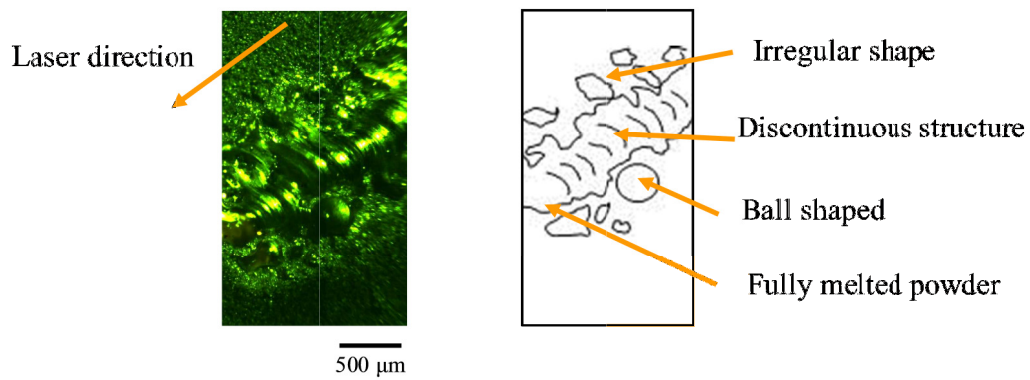


Fig. 5.17 Consolidation of metal powder when  $P = 150$  W,  $V = 100$  mm/s

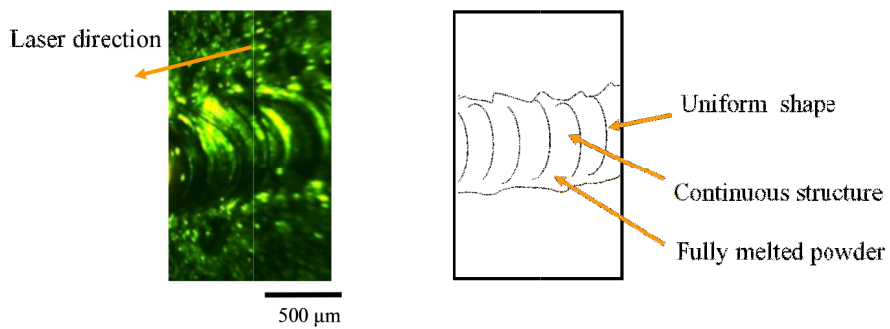


Fig. 5.18 Consolidation of metal powder when  $P = 150$  W,  $V = 250$  mm/s

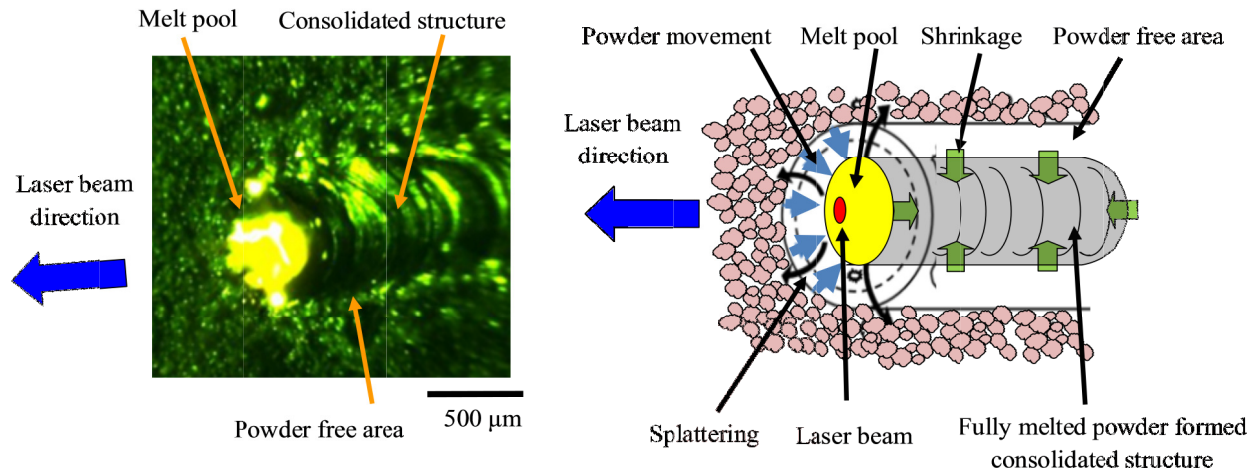


Fig. 5.19 Consolidation mechanism of metal powder

The mechanism of the metal powder consolidation is illustrated in Fig. 5.19. During the laser beam movement, the transformation of the metal powder to a consolidated structure occurred in sequence of stages within the previously defined area during line consolidation. The arrows indicate powder movement direction, splattering direction and shrinkage direction throughout the consolidation process.

When the powder particles outside from the FZ, they were not affected by the heat transferred from the laser beam due to far distance from the moving heat source. At the position where the metal powder near to the FZ, the metal powder started to form liquid around the particles. With the higher amount of heat received by the metal powder, the amount of liquid film around the metal powder increased. At the edge of the FZ, the region experienced a low surface tension. This was caused by temperature difference between the center and the edge of laser-irradiated area. Consequently, the movement of the metal powder started to occur due to the surface tension. Air gaps between the powder particles were heated contributed to existence small explosions due to the entrapped air. As a result, splattering of the metal powder was observed followed by the movement of the metal powder toward the

high surface tension region, which is approximately at the center of the laser beam irradiated area.

Within a large melt pool, chaotic movement of the liquid melt was observed. The chaotic behavior induced by the flow of the high temperature molten powder toward the surface of the melt pool and the flow of the lower temperature molten powder to the bottom of the melt pool. This movement is also known as Marangoni convection [16],[17],[18]. The fluid motion was caused by the difference in the temperature. When the molten powder was heated and has a higher temperature, it becomes less dense. As a result, it moved toward the surface of the melt pool. In contrast, the existing molten powder on the surface moved to the bottom due to its density. At this stage also, the metal powder was fully melted. Later, the melt pool formed a liquid cylinder. However, due to surface tension and Rayleigh's instability, it broke up into the ball shaped [19]. These small ball-shaped molten metals diffused to bigger one. This was caused by Ostwald ripening phenomena. As the laser beam moved, the melt pool started to solidify. Solidification was directional starting from the outer layer towards the center. Further movement of the laser beam away caused the melt pool to undergo the solidification process. As a result, the consolidated structure was formed.

Based on the visualization during the consolidation process, the melt pool area at high laser power was easily distinguishable from the FZ. This was due to dynamic movement of the melt pool over the time and as the laser beam scanned forward. Melt pool area was the main interest in the SLS/SLM due to within the melt pool area, the metal powder was successfully changed to liquid. Generally, a greater melt pool in line consolidation caused bigger line consolidation width after solidification of the melt pool. Furthermore, the larger melt pool area facilitated the flow of the liquid metal to fill the porosity.

At low laser power and at high scan speed, the existence of melt pool was difficult to observe. This is attributed to the area of the melt pool, which was too small. Furthermore, the metal liquid was instantaneously transformed to ball shaped consolidated structure. With the increase of the laser power, melt pool area enlarged significantly as shown in the figure. In contrast, the melt pool area was decreasing with the increase of the scan speed. The melt pool was dependent on the amount of the energy that transferred to the metal powder surface during laser irradiation. Therefore, it was largely affected by the laser power, scan speed, oxygen content in the atmosphere and alloying elements.

The melt pool and the FZ are the most important phenomena observed during the consolidation process. As previously discussed, the size of the melt pool and fusion zone is dependent upon the laser processing parameter used during laser irradiation. Both were increasing with the increment of laser power as illustrated in Fig. 5.20. However, the rate of FZ increased dramatically at 150 W. At this condition, the heat was dissipated to the substrate and its surroundings causing poor quality of consolidated structure in comparison to when the laser power was 100 W. In contrast, too small FZ caused low ability of the molten powder to consolidate.

The consolidated structure at the laser power of 100 W and 150 W is shown in Fig. 5.21. The figure shows the continuous and uniform structure was obtained at lower laser speed of 100 W. Adversely, higher laser power of 150 W produced discontinuous consolidated structure with significant irregularities despite its higher energy density.

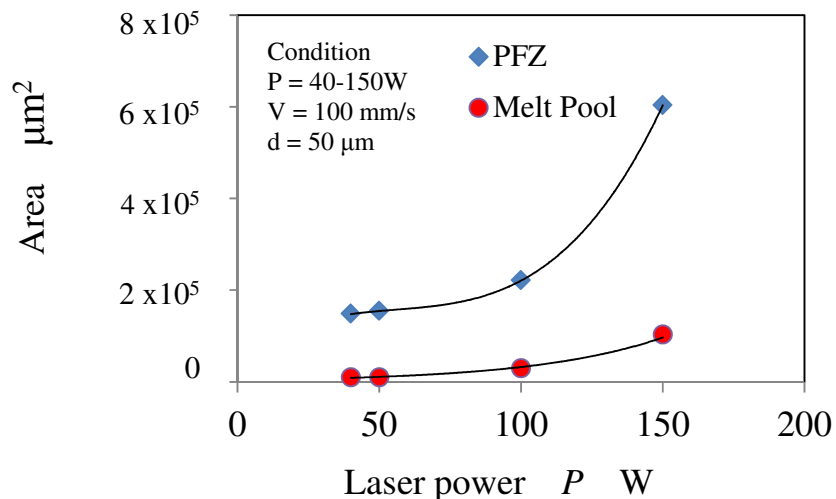


Fig. 5.20 Relation between the FZ and the melt pool area with the increase of laser power

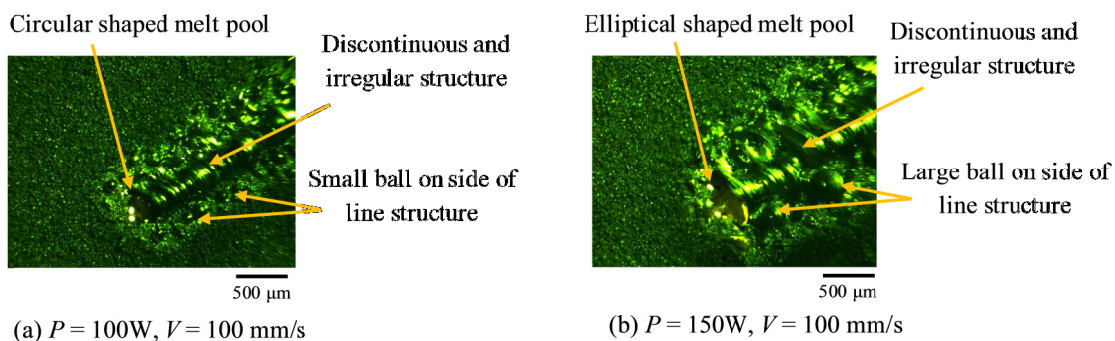


Fig. 5.21 Effect of the melt pool and the FZ on the consolidated structure

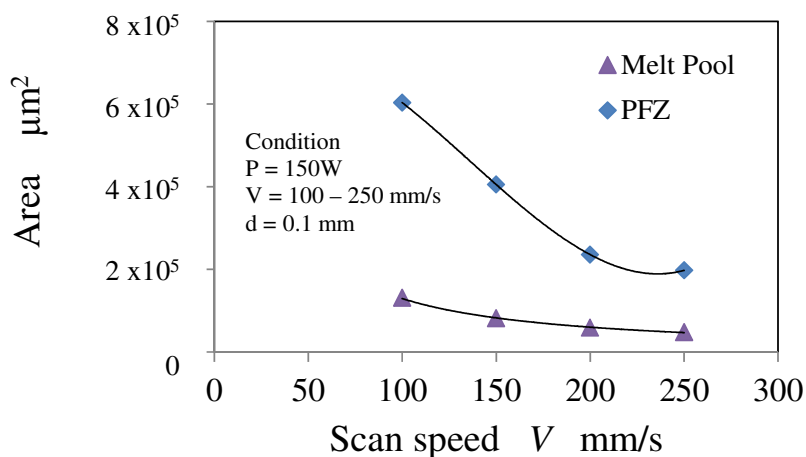


Fig. 5.22 Relation between the FZ and the melt pool area with the increase of scan speed

Comparison of the melt pool and the FZ was also made with the increase of scan speed. This is compared in Fig. 5.22. At low scan speed, the FZ was high. The value was decreasing abruptly with the increase of scan speed. However, starting at 200 mm/s, the FZ was decreasing incrementally. Comparison of the structure quality indicated that better structure was obtained when the scan speed was 250 mm/s. This was despite its lowest energy density compared to other setting conditions.

The results signify the importance of the melt pool and the FZ optimization in producing a good continuous structure. High energy density through increasing the laser power and decreasing did not directly produce a better structure. Therefore, optimization of the laser parameter through observation of the FZ and the melt pool is important. This can be obtained when the difference of the FZ, and the melt pool can be kept at relatively minimum value.

### *5.3.1.2 Influence of Laser Power*

The influence of laser power on consolidation behavior was monitored at different laser powers ranging from 1 to 150 W, and a thickness of 50 microns. Based on the analysis, it was found that the increment of laser power affected line consolidation width. It was found the width was increasing with the rise of laser power. Similar behavior was observed after shrinkage of line consolidation width. This influence of laser power on consolidation width is presented in Fig. 5.23. The figure shows different line consolidation widths obtained at various laser powers. The scan speed was set 50 mm/s at 100 mm/s. Different quality of the line consolidation was observed as the laser power was increased.

As the laser beam was irradiated at low laser power, the amount of the metal powder coalescing with its neighboring powder particles was very small. In addition, the heat that was generated by laser irradiation was not enough to liquefy high amounts of metal powder. Merely outer layer of metal powder particle at the center of the laser beam was liquefied. As a result, only the metal powder directly irradiated by the laser beam and those very close to the center of the laser beam path was coalesced. These metal powder particles randomly coalesced to form consolidated agglomerates.

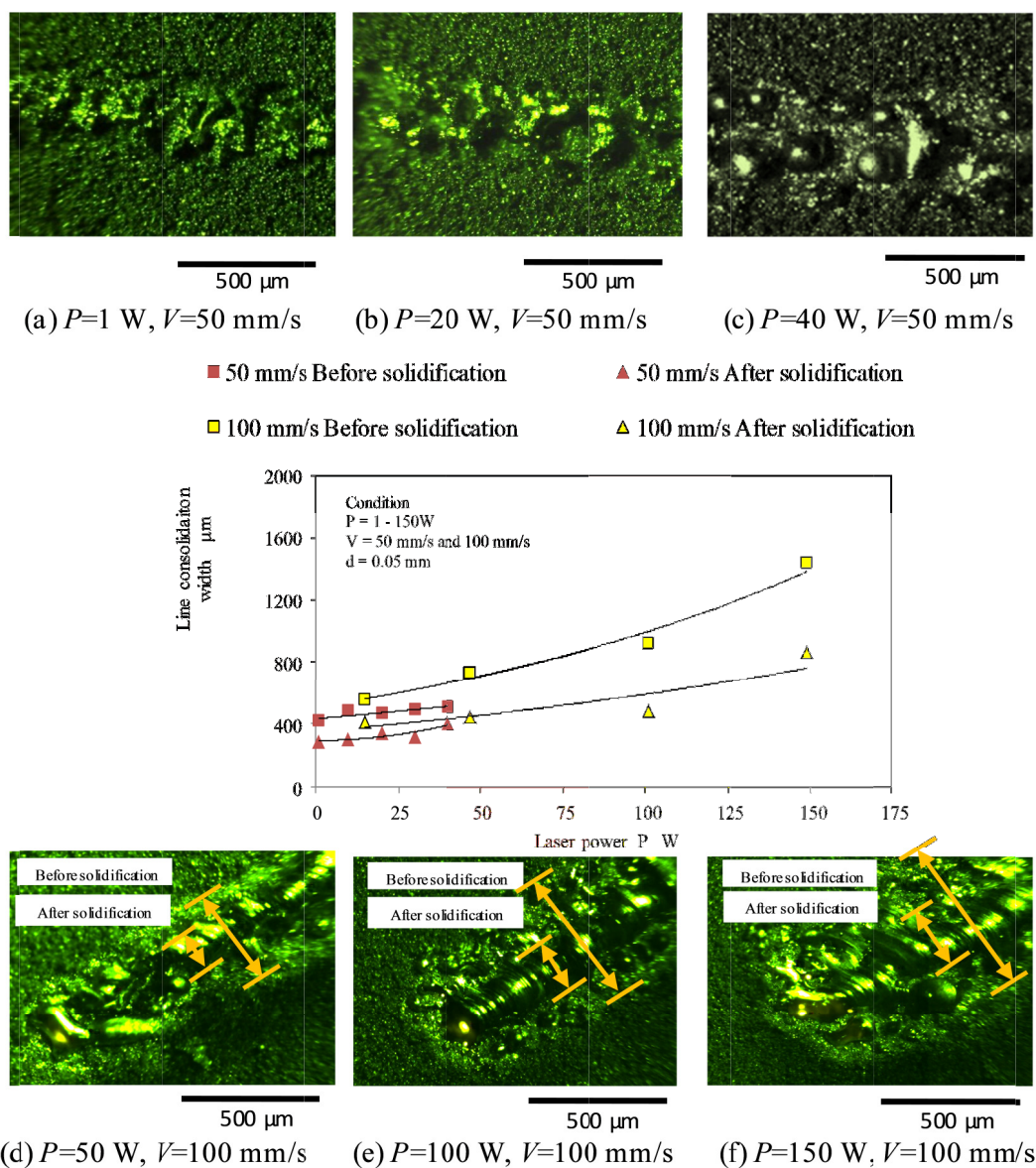


Fig. 5.23 Influence of laser power on line consolidation width

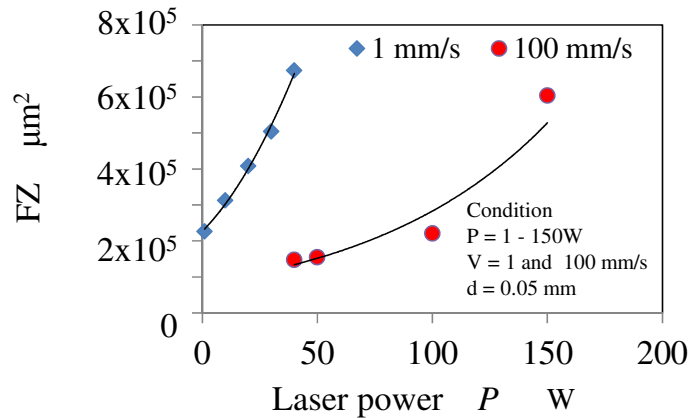


Fig. 5.24 Influence of laser power on the powder FZ

Furthermore, the metal powder particles did not consolidate with the substrate at low laser power. With the increase of laser power, formation of ball-shaped agglomerate was observed. Further increase of the laser power to 150 W had reduced the amount of balling but produced a discontinuous structure. The amount of metal powder coalesced with neighboring powder and formed consolidated structure was growing as the laser power was increased.

The influence of laser power on the FZ at the scan speed of 1 mm/s and 100 mm/s is graphically depicted in Fig. 5.24. Increasing size of the FZ was obtained with the increment of laser power for both scan speed of 1 mm/s and 100 mm/s. It was observed that as the laser beam irradiated on metal powder, a larger FZ region was formed. Even at lowest laser power of 1 W, the size of the FZ measured was approximately at  $2.2 \times 10^5 \mu\text{m}^2$ . This is despite the actual laser beam area of  $2.3 \times 10^3 \mu\text{m}^2$ . The area was enlarged with the increase of laser power. A bigger FZ was obtained compared to the laser beam area attributed to the heat transfer from laser beam area. At higher laser power, very high temperature gradient existed between metal powder particles at different position. Temperature at the center and near to the laser was high in comparison to metal powder at the edge of the FZ. During laser irradiation also, the heat was transferred through the substrate surface so that thermal could be equilibrium achieved.

Accordingly, as the laser power was increased, better consolidation between the metal powders was achieved. As a result, consolidation between the substrate and the metal powder occurred more prominent. At high laser power also, the FZ was larger, which resulted in a bigger line consolidation width. Furthermore, the splattering of the metal particles and the molten powder occurred around line consolidation. Significant amount of the metal particles splattering were observed at the higher laser power. Comparison of the FZ at 1 mm/s and 100 mm/s shows that the rate of FZ increasing is different at these two conditions. When the scan speed was set at 1 mm/s, the size of FZ increased relatively faster with the increment of the laser power compared to when the scan speed was 100 mm/s.

### *5.3.1.3 Influence of Scan Speed*

In contrast to the influence of laser power, the influence of scan speed resulted in an adverse effect. The increase of scan speed has resulted in narrower line consolidation width, smaller FZ and agglomerate size. The influence of scan speed on line consolidation width before solidification and after solidification is illustrated in Fig. 5.25. The phenomena can be linked to the heat transfer process that causes the FZ around the irradiated region. At high scan speed, the amount of heat transferred to the powder surface was less compared to at the low scan speed. The exposure time of each metal particle to laser irradiation that caused the reaction metal powder to take place during the interaction between the laser beam and the metal powder was very low. In contrast to low scan speed, the exposure time of the metal powder to the laser beam was high causing extremely localized heating within a small region. The heat was then transferred from the metal powder to the substrate surface and was further transferred radially, causing the PFZ to have a big diameter. Due to this, rapid heating and

cooling of line consolidation occurred faster at high scan speed. Consequently, a smaller FZ was observed.

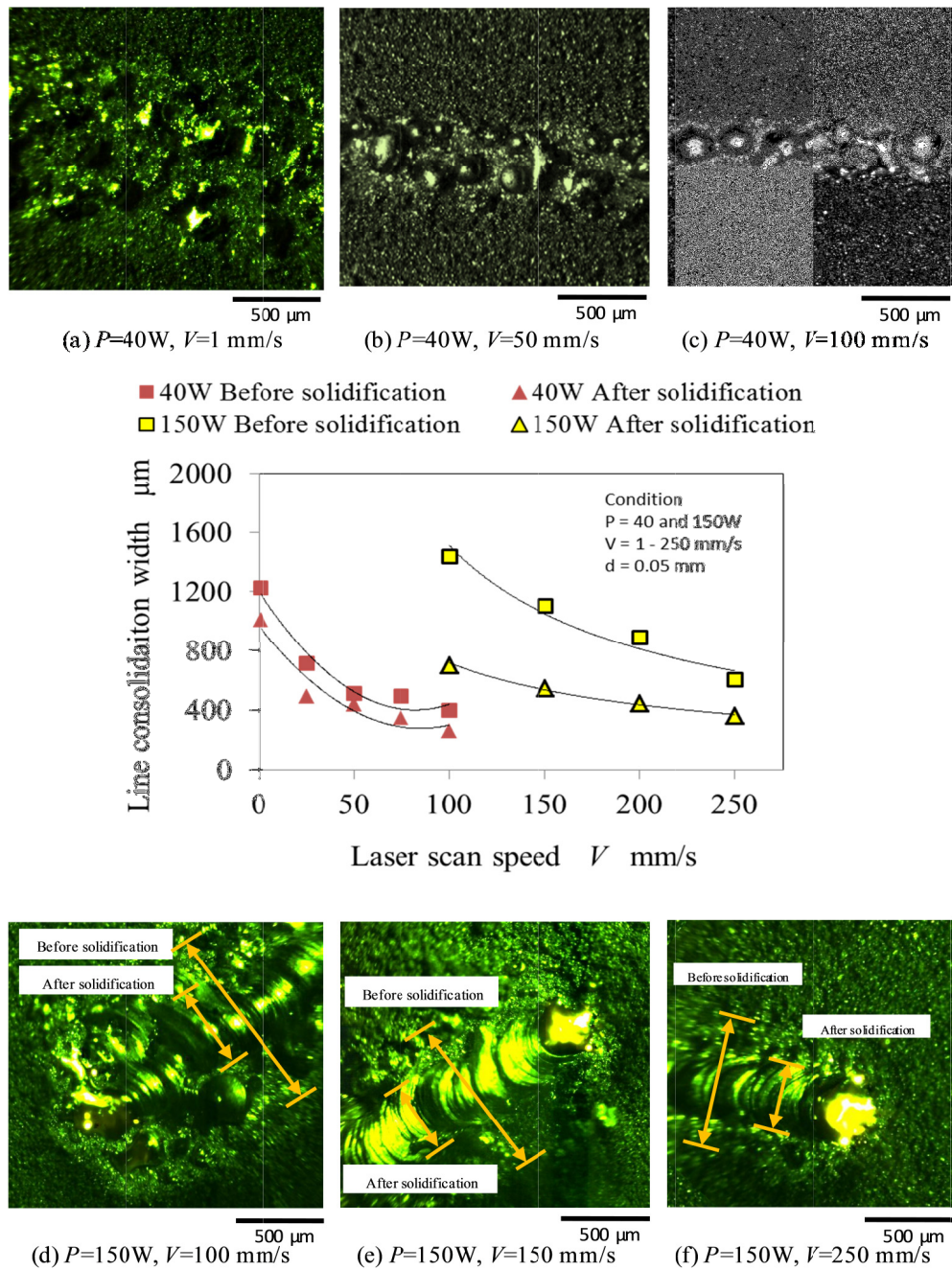


Fig. 5.25 Influence of laser scan speed on line consolidation width

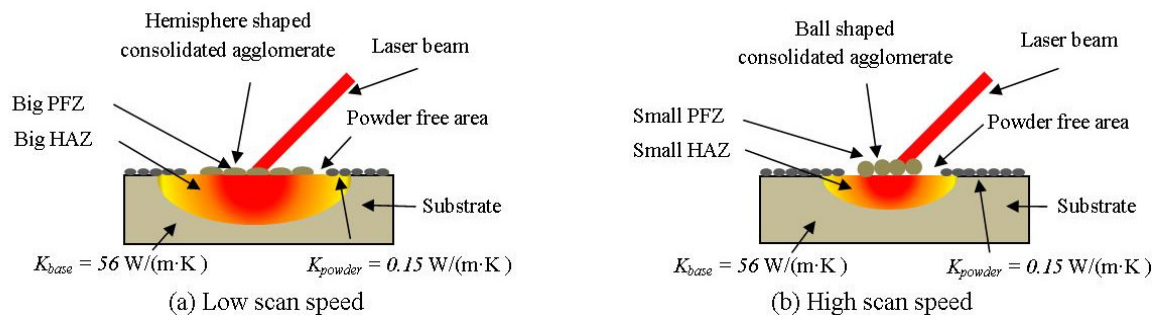


Fig. 5.26 Schematic of laser irradiation on substrate

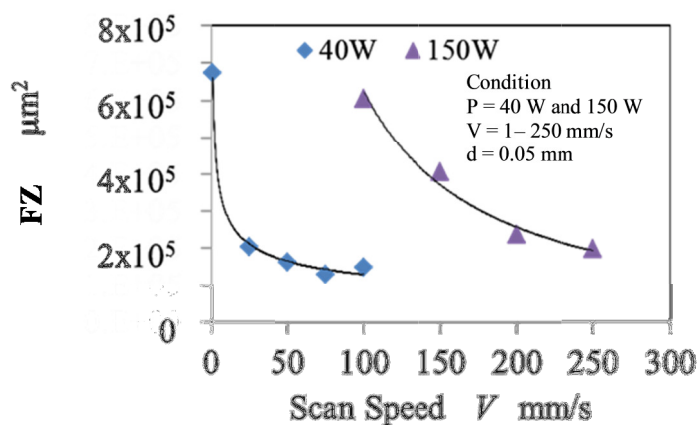


Fig. 5.27 Influence of scan speed on the FZ

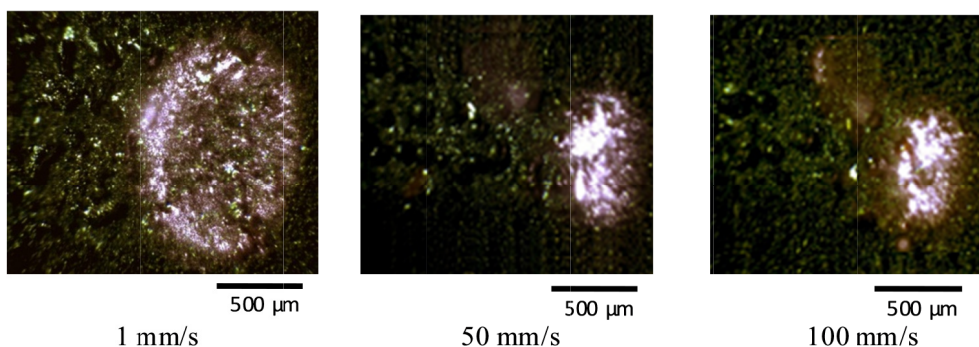


Fig. 5.28 Influence of scan speed on the FZ

In order to explain this behavior, Fig. 5.26 schematically illustrates the FZ and the interaction between laser beam, metal powder and substrate. It is also important to note that the substrate had high thermal conductivity,  $K_{\text{base}}=56 \text{ W}/(\text{m}\cdot\text{K})$  in comparison to the metal powder  $K_{\text{powder}}=0.15 \text{ W}/(\text{m}\cdot\text{K})$ . Therefore, during the heat transfer process, the radial direction of heat transfer mainly occurred through the conduction. This is accomplished through the substrate material.

The influence of scan speed when the scan speed was varied from 1 to 250 mm/s is illustrated in Fig. 5.27. The figure shows at both laser power of 40 W and 150 W, the FZ is decreasing with the increase of scan speed. Graphically, the line consolidations with the FZ images at 1 mm/s, 50 mm/s and 100 mm/s when laser power was 40 W are shown on Fig. 5.28. The region was substantially large when the scan speed was 1 mm/s. However, the value reduced significantly with the increase of scan speed and was almost constant as approaching 100 mm/s. Higher temperature on the irradiated spot caused more localized heating when the scan speed was low in comparison to high scan speed. At low scan speed, the metal powder melted as the greater amount of heat was generated due to laser irradiation to the powder surface. With the increase of scan speed, less heat was transferred to the FZ. This was due to reduced interaction time between the laser and the metal powder. In terms of splattering, significant splattering was observed with the increase of scan speed.

During the start of laser irradiation, the skin or the outermost layer of powder particles were initially liquefied. As more heat absorbed by powder particles, the powder particles coalesced with their surrounding particles forming hemisphere shaped consolidated agglomerate. During the formation, surrounding powder particle was attracted together. Due to increase of the molten powder volume ratio within the FZ, formation of liquid/melt pool

occurred. As a result, viscosity of the liquid/melt pool increased. This caused the flow of the molten powder to move under the influence of the surface tension.

Fig. 5.29 shows consolidation of metal powder when the laser power was set at 40 W and at scan speed of 50 mm/s. The consolidation was recorded at 2 ms intervals. With the increase of scan speed, there was less interaction time between the laser beam and metal powder within the irradiation spot. As a result, only a limited amount of the outer layer of the metal powder was transformed to liquid. This is attributed to the shorter exposure time of the metal powder to the laser beam. Hence, low volume fraction of molten powder was produced. At this point, it was observed that surface tension significantly caused the molten powder particles on its surrounding region to form consolidated agglomerates. As the volume fraction of liquid melt was increasing and sufficiently high, the flow more rapidly toward the center. Surface tension in the SLS/SLM is created due to the attraction force that exists between molten powders. During the movement, the neighboring metal powder stuck to the molten powder surface and attracted together.

Fig. 5.29 shows that the flowing of molten powder toward the center occurred more prominently when the scan speed was increased. Other than that, the tendency of balling to occur increased at the higher scan speed. At the scan speed of 50 mm/s, most of the molten powder still wet on the surface. However, at the higher speeds, some of the molten powders formed ball-shaped consolidated agglomerate. This agglomerates also well known as balling phenomena in the SLS/SLM. It is one of the most common defects in the SLS/SLM because of spheroidisation of the liquid melt pool. Some molten balls formed at this speed tended to coalesce to the substrate surface. However, some of them could be easily being removed as the metal powder was cleaned from the substrate.

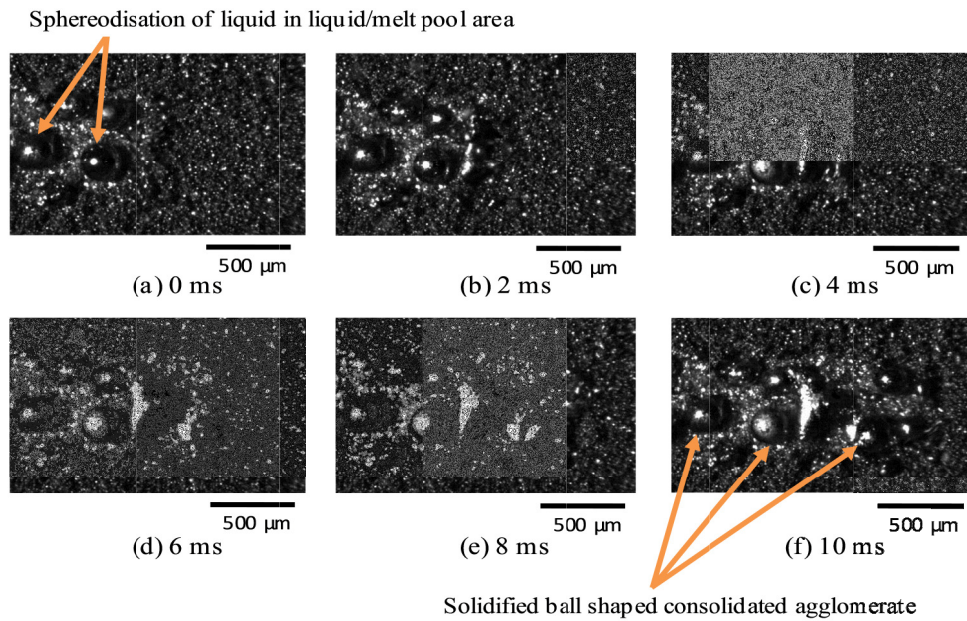


Fig. 5.29 Line consolidation at  $P=40$  W and  $V=50$  mm/s

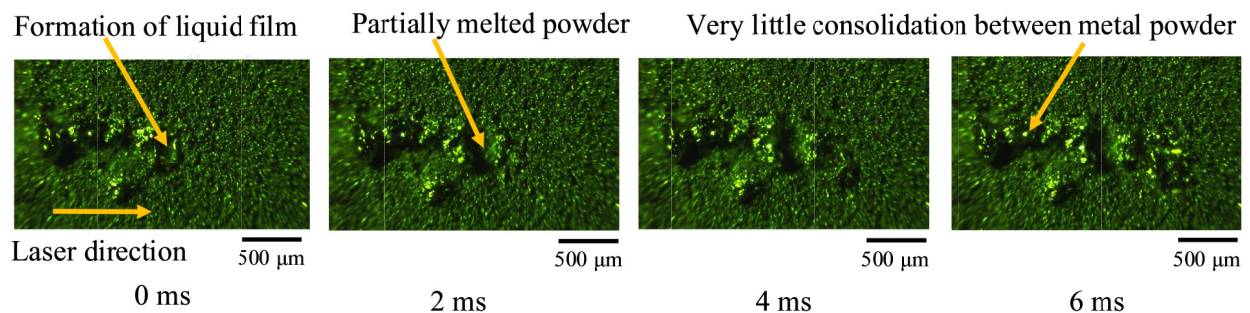


Fig. 5.30 Line consolidation at  $P=10$  W and  $V=50$  mm/s

In order to demonstrate the consolidation at the low laser power, 10 W of laser power was used. Fig. 5.30 shows a sequence of the metal powder consolidation at 2 ms interval. Sintering between the metal powder particles took place as the temperature was recorded below the melting point. Only small amount of liquid films between the powder particles was formed after the laser irradiation.

With the increase of laser power, a more continuous and rigid consolidated structure was obtained. This differs from the structure when low laser power was used. This is demonstrated in the consolidation transformation at 100 W and 150 W as illustrated in Fig. 5.31, Fig. 5.32 and Fig. 5.33. The figures show consolidation of metal powder at 4 ms interval. The figure shows the formation started with the movement of metal powder towards the center of the laser beam. Comparison between laser power at 100 W and 150 W when the scan speed was 100 mm/s indicates that a more consistent width was obtained at the laser power of 100 W. Combination of 150 W and 100 mm/s seems to be unsuitable to produce a good structure. High laser power with relatively low speed caused the structure was heated too long at the irradiation region. This led to re-melting of previously formed structure and big FZ. As a result, distortion and inconsistency of line width were observed.

However, as the scan speed was increased to 250 mm/s, a more continuous and consistent consolidated structure was recorded with the high-speed camera. This is depicted in Fig. 5.33. Higher speed of 250 mm/s compared to 100 mm/s allowed the heat from the laser beam to be transferred to the metal powder and the substrate material at the appropriate time. At the high laser power also, the melt pool could be observed and the size was enlarging with the increase of laser power.

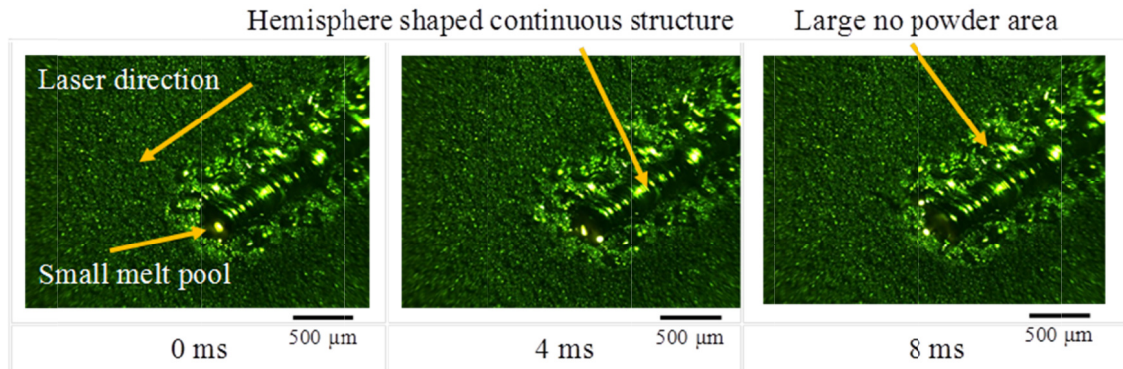


Fig. 5.31 Line consolidation at  $P=100$  W and  $V=100$  mm/s

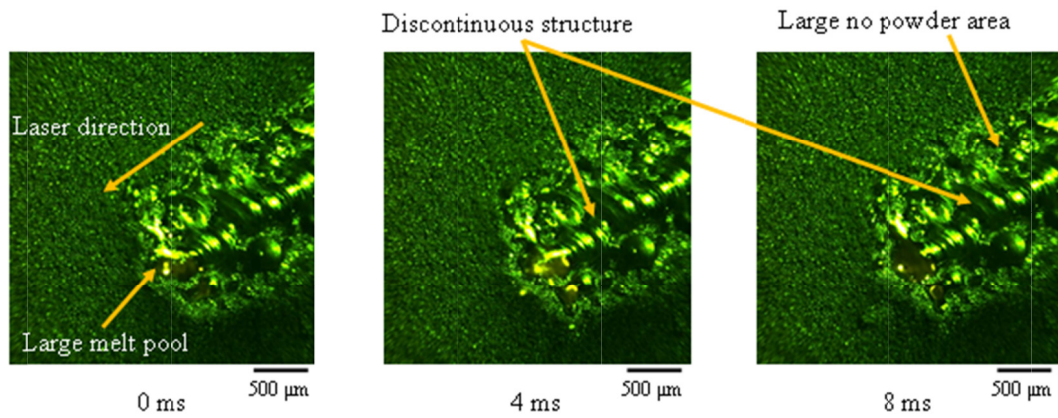


Fig. 5.32 Line consolidation at  $P=150$  W and  $V=100$  mm/s

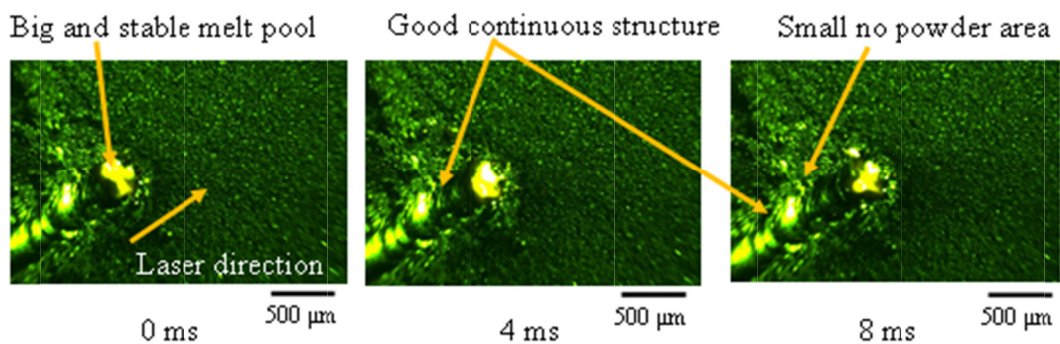


Fig. 5.33 Line consolidation at  $P=150$  W and  $V=250$  mm/s

5.3.1.4 Influence of Surface Condition

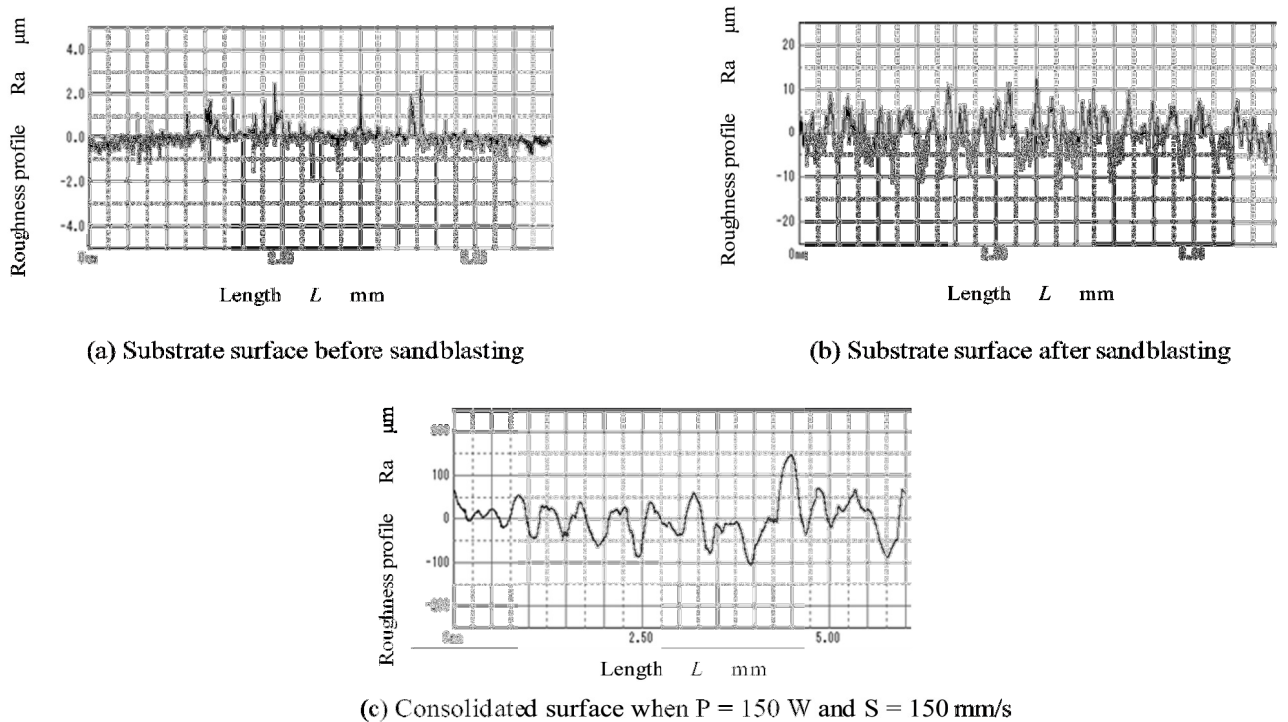


Fig. 5.34 Surface roughness of different surface conditions

Since in the SLS/SLM process involves the laser irradiation on the different surface condition, it is essential to understand the influence of the surface condition. The substrate surface was sandblasted in order to improve wettability of the molten metal. The surface roughness of the surface at different surface condition is shown in Fig. 5.34. The thickness of the metal powder was maintained at 50  $\mu\text{m}$ . The first layer consolidation on was made on the sandblasted substrate surface. In contrast, the second layer was performed on the consolidated surface. Comparison was made between the first and the second layer consolidation. This is shown on the Fig. 5.35 and Fig. 5.36 respectively.

The first layer consolidation on the sandblasted substrate surface produced a relatively continuous and straight structure. This was attributed to the smooth substrate surface as shown in Fig. 5.35. The surface roughness,  $Ra$  before sandblasting was  $0.2155 \mu\text{m}$ , after sandblasting was  $2.4893 \mu\text{m}$  and the roughness of the consolidated surface was  $9.0229 \mu\text{m}$ . During consolidation process, faster movement of the metal powder was observed on the sandblasted substrate surface in comparison to the consolidated surface. This is due to a better surface finish of the sandblasted substrate. In contrast, formation of the subsequent structure on the consolidated surface showed movement of the metal powder relatively slower compared to on the sandblasted substrate surface at the same processing setting. There was increased splattering contributed by the collision of the molten metal to the rough surface of the bottom layer. Furthermore, at high laser power, the movement of melt pool and its surrounding metal powder is relatively dependent by the quality of the surface condition. The line consolidated structure distorted and not continuous compared on the when the laser is irradiated on the sandblasted substrate surface. This is demonstrated in Fig. 5.36.

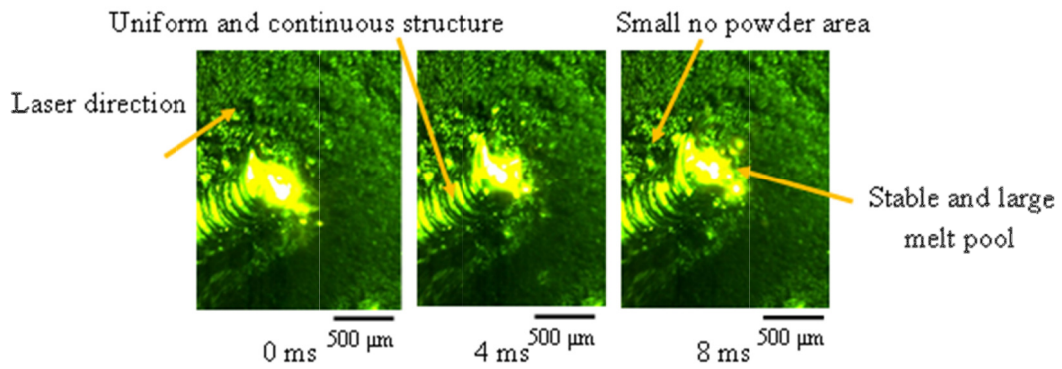


Fig. 5.35 Line consolidation on substrate surface at  $P = 150 \text{ W}$  and  $V = 150 \text{ mm/s}$

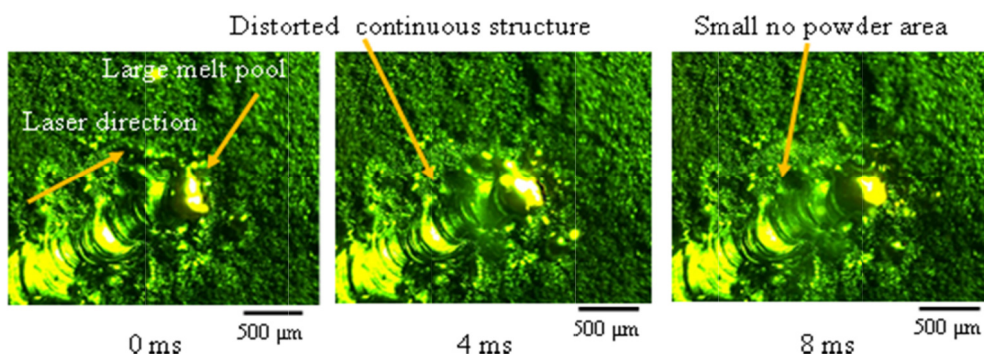


Fig. 5.36 Line consolidation on consolidated surface at  $P = 150 \text{ W}$  and  $V = 150 \text{ mm/s}$

### 5.3.1.5 Influence of Layer Thickness

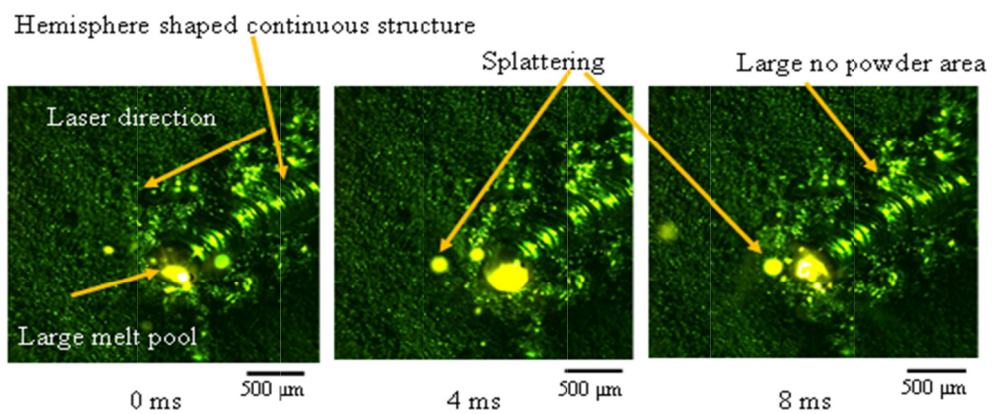


Fig. 5.37 Line consolidation at  $P = 150 \text{ W}$ ,  $V = 150 \text{ mm/s}$ ,  $t = 0.10 \text{ mm}$

The thickness of metal powder is one of the parameters that was investigated by researchers such as by [20],[21],[22]. However, the study did not emphasize on visualization of the consolidation process at different thickness. In this research, process visualization using the high-speed camera with the thickness from 0.05 to 1.00 mm was made. The consolidation at the thickness of 0.05 mm was previously shown in Fig. 5.35. Therefore, the following describes the process visualization at the thickness of 0.10, 0.20 and 1.00 mm.

Layer thickness of 0.10 mm permitted higher amount of metal powder supplied to the laser irradiation region compared to when the layer thickness was set at 0.05 mm. Therefore, the depth of the melt pool was greater. As a result, a higher thickness of consolidated material was attained with relatively a hemisphere shaped structure. Chaotic movement of the melt pool was also observed. Furthermore, significant splattering of the molten powder was produced at the layer thickness of 0.10 mm. As mentioned earlier, the high splattering was not desirable as subsequent laser sintering/melting was affected and contributed to the surface irregularities. The sequence of high-speed image is illustrated in Fig. 5.37.

Consolidation of metal powder at the thickness of 0.20 mm is shown in Fig. 5.38. This was induced by additional and continuous metal powder supply during laser irradiation. However, examination of the high-speed images indicates increasing of splattering occurred as the laser beam irradiated on the relatively thicker metal powder. The splattering of metal was unavoidable during SLS/SLM. Increasing amount splatter was not preferable as it contributed to the surface irregularities. As a result, overall consolidation process and surface quality were affected when the successive line consolidation was performed. This was because the splattered molten powder either adhered to the consolidated surface of produce a ball-shaped agglomerate that was scattered on the powdered surface. The figure shows the splattered molten powder in the radial direction.

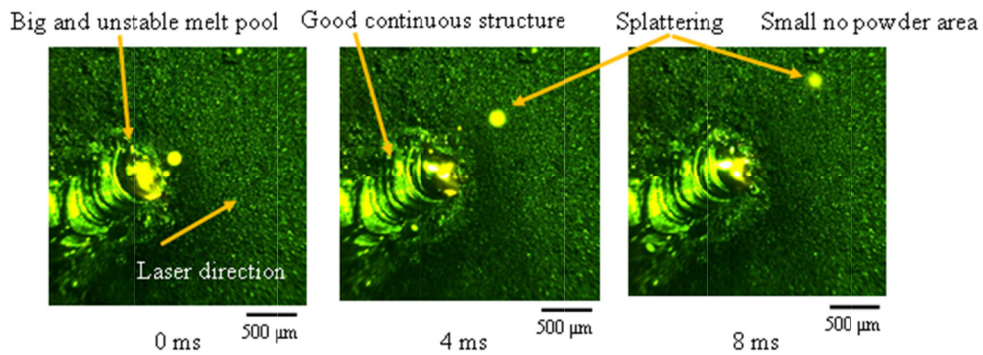


Fig. 5.38 Line consolidation at  $P = 150$  W,  $V = 150$  mm/s,  $t = 0.20$  mm

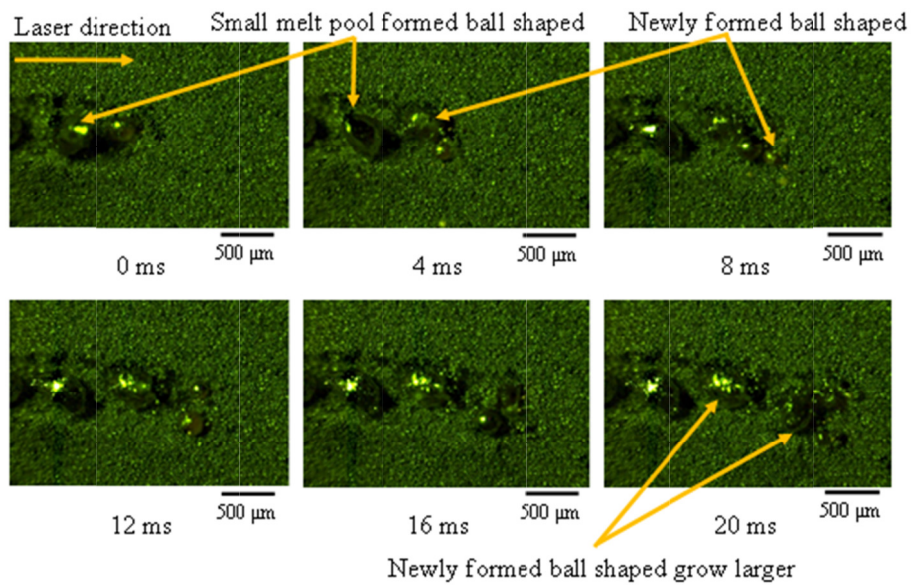


Fig. 5.39 Line consolidation at  $P = 40$  W,  $V = 1$  mm/s,  $t = 1.00$  mm

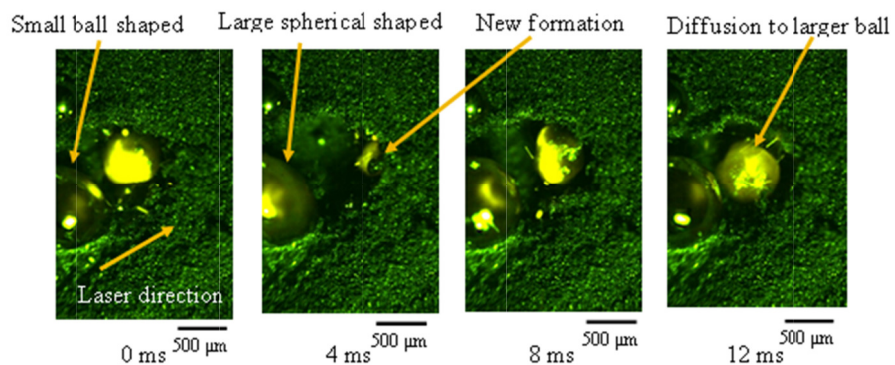


Fig. 5.40 Line consolidation at  $P = 150$  W and  $V = 150$  mm/s,  $t = 1.00$  mm

When the thickness of metal powder was sufficient very high for SLS/SLM at 1 mm, the laser beam irradiation on the metal powder caused the metal powder to change to a liquid state. Due to the surface tension, the molten powder was transformed to spherical shaped. Successive laser irradiation on the metal powder caused molten powder diameters to increase in its size as illustrated in the Fig. 5.39. The spherical shaped molten solidified as the laser beam moved away from the irradiation area. As the laser power was increased to 150 W, the diameters and formation were more prominent. The sizes grew larger as the smaller tended to move and diffuse to the greater one. This is illustrated in Fig. 5.40.

In analyzing the influence of the thickness in the SLS/SLM, it is important to note that a large amount of air exists entrapped within the metal powder. When the metal powder particles melted, the air trapped as bubbles [20]. Therefore, at low layer thickness, penetration of the laser beam to the bottom layer is larger. As a result, a greater amount of energy was transferred to the metal powder on the laser-irradiated region and around its immediate vicinity. Hence, it led the molten powder, to a higher degree of melting [21]. In the case of high layer thickness, the penetration was low. Greater amount of energy was transferred to the metal powder without sufficient wetting to the substrate surface. Accordingly, a spherical shaped molten powder was produced. With the increment of the layer thickness also, the most apparent difference observed was the significant amount of splattering and consistency of the consolidated width. This was induced by the greater amount of air existed in the loose powder of thicker layer. Due to laser irradiation on the metal powder, the air was trapped and recoiled. Consequently, the metal powder was splattered. On the other hand, consistency of the consolidated width was accomplished caused by the continuous metal powder supplied during laser irradiation.

### 5.3.2 Area Consolidation

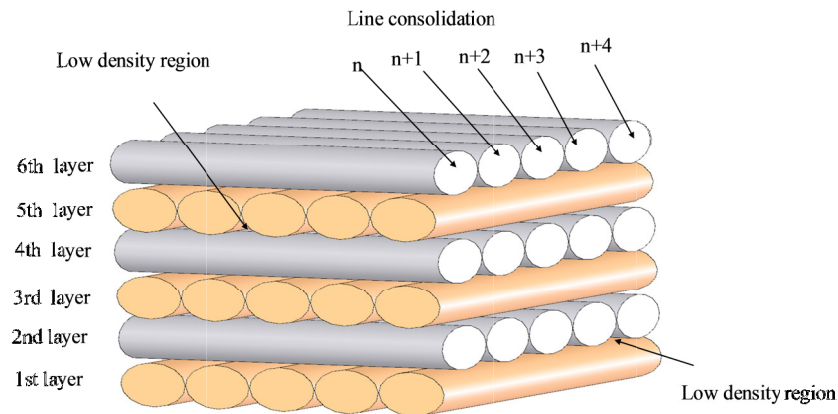


Fig. 5.41 Schematic of low density region in area consolidation

In order to ensure a successful 3D part fabrication, area consolidation is essential. In this research, other than line consolidation, area consolidation was also monitored so that the actual laser sintering/melting process could be visualized. Therefore, instead of having only one single line during laser beam irradiation, the laser was irradiated successively next to each other at the distance of the hatching size. Throughout the experiment, the hatching size was maintained at  $45\ \mu\text{m}$ . The experimental setup was similar as previously elaborated.

Previous shown results indicated that after laser irradiation on metal powder, a line structure was formed with the width varies range from  $250\ \mu\text{m}$  to  $600\ \mu\text{m}$ . This depended on the processing condition used. However, the size of the laser beam was  $45\ \mu\text{m} \times 64\ \mu\text{m}$  (due to laser orientation), and the hatching size was  $45\ \mu\text{m}$ . Therefore, in area consolidation, previously formed structure was wider than the hatching size. As a result, the laser beam was actually being irradiated on the formed consolidated structure repeatedly with additional metal powder continuously sintered/melted to produce a new structure. Hence, the laser line consolidated structure overlapped, and the melted powder bonded to the other lines structure

near its surroundings. The low-density region is schematically illustrated in Fig. 5.41. Utilizing the high-speed camera allows these overlapping to be visualized.

Similar to the line consolidation, when the laser beam was irradiated on the metal powder, localized heating at laser irradiated area was initiated. Localized heating that occurred at very short duration of time and low laser power produced insufficient energy. This caused merely sintering of the metal powder. Laser sintering only liquefied particle surface, but the powder particle core remained unchanged. Laser melting in contrast thoroughly transformed all metal powder particles to a liquid state. This enhanced the flow of the molten metal. During area consolidation, repeated process where the structure undergone the iterative process of being reheated, re-sintered/ re-melted and re-solidified as the uppermost layer of the metal powder being irradiated with the laser beam. In this stage, the layer experienced the re-melting process. Due to the existence of pore between the structure, the molten metal flowed towards pore filling. As a result, densification of the material occurred.

### *5.3.2.1 Area Consolidation Mechanism*

During the SLM/SLS, material state changed from solid state (powder) to semi-liquid state or liquid state (molten powder) then back solid state (consolidated). In contrast to the line consolidation, area consolidation involves existence of additional semi-liquid state and solid state on laser irradiated area due to prior sintering/melting of the adjacent consolidated tracks. Therefore, the analysis of the mechanism that occurred during laser beam interaction becomes more complex. Analysis of the high-speed camera images revealed that the area consolidation could be linked to line consolidation. Furthermore, SLS/SLM involves layer-

by-layer laser irradiation and powder deposition. Each subsequent consolidation of a new layer occurs on the top of the previously formed surface. As a result, the bottom layer experienced these different changes repeatedly until the 3D object was fabricated.

Main region in area consolidation is presented in Fig. 5.42. The region represents typical stages involved at any instantaneous point during the area consolidation process. The figure shows within the fusion zone, both powder fusion and re-melting/re-sintering of previously formed consolidated tracks are heated. Re-melting/re-sintering of the structure occurred within overlapping region. When the laser power was increased, fusion zone was bigger causing larger re-melting/re-sintering area. Furthermore, it was observed that, in area consolidation, laser was irradiated on the semi-liquid molten metal rather than directly on the metal powder. This was due to prior adjacent laser irradiation on metal powder at the distance of 45  $\mu\text{m}$  of hatching size. Repetitive laser irradiation melted the metal powder and re-melted the liquid metal to a higher degree of melting. As a result, the molten metal penetrated into the underlying structure through porosity that existed between solid structures and between line consolidation tracks. Accordingly, a better surface roughness of the consolidated surface was attained.

Observation on the high-speed images indicates the existence of relatively large size of the powder-free area. Successive laser irradiation on molten metal further improved its spread and wettability with the substrate surface. As the irradiation continued, the tendency of laser irradiation made on substrate material only was very high. Therefore, there was no metal powder supplied to the melt pool area and a small amount of the molten metal inside the area. As a result, a non-uniform surface structure was produced. This non-uniform structure could contribute to the existence of the low-density region, which then formed the

porous area. With repetitive laser irradiation, the phenomena periodically occurred. Proper selection of processing parameters could reduce the periodical existence of these porous areas.

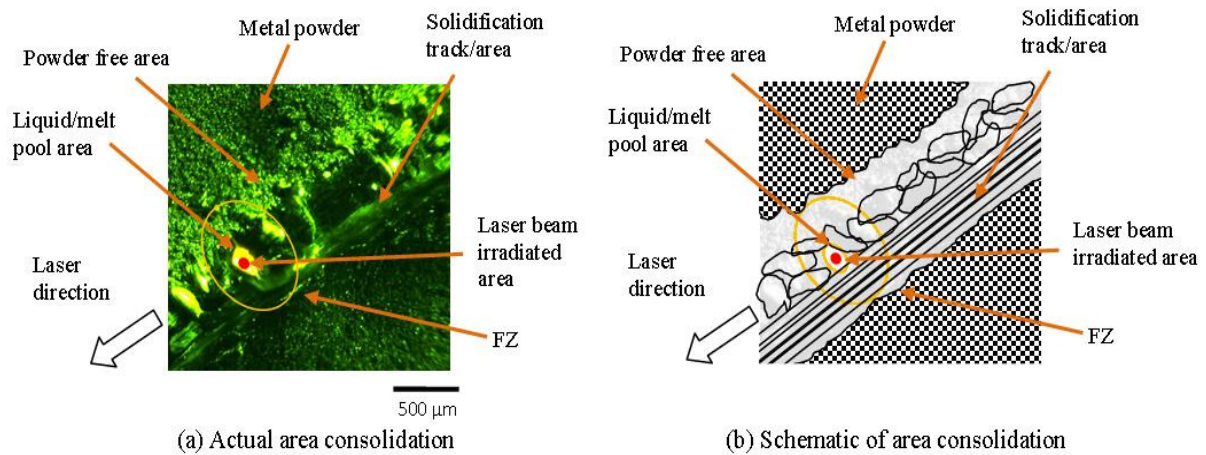


Fig. 5.42 Main region and stages in area consolidation structure

Differ from the line consolidation, the area consolidation mechanism was more complicated. This was because throughout the successive laser irradiation process, changes of the metal powder to sintering, melting and solidification occurred continuously and periodically. Furthermore, significant overlapping region and different phase changes contributed to the complexity of the area consolidation mechanism.

Initially, the metal powder already experienced liquid film formation, although the location was not within the FZ. The formation was mainly due to prior adjacent track consolidation, which affected the neighboring metal powder. As the position of the metal powder nearer to laser beam area and within the FZ, a higher amount of liquid was formed due to increase of temperature. As a result, movement of the metal powder occurred. Due to the temperature differences between the center and edge near laser irradiated area, surface tension existed between these regions. Hence, movement of the metal powder from the edge toward the center of the laser beam was observed.

When the metal powder was irradiated at high energy density, the metal powder transformed to the liquid state. Hence, the melt pool was formed. Chaotic flow was due to the movement of molten powder under the influence of high temperature. Later, the spreading of the liquid melt was observed. The previously formed consolidated track was also re-melted. The higher temperature enhanced its flow and spread on the surface. This allowed the molten powder penetration through the porosity within the consolidated material.

The melt pool was transformed to the liquid cylinder under the influence of the surface tension. Nevertheless, due to its instability, the liquid cylinder tended to break into little drops [19]. At this stage also, the small ball diffused to the bigger one caused by Ostwald ripening phenomena. Later, wetting of the ball shape drops occurred where they coalesced with the substrate. Hence reduced its thickness and increased wetting contact area to the substrate surface. As the laser beam moved away from the melt pool, solidification of the molten powder took place. Solidification caused the shrinkage of the molten powder and reduced its size. Some of the molten powder adhered to the previously formed track due to its spread and most of them to the substrate surface. Due to the entrapped gases within the molten powder, pores were scattered within the consolidated structure.

Similar to the line consolidation, the melt pool and the FZ are important phenomena in the area consolidation. At low laser power below than 20 W, melt pool was very small and difficult to be observed. The melt pool area was increasing with the increment of laser power. The relationship of the melt pool area during the area consolidation is presented in Fig. 5.43. The figure shows the FZ increases significantly compared to the melt pool. This is more apparent when the laser power was 150 W. As a result, the difference between the FZ and the melt pool was relatively high. This indicates the heat was effectively transferred in the radial direction. Too high energy difference between the FZ and the melt pool caused the heat to be

dissipated radially too fast. Hence, the amount of energy within the melt pool was not enough to cause good consolidation of metal powder.

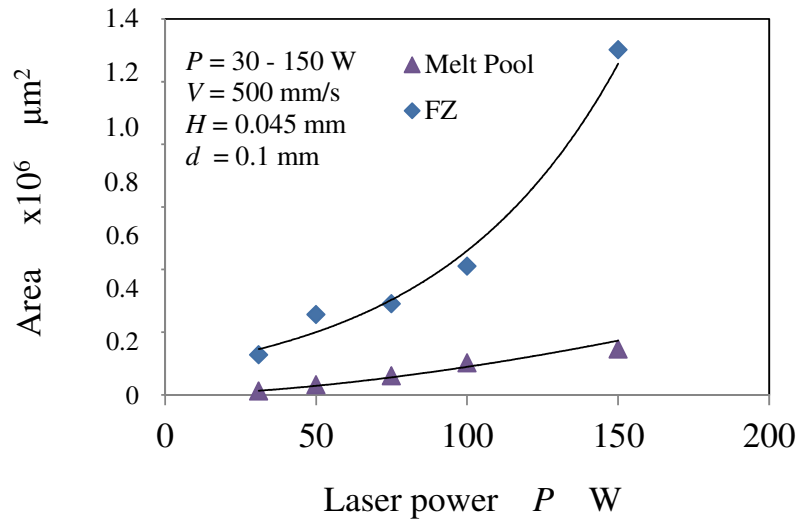


Fig. 5.43 Melt pool area and FZ at various laser setting during area consolidation

In the area consolidation, the melt pool developed during SLS/SLM was larger than the melt pool during the line consolidation at the same laser conditions. This was caused by the sintering/melting of prior adjacent tracks significantly changed the metal powder to the molten metal and increased its temperature. Therefore, successive laser irradiation on the next track further improved the degree of melting and viscosity of the previously formed track. As a result, the melt pool was larger. This was because the amount of liquid formations within the melt pool was a function of temperature. The temperature was dependent on laser processing condition such as laser power, scan speed, hatching size and others. In this experiment, this phenomenon was observed to be more prominent at high laser power and low scan speed. Higher temperature increased the viscosity of the melt pool and improved its rheological characteristics to enhance its flow and spread. Besides, its penetration through

porosity was also improved. Consequently, a more dense consolidated structure and better surface roughness was obtained.

### *5.3.2.2 Influence of Processing Parameters*

Fig. 5.44 shows a series of the area consolidation process of metal powder at 50 W and 500 mm/s. Similar observation in the line consolidation was found in the area consolidation. The powder was attracted towards the center of the laser beam. However, in the area consolidation, adjacent line irradiation already formed a structure, which was wider than the size of the laser beam diameter of 45  $\mu\text{m}$ . Hence, subsequent laser irradiation was beamed on the previously formed structure. As a result, a small amount of metal powder started to be liquefied and coalesced with the existing consolidated structure. A relatively low laser power did not able to re-melt the previously formed structures to molten state again and only reheated them. The melt pool during laser irradiation is indicated by the arrow on the figure. At the laser power 50 W, the structure formed ball shaped agglomerate during the area consolidation. Consequently, this produced irregular protruded surface after the solidification completed. The consolidation behavior of the metal powder when laser power was increased to 100 W is shown on Fig. 5.45. The figure indicates more elongated consolidated agglomerate instead a ball-shaped structure as previously observed at laser power of 50 W.

Formation of the consolidated structure was more prominent with the higher amount of overlapping during laser movement. It was also clear that the melt pool produced bigger than spot size of the beam diameter. Thus, the high temperature within melt pool was observed to re-melt formerly produced adjacent tracks and overlapped to each other. The melt pool is indicated by an arrow in the figure. The melt pool flowed and spread between successively

formed tracks. Hence, the molten powder flowed and filled the porosity. Consequently, it decreased the porosity and escaped the entrapped gas. As a result, more continuous and smooth consolidated structure was obtained compared to when the laser power was 50 W. As the laser power was increased further to 150 W during area consolidation, smoother surface formation was observed. The transformation of the metal powder is shown in Fig. 5.46. Sequence of the images shows that a high amount of molten metal produced at elevated laser power. Viscosity of the liquid melt increased due to higher laser energy was irradiated on the localized region. A larger melt pool and FZ were observed when the laser power was set at 150 W in comparison when the laser power was set at 100 W. The melt pool is indicated by an arrow. Successive laser irradiation on the previously formed consolidated structure had re-melted the structure again. Metal powder on its surrounding was also attracted toward the center of the laser beam. Combination of the re-melting of the structure and uninterrupted flow of molten powder on its surrounding occurred. This enabled relatively a good continuous structure formation as illustrated in the figure.

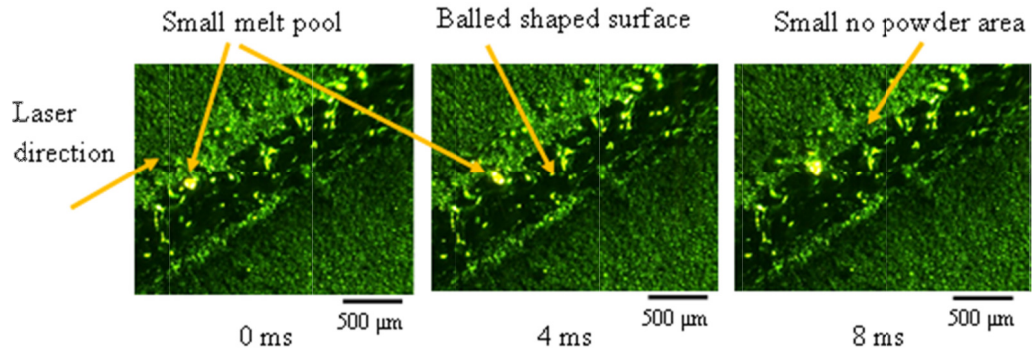


Fig. 5.44 Area consolidation at  $P=50$  W and  $V=500$  mm/s

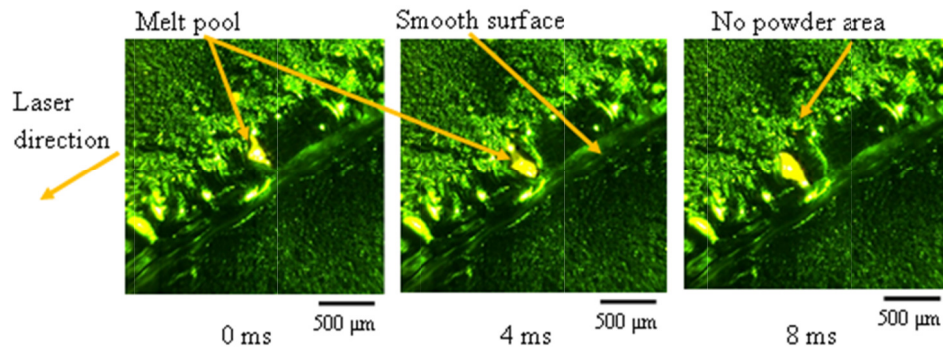


Fig. 5.45 Area consolidation at  $P=100$  W and  $V=500$  mm/s

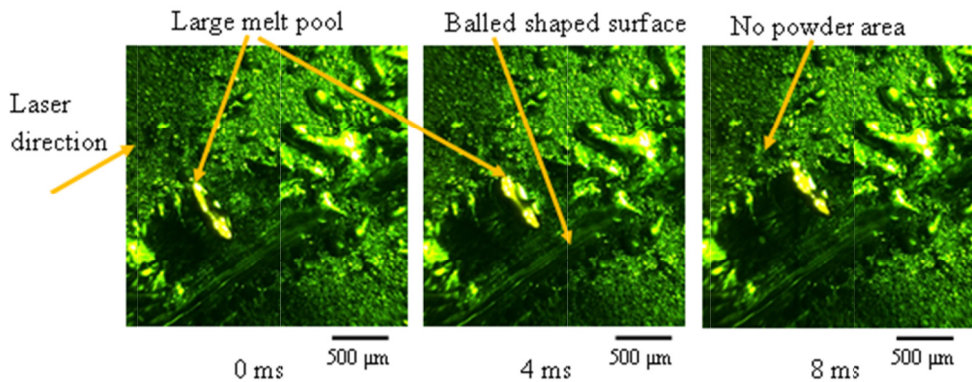


Fig. 5.46 Area consolidation at  $P=150$  W and  $V=500$  mm/s

## 5.4 CONCLUSIONS

Consolidation characteristics of ferrous-based metal powder during SLM/SLS were successfully monitored and analyzed with the utilization of a high-speed camera. Based on the study, the mechanism of metal powder consolidation within a FZ under the influence of the laser beam was explained. It can be concluded that

1. Despite challenges in acquiring process visualization of SLS/SLM due to temperature, area and accessibility constraint, it is demonstrated that it is feasible through proper equipment design and experimental setup. The SLS/SLM visualization revealed consolidation mechanisms that occurred during laser irradiation, and the subsequent solidification after the laser moved away from laser irradiation area.
2. The FZ is an important characteristic in the SLS/SLM process due to all microstructural, changes and the transformation of the metal powder to a consolidated structure occurring in this region. The result showed the line consolidation width was approximately the same diameter as the FZ diameter. Within FZ, existence of melt pool was observed.
3. The melt pool, which is located inside the FZ, is the most important behavior observed. This is due to the flow and spread of molten metal occurs within this region. The melt pool formed during laser irradiation relatively larger than the size of the spot size of the laser beam. The melt pool was observed to increase with energy density.
4. High temperature is required to melt the metal powder to form a good and continuous structure. However, too high temperature caused overheating of the laser irradiation area. At too high temperature, the heat was transferred radially at the rate where it affected the surrounding metal powder. As a result, a poor consolidated structure was produced.
5. Line consolidation width, FZ and splattering are increasing with the increase of laser

power. In contrast, with the increase of scan speed, the result is vice versa. At low power, the tendency of balling formation is also higher with the increase of scan speed. This is due to a lack of wettability of the molten powder with the substrate surface. As a result, poor consolidation between the metal powders due to less interaction time between the laser beam, metal powder and substrate that can prompt a reaction to occur. Line consolidation width, the FZ and splattering behavior are related to the heat transfer process that occurred during the interaction of the laser beam, metal powder and substrate surface.

6. Surface condition affected the width and the quality of the consolidated structure. During the laser irradiation, the movement of the metal powder was not smooth on the rough surface. As a result, a distorted consolidated structure was obtained. This was also attributed to the wettability of the molten metal, which is affected by the surface roughness.
7. With the increase of layer thickness, splattering occurs more prominent, and the movement of the metal during laser irradiation shows more chaotic without proper wetting with the substrate surface.
8. During the area consolidation, overlapping of the line consolidation occurred due to wide line consolidation compared to the hatching distance. Overlapping of the consolidated track lead to better surface finish as the overlapping pattern produces the continuous structure. Nevertheless, improper selection of the laser parameters caused a large FZ, which then lead to periodic occurrence of the porous area.
9. Relation between the FZ and the melt pool determined the ability of the metal powder to produce a relatively good and continuous structure. Too large FZ signifies large amount of the heat dissipates to the substrate and its surroundings. Hence, a poor quality of consolidated structure was obtained. In contrast, too small FZ caused the low ability of

the molten powder to consolidate. Therefore, optimization of the laser parameters through observation of the FZ and the melt pool is important so that a good continuous consolidated structure could be produced.

## REFERENCES

- [1] C. Hauser, T. H. C. Childs, C. M. Taylor, and M. Badrossamay, "Direct Selective Laser Sintering of Tool Steel Powders to High Density: Part A - Effects of Laser Beam Width and Scan Strategy," in *Proceedings of Solid Freeform Fabrication Symposium (SFF)*, 2003.
- [2] T. H. C. Childs, C. Hauser, and M. Badrossamay, "Selective laser sintering (melting) of stainless and tool steel powders: experiments and modelling," *Proc. Inst. Mech. Eng. Part B J. Eng. Manuf.*, vol. 219, no. 4, pp. 339–357, Jan. 2005.
- [3] F. Bayle and M. Doubenskaia, "Selective Laser Melting process monitoring with high speed infra-red camera and pyrometer," in *Proc. of SPIE Vol. 6985, 698505*, 2008, vol. 6985, no. 33, pp. 698505–698505–8.
- [4] J. P. Kruth, P. Mercelis, J. Van Vaerenbergh, and T. Craeghs, "Feedback control of Selective Laser Melting," in *Proceedings of the 3rd International Conference on Advanced Research in Virtual and Rapid Prototyping*, 2007, pp. 1–7.
- [5] J. P. Kruth, J. Duflou, P. Mercelis, J. Van Vaerenbergh, T. Craeghs, and J. De Keuster, "On-line monitoring and process control in selective laser melting and laser cutting," in *Proceedings of the 5th Lane Conference, Laser Assisted Net Shape Engineering*, 2007, pp. 23–27.
- [6] P. Lott, H. Schleifenbaum, W. Meiners, K. Wissenbach, C. Hinke, and J. Bültmann, "Design of an Optical system for the In Situ Process Monitoring of Selective Laser Melting (SLM)," *Phys. Procedia*, vol. 12, pp. 683–690, Jan. 2011.
- [7] Y.-C. Hagedorn, N. Balachandran, W. Meiners, K. Wissenbach, and R. Poprawet, "SLM of Net-Shaped High Strength Ceramics: New Opportunities For Producing Dental Restorations," in *Proceedings of the Solid Freeform Fabrication Symposium*, 2011, pp. 536–546.
- [8] T. Craeghs, S. Clijsters, J.-P. Kruth, F. Bechmann, and M.-C. Ebert, "Detection of Process Failures in Layerwise Laser Melting with Optical Process Monitoring," *Phys. Procedia*, vol. 39, pp. 753–759, Jan. 2012.

- [9] Y. Chivel, "Optical In-Process Temperature Monitoring of Selective Laser Melting," *Phys. Procedia*, vol. 41, pp. 897–903, Jan. 2013.
- [10] D. Rosenthal, "The theory of moving sources of heat and its application to metal treatment," *Trans. ASME*, p. 849, 1948.
- [11] J. P. Kruth, P. Mercelis, J. Van Vaerenbergh, L. Froyen, and M. Rombouts, "Binding mechanisms in selective laser sintering and selective laser melting," *Rapid Prototyp. J.*, vol. 11, no. 1, pp. 26–36, 2005.
- [12] J. P. Kruth, L. Froyen, J. Van Vaerenbergh, P. Mercelis, M. Rombouts, and B. Lauwers, "Selective laser melting of iron-based powder," *J. Mater. Process. Technol.*, vol. 149, no. 1–3, pp. 616–622, Jun. 2004.
- [13] M. Khan and P. Dickens, "Selective laser melting (SLM) of gold (Au)," *Rapid Prototyp. J.*, vol. 18, no. 1, pp. 81–94, 2012.
- [14] E. O. Olakanmi, "Selective laser sintering/melting (SLS/SLM) of pure Al, Al–Mg, and Al–Si powders: Effect of processing conditions and powder properties," *J. Mater. Process. Technol.*, vol. 213, no. 8, pp. 1387–1405, Aug. 2013.
- [15] T. Furumoto, T. Ueda, M. R. Alkahari, and A. Hosokawa, "Investigation of Laser Consolidation Process for Metal Powder by Two-Color Pyrometer and High-Speed Video Camera," *CIRP Ann. - Manuf. Technol.*, vol. 62, no. 1, pp. 223–226, Jan. 2013.
- [16] B. Xiao and Y. Zhang, "Marangoni and Buoyancy Effects on Direct Metal Laser Sintering with a Moving Laser Beam," *Numer. Heat Transf. Part A Appl.*, vol. 51, no. 8, pp. 715–733, Apr. 2007.
- [17] M. Rombouts, J. P. Kruth, L. Froyen, and P. Merce, "Fundamentals of Selective Laser Melting of alloyed steel powders Fundamentals of Selective Laser Melting of alloyed steel powders," *CIRP Ann. - Manuf. Technol.*, vol. 55, no. 1, pp. 187–192, 2006.
- [18] A. Mills, K.C., Keene, B.J., Brooks, R.F., Shirali, "Marangoni effects in welding, in Marangoni and interfacial phenomena in materials processing," *IOM Commun.*, 1998.
- [19] H. J. Niu and I. T. H. Chang, "Instability of scan tracks of selective laser sintering of high speed steel powder," *Scr. Mater.*, vol. 41, no. 11, pp. 1229–1234, Nov. 1999.
- [20] A. N. Chatterjee, S. Kumar, P. Saha, P. K. Mishra, and A. R. Choudhury, "An experimental design approach to selective laser sintering of low carbon steel," *J. Mater. Process. Technol.*, vol. 136, no. 1–3, pp. 151–157, May 2003.
- [21] D. Gu and Y. Shen, "Processing conditions and microstructural features of porous 316L stainless steel components by DMLS," *Appl. Surf. Sci.*, vol. 255, no. 5, pp. 1880–1887, Dec. 2008.
- [22] I. Yadroitsev and I. Smurov, "Selective laser melting technology: From the single laser melted track stability to 3D parts of complex shape," *Phys. Procedia*, vol. 5, pp. 551–560, Jan. 2010.

# **CHAPTER 6 : PROPERTIES OF CONSOLIDATED STRUCTURE**

## **6.1 INTRODUCTION**

Since the advancement of AM technology, there are many types of materials have been developed. This is to pursue a high quality product for various functional requirements. In the early development of AM, polymer has been used extensively as raw material. Later, metal powder and ceramic binder were used as more demand for functional parts in rapid manufacturing applications. Similarly, in the SLS/SLM, the potential of a developing metal part directly is high due to its distinctive capability compared to other AM processes. However, the main bottlenecks are accuracy and appropriate material properties that give the best properties that comparable to bulk materials. Critical factors in AM are the material capability, accuracy and surface finish [1]. Various types of materials have been investigated by researchers for use in the SLS/SLM. In addition, many SLS/SLM machine manufacturers develop their own material alloy and mixture to be used with their respective machine. Comparison of the properties of commercial materials were made by [2],[3]. Other researchers also reported properties of pure metal, for instances SUS304 [4], SUS316 [5], Inconel [6] and magnesium [7].

The application of different types of materials used in the SLS/SLM process requires detail studies on the consolidated material properties. This reveals its potential and limitation.

Porosity is main shortcomings associated with the material produced via the SLS/SLM. In this research, the drawback of porosity in the consolidated material is used as a value added feature so that the materials can also be used for any specific engineering applications. There are many engineering applications where the porous materials from other manufacturing processes are well known and have been to be utilized. Some of these engineering applications are as filters, flow control devices, breathers, pressure equalizers, flame arrestors, spargers, rollers, fluidizers, gauge snubbers, silencers and others.

Recently, there has been a great interest in developing an injection mold using AM due to its capability in reducing the product development time. Conventionally, the injection mold is manufactured through subtractive process utilizing Computer Numerical Control (CNC) system. With the advent of computer-aided design (CAD) and various rapid tooling technologies, current mold manufacturing technique starts to be fabricated using the additive process. In fact, SLS/SLM, which is also known as one of the fast growing Rapid Tooling (RT) technologies due to its potential for mold development. A number of research investigates the potential of SLS/SLM capability and the developing injection mold from different aspects as reported by [8],[9],[10],[11],[12].

One of applications where the porosity characteristics of the materials may be optimized is in the development of permeable structure in the mold manufacturing. In the development of the injection mold, the porous area may be used as a breather, to remove air bubbles from the injection mold. This enables some common problems associated with injection-molded part such as blister, sink mark, air trap, short shot and other can be improved. The permeable mold insert is an innovation in mold manufacturing techniques. The inserts are sintered and pre-hardened with 20 to 30 % porosity. Within the gas permeable mold material, interconnected micron-sized pores are dispersed.

Since the introduction of the gas permeable mold steel insert in the mold manufacturing, many mold manufacturers start to integrate the insert in their mold. The insert allows effective flow of entrapped gas. There are a number of industries supplying this type of materials to the mold making manufacturers such as [13],[14] and [15]. The inserts manufactured by these companies range from 0.25 to 0.50 inch in diameter, produced in cylindrical shapes, and available at the predetermined sizes. Nevertheless, the utilization of the permeable insert requires a secondary process. Hence, the mold needs to be machined and the insert being placed manually at any possible problematic locations. This is rather time consuming compared to the SLS/SLM where the permeable area and mold can be manufactured simultaneously in a single setup.

The effectiveness of the permeable mold insert encourages rapid manufacturing researchers to develop the permeable mold directly from CAD data using the SLS/SLM. This is because mold manufacturing through additive manufacturing enables simultaneous reduction of mold manufacturing time and improved injection-molded part quality. The SLS/SLM has a very high potential to be developed as permeable mold, owing to its capability of sintering and melting powder metal with a controlled amount of porosity. Therefore, a number of research studies permeability of the consolidated part manufactured via the SLS/SLM [16],[17],[18],[19],[20].

In this research, ferrous-based material has been used as the main material for investigation. Chapter 4 discusses the consolidation process of metal powder using a high-speed camera. The result showed the formation of the consolidated structure with potential of producing relatively weak structure with high surface irregularities. These will affect the properties of the material. Therefore, in this Chapter 5, the properties of the consolidated material manufactured via SLS/SLM are investigated for the development of injection mold.

In this research, properties of the material with respect to surface quality, permeability, hardness and strength were evaluated. The permeability was studied in order to investigate its feasibility of developing the gas permeable structure through SLS/SLM. The relations of properties to the porosity and the processing parameter were analyzed.

## 6.2 EXPERIMENTAL SETUP

### 6.2.1 Surface Quality Observation

Surface quality is one of the technical barriers that currently faced by the relatively new process as SLS/SLM. In order to perform the surface quality observation, the samples with various laser parameter settings were prepared. The sample size is 10 mm x 10 mm as shown in Fig. 6.1. The top surface and bottom surface were observed using an optical microscope and scanning electron microscope (SEM). Furthermore, the samples were sectioned in the middle (indicated by X-X) when the examination on the cross section was required. The samples were prepared under the setting conditions as tabulated in the Table 6.1.

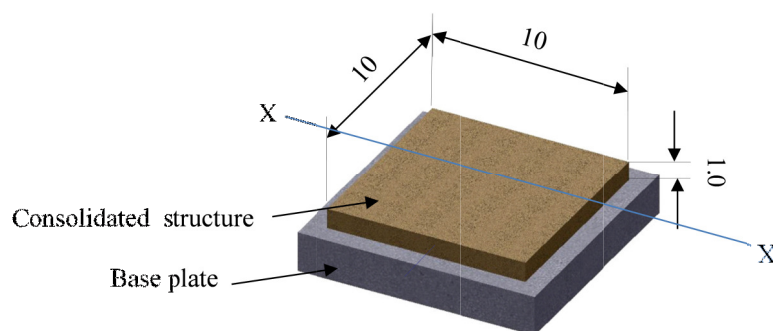


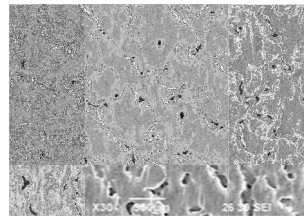
Fig. 6.1 Sample preparation for surface quality observation

Table 6.1 Setting condition used in samples preparation

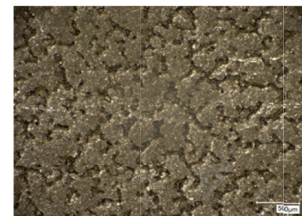
Model		LUMEX 25C
Type		Yb: fiber (CW)
Wavelength [nm]	$\lambda$	1070
Beam diameter	$\phi$	0.1 - 0.4
Power [W]	$P$	100 - 500
Scan speed [mm/s]	$V$	444 - 4500
Hatching distance [mm]	$H$	0.045
Scan length [mm]	$L$	5
Processing atmosphere		N <sub>2</sub>



(a) Optical microscope image of consolidated surface before wire cut



(b) SEM image of consolidated surface before wire cut



(a) Optical microscope image of consolidated surface after wire cut

Fig. 6.2 Example of surface quality observation

The surface quality observation was performed using a SEM equipment model JSM-6390LVU manufactured by JEOL Ltd and Keyence digital microscope VHX-1000. The material was sectioned using a wire cut machine model AQ325L by Sodick Co. Ltd. The

utilization of wire cutting is important in order to reveal the actual porosity and surface quality of the consolidated surface. Studies have proven that subsequent post-processing of porous material is significant so that a correct interpretation of porosity can be made [13]. Sufficient porosity can be revealed through wire EDM. Other secondary processes such as grinding and milling might alter the surface quality and close the porous area. Therefore, throughout the experiment, the wire EDM was used. Examples of the observation are illustrated in Fig. 6.2. The figure shows the surface quality when  $P=200$  W,  $V=1000$  mm/s,  $d$ =spot size 0.1 mm and  $H=0.045$  mm.

### 6.2.2 Roughness

Surface roughness is another problem associated with parts manufactured via the SLS/SLM. In this research, the surface roughness of 2D and 3D profiles were evaluated using Surfcom 2000DX2. The equipment was manufactured by Tokyo Seimitsu Co. Ltd. The conditions that were set during the 2D and 3D profiles measurements are tabulated in Table 6.2 and Table 6.3 respectively. The measurement was made 5 times, and average value was calculated.

Table 6.2 Setting condition for 2D profile measurement

Travelled distance [mm]	6
Travelled speed [mm/s]	0.3
Return speed [mm/s]	6

Table 6.3 Setting condition for 3D profile measurement

Measured area [mm]	2 x 2
Travelled speed [mm/s]	0.3
Return speed [mm/s]	6
Y pitch [mm]	0.005
X pitch[mm]	0.0010

### 6.2.3 Permeability

Permeability,  $\mu$  is the measurement of the flow resistance through a material. In the experiment, the permeability describes how easily the compressed air is able to move through the porous consolidated material. The permeability of the porous material can be associated to Darcy`s Law that describes the flow of a fluid which can be applied in the analysis of the porous material [21]. Theoretically, Darcy`s Law is given by the following Eq. 5.1. The relation between the parameters described is presented in the Fig. 6.3.

$$\text{Permeability, } \mu = \eta \cdot \frac{\delta}{A} \cdot \frac{Q}{p_1 - p_2} \quad (5.1)$$

where

$\mu$  = permeability ( $\text{m}^2$ )

$Q$  = flow rate ( $\text{m}^3/\text{s}$ )

$A$  = the cross sectional of area to flow ( $m^2$ )

$p_1 - p_2$  = pressure difference (Pa)

$\delta$  = thickness of the permeable structure (m)

$\eta$  = viscosity of the fluid (Pa·s)

The specification of the consolidated material that was prepared as the specimen for permeability test is shown in Fig. 6.4. The material was prepared in a circular shape with the diameter of 60 mm. The thickness of the specimens was 3.5 mm. The outer region of the specimens prepared at a melting condition whereas the inner region was a porous material that was prepared at a sintering condition. The sintering region was prepared by using various processing parameters in order to investigate the effect of the different processing parameters on the permeability. In contrast, the melting region was manufactured at the setting of  $P=200$  W,  $V=444$  mm/s,  $d=0.1$  mm,  $H=0.045$  mm. The condition for specimen preparation is as tabulated in Table 6.1.

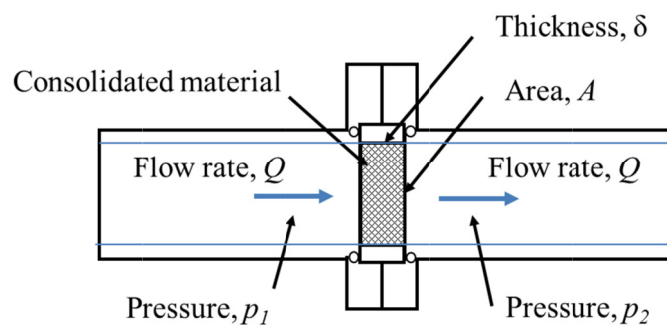


Fig. 6.3 Fluid flow in porous medium and its relation to Darcy`s Law

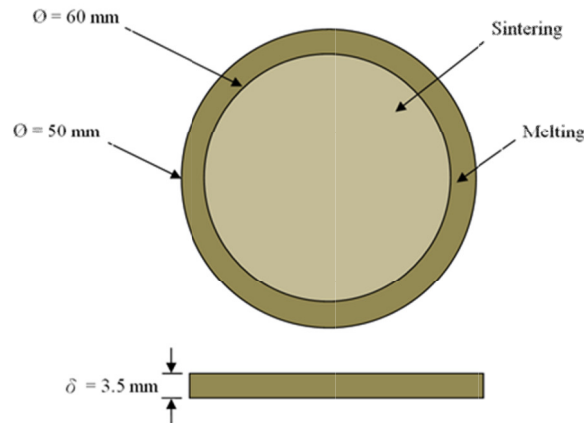


Fig. 6.4 Permeability specimen specification

Table 6.4 Condition for test specimen preparation

Condition		Melted area	Sintered area
Scan speed [mm/s]	$V$	444	500 - 4000
Laser power [W]	$P$	200	300
Spot size [mm]	$d$	0.1	0.1
Hatching space [mm]	$H$	0.045	0.045

The schematic of permeability test setup is depicted in Fig. 6.5. The compressed air from the compressor flowed through a control valve and then traveled through a pressure regulator in order to control the amount of the air that flowed to the test holder. A flow meter was used to confirm and maintain the flow rate of the compressed air, prior to its flow inside the specimen test holder. When the specimen was mounted inside the test holder, the specimen separates the test holder into two different chambers. The chambers contained the pressured air before and after flowing through the porous consolidated material. In order to analyze the permeability of the specimen, the pressure at each chamber was measured with a

pressure transducer. The pressure transducer was also connected to the oscilloscope for pressure measurement. The specimen test holder was designed and fabricated to measure the permeability of the prepared specimen. The sectional view of the specimen test holder is shown in Fig. 6.6.

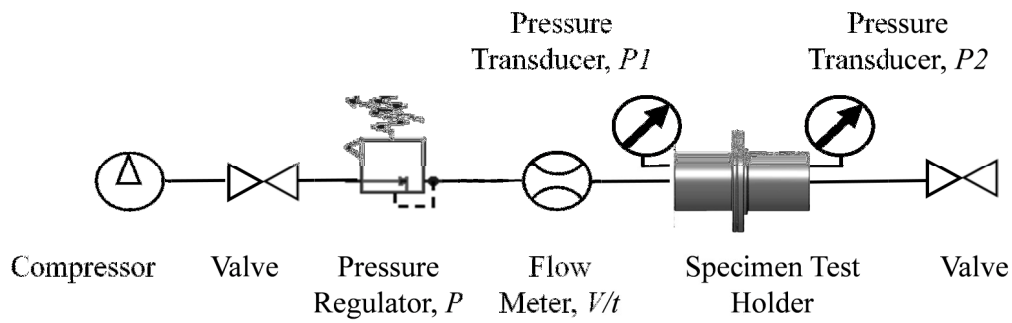


Fig. 6.5 Schematic of permeability measurement setup

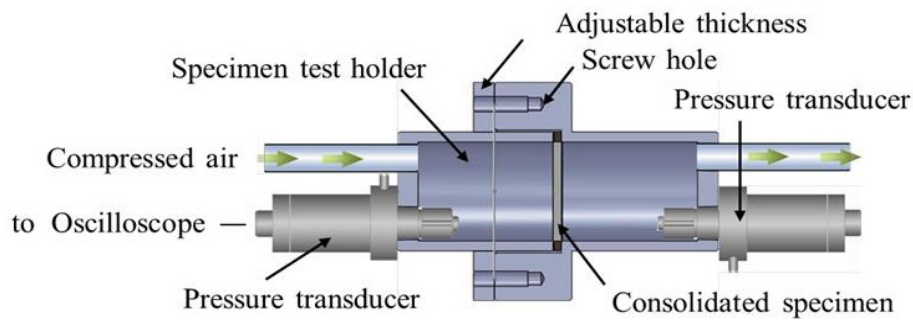


Fig. 6.6 Permeability specimen test holder

Table 6.5 Condition for permeability measurement

Pressure [MPa]	$p$	0.3
Flow [L/min]	$Q$	4
Temperature [C]	$T$	20
Viscosity [Pa · s]	$\eta$	$18.2 \times 10^{-6}$

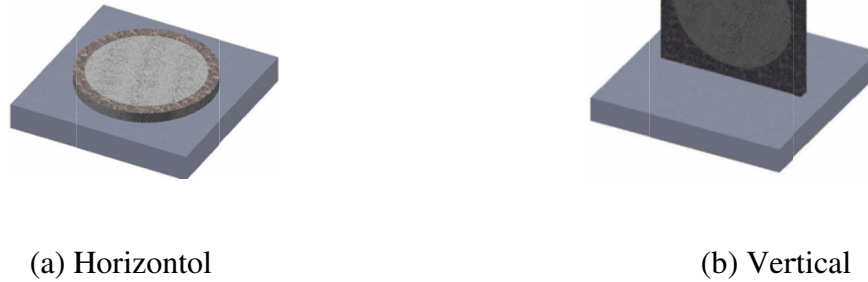


Fig. 6.7 Specimen orientation during consolidation process

The condition used throughout the permeability measurement is as tabulated in Table 6.5. During the specimen preparation, the orientation of the specimen was in horizontal. In order to investigate the influence of the specimen orientation, the permeability of the consolidated material was also investigated at vertical orientation. The orientation of the specimen is shown in Fig. 6.7. The processing parameters, sintering area diameter and thickness, were maintained in both orientations so that the permeability results were comparable.

#### 6.2.4 Hardness

Hardness tests were performed with measurement on different areas on the consolidated structure, and the average values were taken. Testing machine micro-hardness from Mitutoyo Corporation (HM-101) was used during the hardness test. Previous study showed that the hardness of the material varies with its position from the surface. The hardness of the consolidated material on the external surface was superior to the inner surface. In addition, the internal surface has uniform hardness [22]. Therefore, the hardness values were measured

at various positions of the inner surface of the consolidated material cross section since the hardness values are more consistent.

### **6.2.5 Strength**

Capability to operate and withstand certain design limit indicates the performance of any material. Hence, investigation of the strength of the material is crucial. The strength of the material was evaluated with regard to the Japan Standard JIS Z2201-2011 : Tensile specimen metal material. The specification of the strength test specimen is as illustrated in the Fig. 6.8. The length of the specimen was 100 mm with width of 12.5 mm and thickness of 4 mm. The end part of the specimen was manufactured using melting condition of laser power 200 W and scan speed 444 mm/s. Whereas, the sintering part, was prepared with laser power of 300 W and scan speed that varied from 500 mm/s to 4000 mm/s. All the specimens for the strength test used spot size of 0.1 mm and hatching size 0.045 mm. The detail of the laser parameters used for preparation of the strength test specimen is same as previously illustrated in Table 6.1. Fig. 6.9 shows the tensile machine used in the experiment. Strength test machine that was used in the experiment was AUTOGRAPH AG-X/R manufactured by Shimadzu Co. During the strength test experiment, the speed was set 0.05 mm/s.

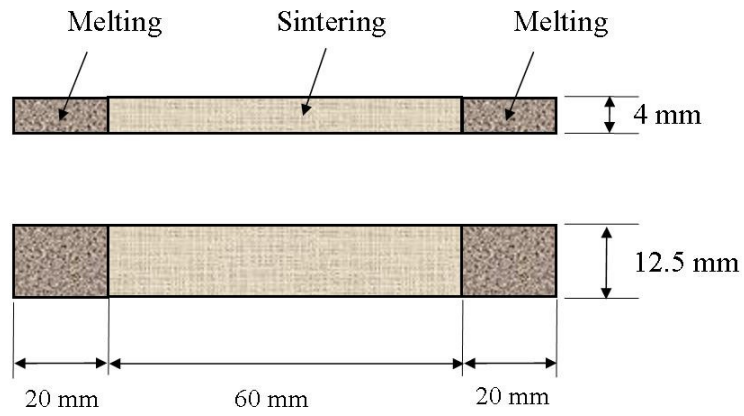
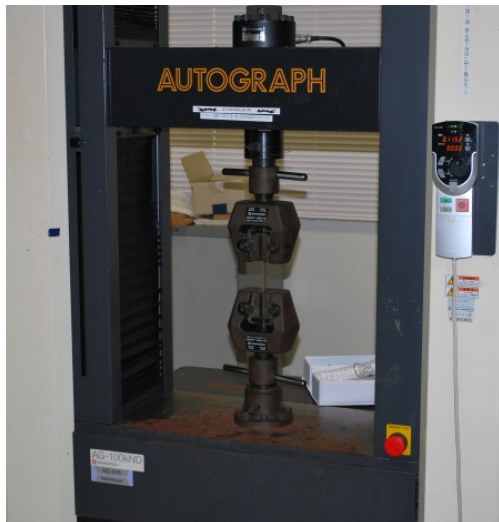


Fig. 6.8 Specimen specification for strength test



(a) Tensile machine



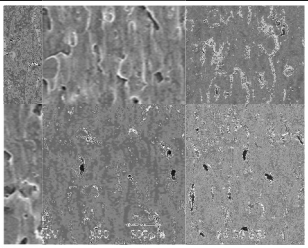
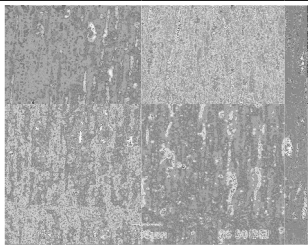
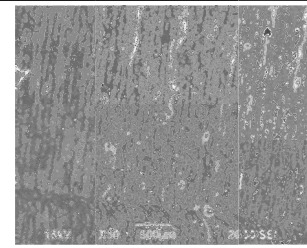
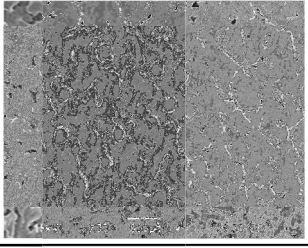
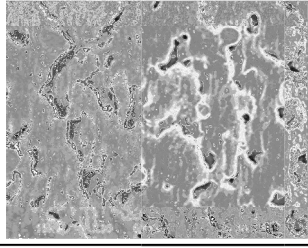
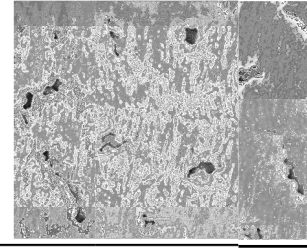
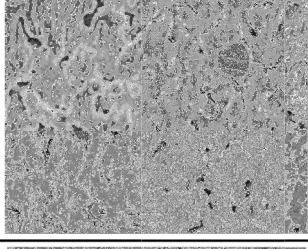
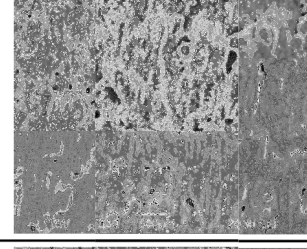
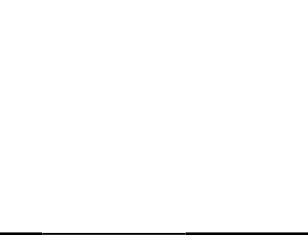
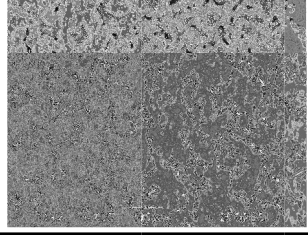
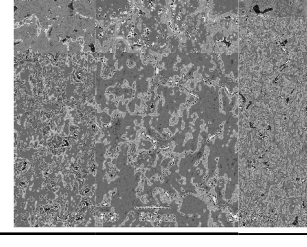
(b) Specimen during tensile test

Fig. 6.9 Specimen during strength test

### 6.3 EXPERIMENTAL RESULTS AND DISCUSSION

#### 6.3.1 Surface Quality Observation

Table 6.6 Influence of laser power and scan speed on surface quality

		Laser power		
		200W	300W	400W
Scan speed	1000 mm/s			
	2000 mm/s			
	3000 mm/s			
	4000 mm/s			

Using SEM and optical microscope, observation was made on the consolidated material that was produced via the SLS/SLM. Influences of processing parameters were investigated. The surface quality observation is tabulated in Table 6.6.

### *6.3.1.1 Influence of Laser Power*

Surface quality observation of the consolidated material was studied. The influence of the laser power when the scan speed was set at 1000 mm/s shows the existence of pores within the material reduced with the increase of the laser power. At 200 W, the porosity scattered randomly on the surface. However, as the laser power was increased, a denser structure was produced. Similar behavior was observed when scan speed was constant at 2000 mm/s. As shown in the figure, the size of the agglomerate was increasing with the rise of laser power. When the scan speed was set at 2000 mm/s and power of 200 W also, high amounts of pores were produced, but the sizes were relatively small. In contrast, at 400 W the sizes of pores were larger but the amount of the pore was less.

### *6.3.1.2 Influence of Scan Speed*

Influence of scan speed was studied at laser power 200 to 400 W. On the other hand, the scan speed was varied range from 1000 mm/s to 4000 mm/s. It was observed that denser surface obtained when scan speed was set at 1000 mm/s. An increment in the scan speed reduced the energy density per unit area. As a result, the accumulated energy within the laser-

irradiated area was low. This was not enough to allow the smooth flow of the molten metal. Hence, the surface quality deteriorated.

### 6.3.1.3 *Influence of Laser Spot Size*

The influence of the laser spot size on parameters the surface quality was investigated. It is known that the combined effect of laser scan speed, laser power and hatching size can be presented by the energy density. Therefore, in investigating the influence of the laser spot size, the energy density was set at  $1.5 \text{ J/mm}^2$  and hatching size at 0.045 mm. The laser power and scan speed were changed in order to equate the energy density value. For 0.1 mm spot size, the laser power,  $P$  was set at 300 W and scan speed,  $V$  at 2000 mm/s. At different laser spot size, following setting was used 0.2 mm ( $P=300 \text{ W}$ ,  $V=1000 \text{ mm/s}$ ), 0.3 mm ( $P=270 \text{ W}$ ,  $V=600 \text{ mm/s}$ ) and 0.4 mm ( $P=300 \text{ W}$ ,  $V=500 \text{ mm/s}$ ) was set accordingly. The result is shown in Fig. 6.10. The SEM image shows that the surface quality of the consolidated material with the increase of the laser spot size. At 0.1 mm laser spot size, existence of porosity was observed. However, the amount of porosity at bigger laser spot size reduced.

The phenomena were obtained due to the overlapping phenomena occurred on the consolidated surface during laser irradiation. When the laser spot size was sufficiently high, wider line consolidation was produced. Therefore, a successive adjacent line irradiation produced a bigger overlapped region between former line and the newly consolidated line. In contrast, when the laser spot size is small, amount of the overlapped region was reduced. The bigger overlapped region allowed the molten metal to flow and penetrate through the porosity resulting in the denser consolidated material. This is illustrated in Fig. 6.11.

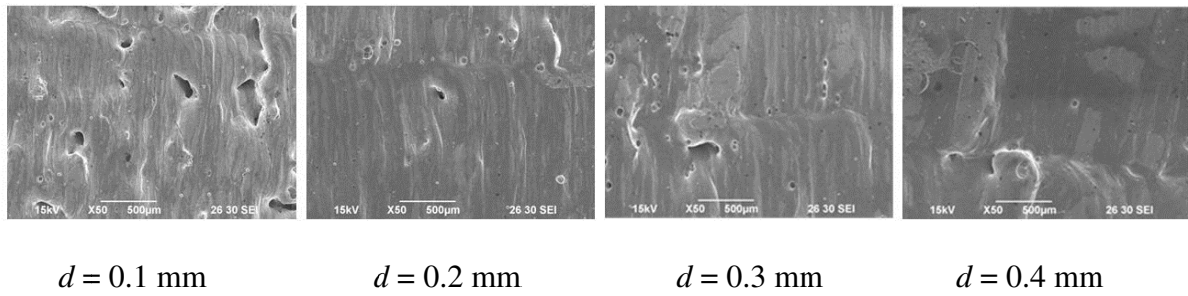


Fig. 6.10 Influence of laser spot size

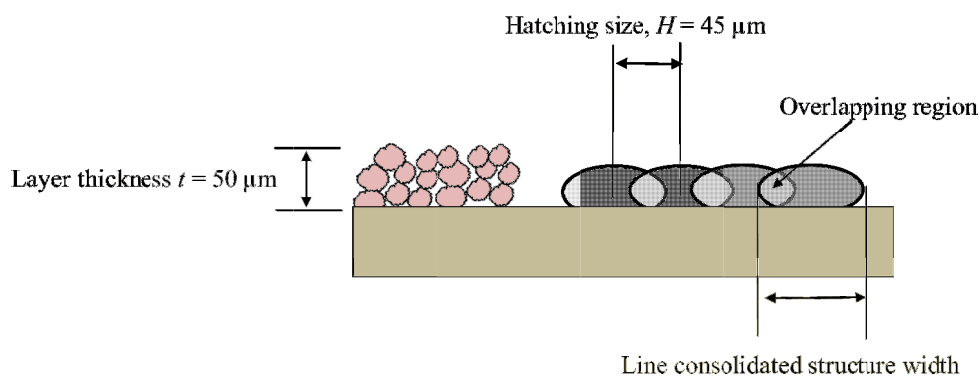


Fig. 6.11 Influence of overlapping region

### 6.3.2 Surface Roughness

The tendency of the permeable structure to have poor surface roughness is high due to the existence of porosity on the consolidated surface. Nevertheless, most of the engineering applications require relatively good surface roughness so that post processing can be minimized. Therefore, observation on the surface quality of the consolidated material was made at a higher magnification. This is depicted in Fig. 6.12 with their respective measured temperature. The figure shows that relatively smoother surface can be obtained at a higher laser power setting. At the high laser power, the surface texture was observed to be

contoured and unidirectional due to the laser beam direction during consolidation. However, at the low laser power of 100 W, the surface texture was observed to be coarser with the greater amount of the ball surface. Therefore, as the laser power was increased, a better surface quality was attained. In order to get a more accurate presentation of the surface texture attained from consolidated structure, 3D profile of the surface was analyzed. The 3D profile was also captured using Surfcom 2000DX2 (Tokyo Seimitsu Co. Ltd). Fig. 6.13 shows the 3D profile of surface roughness with the increase of laser power.

The surface roughness at various laser power shows that the surface roughness values were decreasing with the increase of laser power. The result is depicted in Fig. 6.14 with their respective measured temperature. From the figure, a clear difference in the surface roughness can be seen when  $P=100$  W in comparison to when the  $P=500$  W. At 100 W laser power and scan speed of 444 mm/s, the surface shows randomly scattered and relatively large protrusion of the consolidated structure. These formed protruded peak and valley on the surface. Comparing energy density per unit area between 100 W and 500 W might suggest the reason for the decreasing trend of surface roughness with the increase of laser power. At lower laser power, formation of the liquid pool developed. However, the viscosity of the molten metal was relatively high. This did not allow its smooth flow on the consolidated surface. Poor wettability and high viscosity caused the tendency of the molten metal to spread and flow uniformly on the surface was relatively low. As a result, scattered protruded peak was formed on the surface after the solidification of the molten metal.

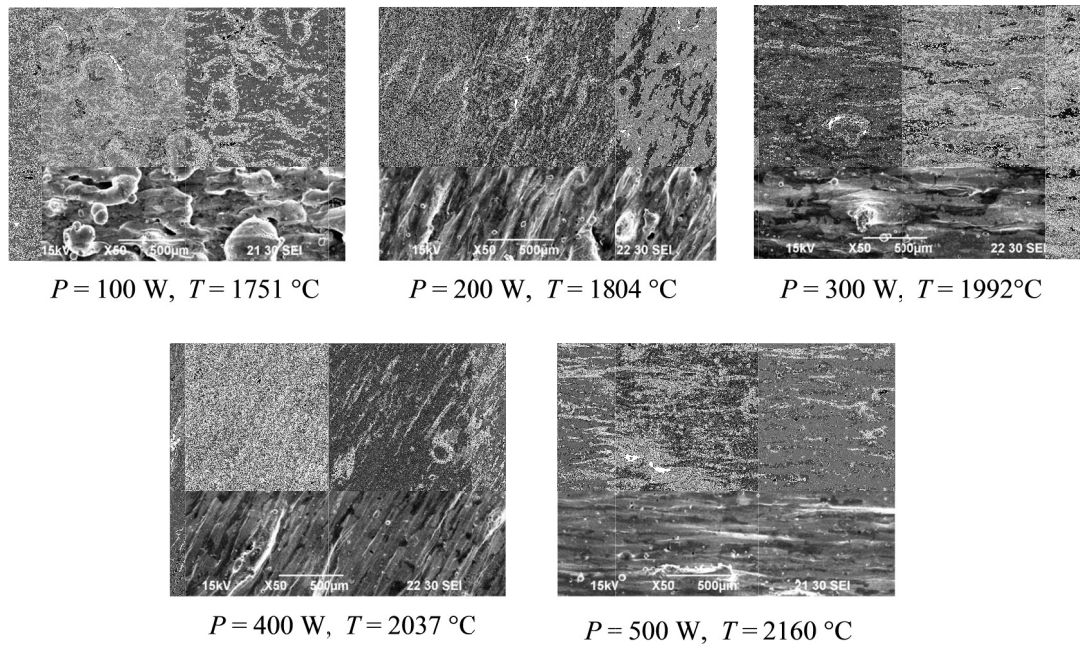


Fig. 6.12 Influence of laser power

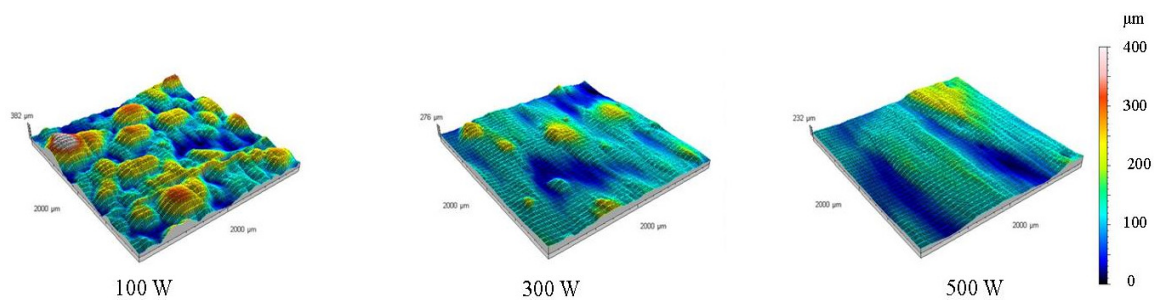


Fig. 6.13 3D profile of surface roughness with the increase of laser power

In contrast, with a further rise of the laser power to 500 W, the temperature was also increased. Therefore, the flowing of the molten metal was more prominent with lower viscosity and improved wettability. Hence, the viscosity of the molten metal increased thereby facilitating its flow to surroundings. In addition, line-by-line irradiation enhanced the fluid flow on the consolidated surface. When the protruded peak of the adjacent line consolidation was irradiated by the laser, the flow of the molten metal enabled porosity and valley region to be filled. As a result, relatively better surface roughness was produced.

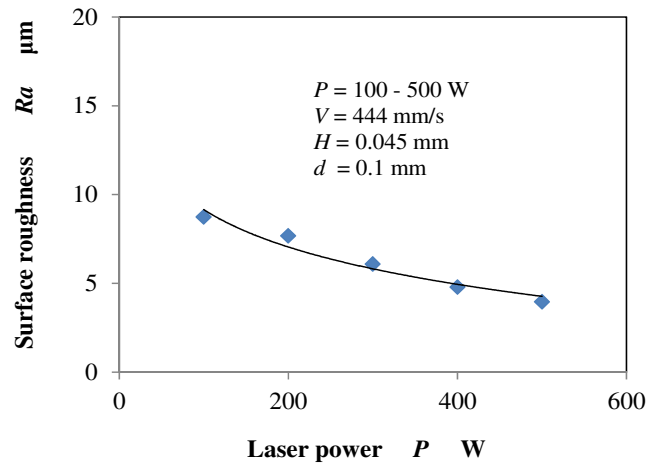


Fig. 6.14 Effect of laser power on surface roughness

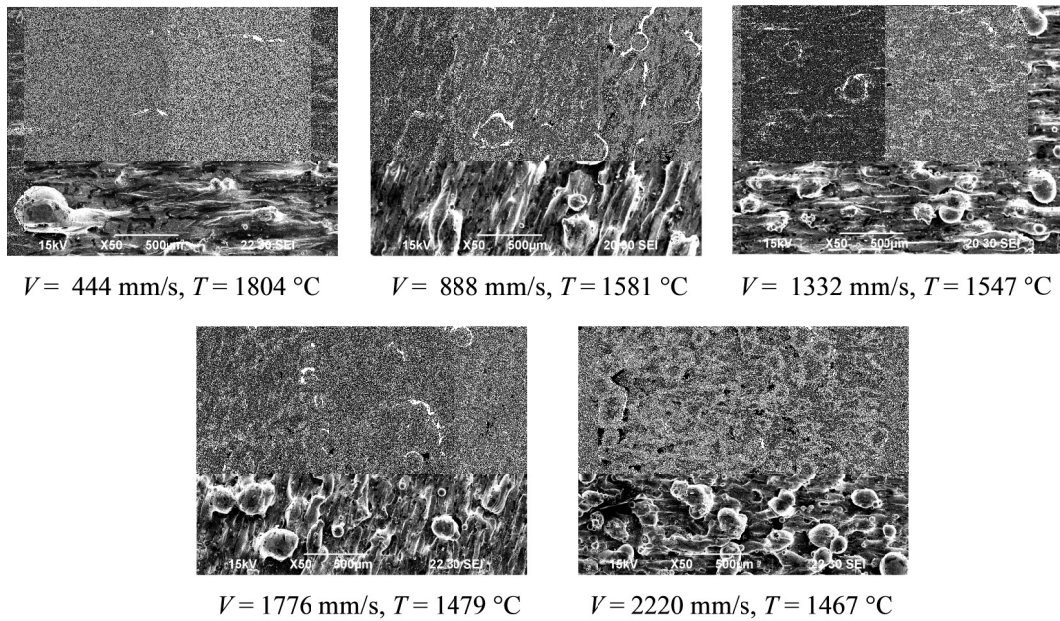


Fig. 6.15 Influence of scan speed

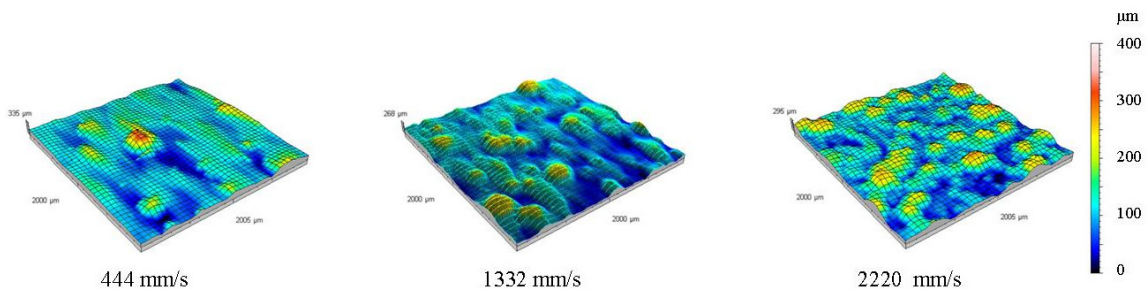


Fig. 6.16 3D profile of surface roughness with the increase of scan speed

Fig. 6.15 indicates the consolidated surface quality as the scan speed was increased. Generally, the surface produced getting coarser with the increase of scan speed. Unidirectional surface texture was observed at low scan speed where the surface texture where the peaks and valleys were elongated in one direction. However, with the increase of scan speed random peaks and valleys can be observed producing a substantially coarse and rougher surface. The 3D profile of the respective surface quality is shown in Fig. 6.16.

Based on the 3D profile, the surface roughness  $Ra$  at various positions using different scan speed can be determined. The average values of  $Ra$  were calculated. The result is presented in Fig. 6.17. The trend shows that the surface quality of the consolidated material is deteriorating with the increase of scan speed.

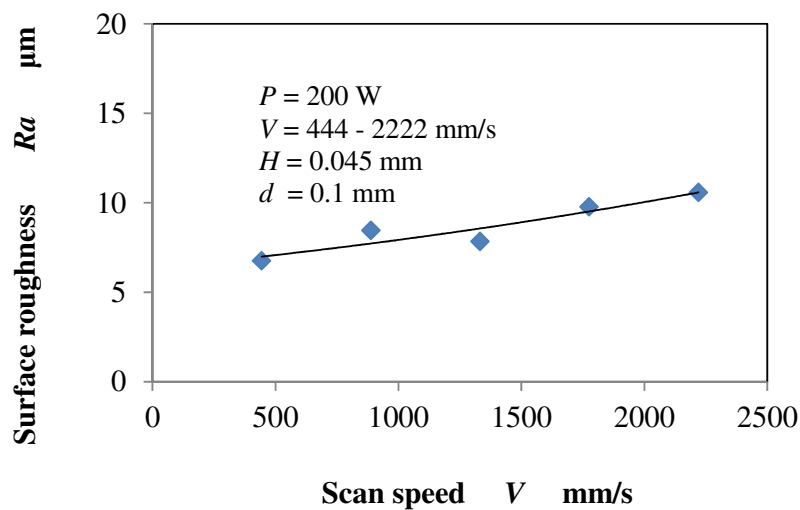


Fig. 6.17 Effect of scan speed on surface roughness

### 6.3.3 Permeability

Table 6.7 Influence of laser power on porosity and permeability

Laser power (W)	Feasibility study result	
	Porosity (%)	Permeability ( $\times 10^{-14} \text{m}^2$ )
200	20 to 45	0.003 – 0.040
300	5 to 30	2 – 25

In order to investigate the potential of consolidated material as a permeable structure through varying the laser parameter. Initially, a preliminary study was performed using laser power of 200 W, 300 W and 400 W. The result obtained is tabulated in Table 6.7. The porosity of the consolidated material was determined using the method that previously described in Section 3.3.4 using Eq. 3.4. Based on the table, it can be concluded that the existence of high porosity on the consolidated material did not ensure the consolidated material produced a permeable structure. For instance, although a high porosity was obtained at the laser power of 200 W, the permeability of the consolidated material was poor due to type of the pore produced during the SLS/SLM. Actually, the pore can be divided into four types, i.e blind pore, open pore, through pore and closed pore as indicated in Fig. 6.18.

The through pore within the consolidated material is important for developing a permeable structure. At laser power of 200 W, it is believed that, the large amount of blind pore and open pore existed within the material. Laser power of 400 W, contrariwise, produced significant balling at high scan speed. Based on the preliminary study conducted, laser power of 300 W is potential for the development of the permeable structure. Therefore, detail study was performed on the permeability at the laser power of 300 W.

The consolidated material was prepared the laser power of 300 W, hatching size of 0.045 mm and spot diameter of 0.1 mm. The scan speed was varied range from 1000 mm/s to 4500 mm/s. Relation of the permeability and the porosity is indicated in Fig. 6.20. The result indicates that the permeability of the consolidated material is a function of the material porosity. The existence of porosity within the material allowed the compressed air to flow through the material. The permeability was increasing linearly after approximately 18% of the porosity. However, when the porosity was below than that, the increment was not significant. This was due to the existence of blind, open and closed porosity.

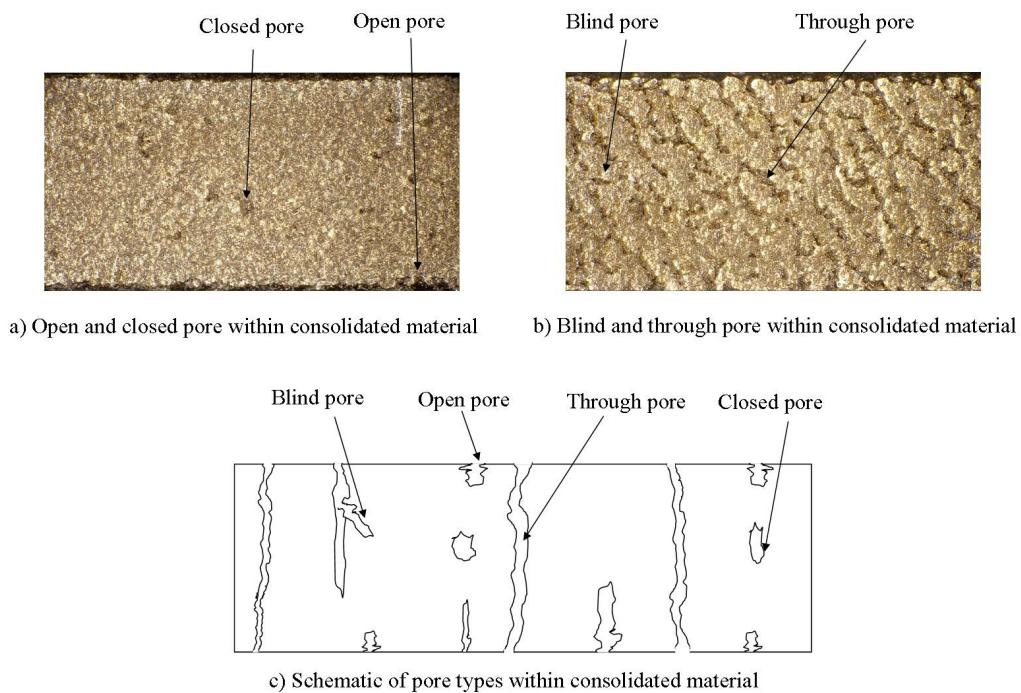


Fig. 6.18 Type of pore within sectioned consolidated material

6.3.3.1 Influence of Porosity on Permeability

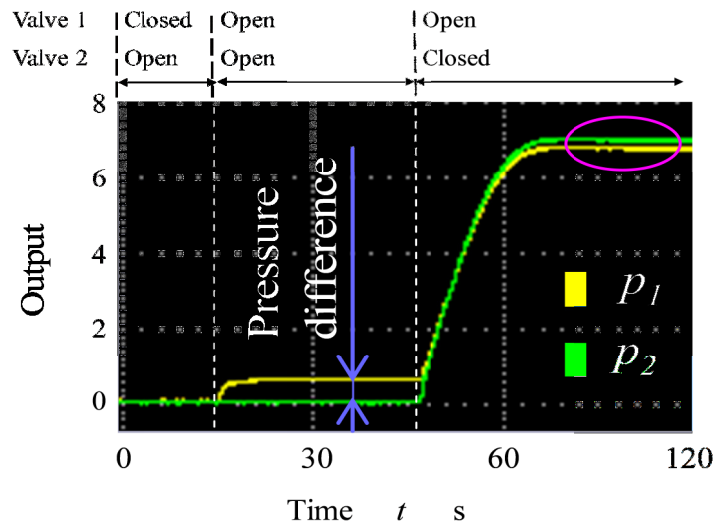


Fig. 6.19 Typical result from permeability measurement

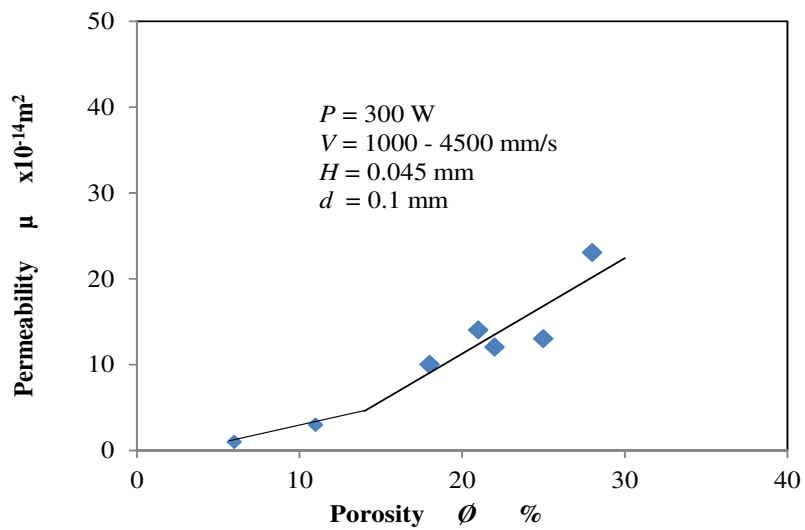


Fig. 6.20 Influence of porosity on permeability

A typical result obtained from the permeability measurement is as illustrated in Fig. 6.19. The figure shows the pressure inside the specimen test holder at the different chamber.  $P_1$  and  $P_2$  are the chambers before and after the airflow through the material respectively. Initially, both  $P_1$  and  $P_2$  are zero when there is no compressed air supplied. In order to measure the permeability of the specimen, Chamber 1 was filled with compressed air. Valve 1 and valve 2 was opened. Therefore, the pressure inside  $P_1$  increased. The pressure inside  $P_2$  was zero due to all air that passed through the porous consolidated material escaped freely through the valve 2. Once the valve 2 was closed,  $P_2$  increased as the air unable to escape anymore. After equilibrium had been achieved, the difference of the pressure was recorded.

### 6.3.3.2 Influence of Orientation Strategy on Permeability

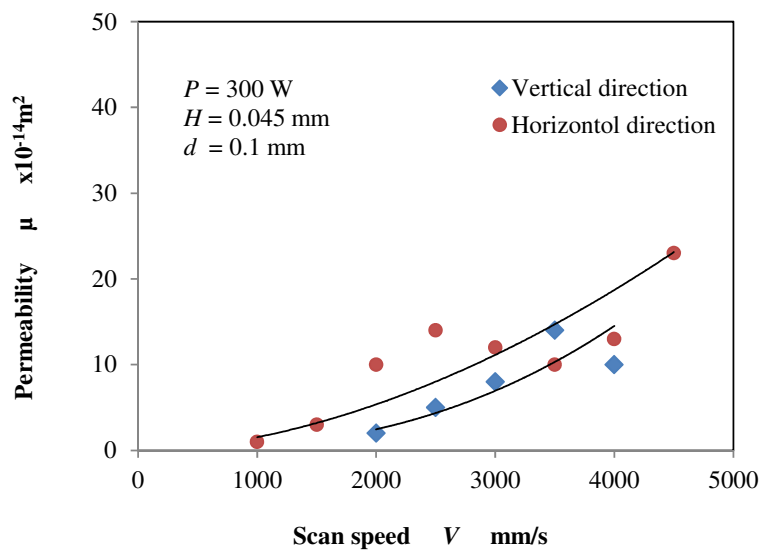
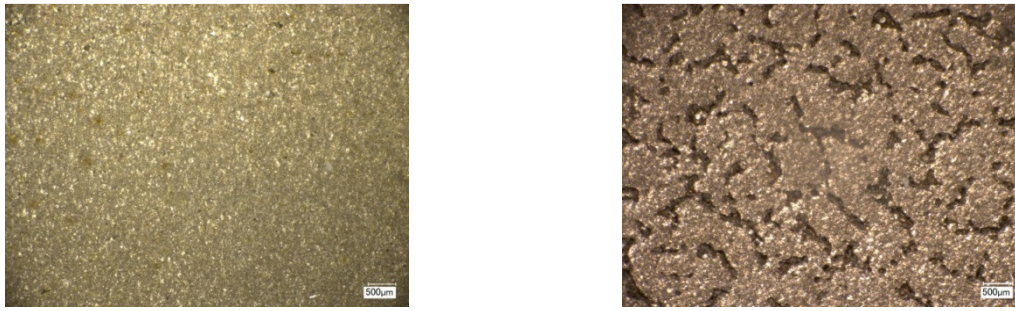


Fig. 6.21 Influence of orientation strategy on permeability



(a) Vertical orientation

(b) Horizontal orientation

Fig. 6.22 Specimen surface produced using different orientation strategy at  $P=300$  W and  $V=2000$  mm/s

Investigation on the permeability of revealed the specimen orientation had affected the permeability of the consolidated material. The result is shown in Fig. 6.21. It was found that the permeability was increasing with the increment of the scan speed. Based on the graph, generally the permeability of the material was higher when the specimen was prepared in the horizontal direction. In the vertical direction, the molten metal was deposited on the previously formed underneath consolidated tracks. Since the track did not fully solidify yet, additional weight caused the semi-molten metal to experience compression that reduced the porosity of the overall consolidated material. Furthermore, when the viscosity of the molten powder was sufficiently high, the fluid flowed downward under the influence of gravitational force. As a result, the porosity within the consolidated material was closed. Hence, specimens that were prepared vertically during processing resulted in the reduced porosity and low permeability.

The surfaces of the consolidated materials using different orientation strategies were examined. The results are compared in Fig. 6.22 and Fig. 6.23 at 2000 m/s and 4000 mm/s respectively. Both figures were set at laser power of 300 W. At scan speed of 2000 mm/s,

high porosity was observed for the specimens that were prepared in the horizontal direction. In contrast, when the specimens were prepared in the vertical direction, denser specimens were manufactured. As a result, the permeability was affected.

In order to analyze the effect of orientation further, observation was repeated at different scan speed. Similarly, comparison was made when the laser scan speed at 4000 mm/s. The porosity images of respective settings are depicted in Fig. 6.23. Visually, it is difficult to determine the condition that shows higher porosity. The specimens that are vertically manufactured shows porosity occurred in one line and directional. However, the specimens manufactured in the horizontal direction display randomly distributed pores. Nevertheless, the permeability inspection on both samples indicates the similar result as when  $V = 2000$  mm/s. It was found higher permeability was observed for specimen manufactured in the horizontal direction.

The higher permeability of the specimens prepared in the horizontal direction might be explained by referring to layer deposition behavior. This is because SLS/SLM involves building of layer-by-layer deposition of the molten powder, which affected the permeability result. During successive upper layer deposition with the increase of thickness, underneath layer was not fully solidified yet. Therefore, the additional weight of the liquid melt on the top layer caused the semi-molten metal to experience compression and penetrated through its porosity as previously mentioned. As a result, the pores that existed within the material were closed by the liquid melt due to the additional weight. This lowered the material permeability.

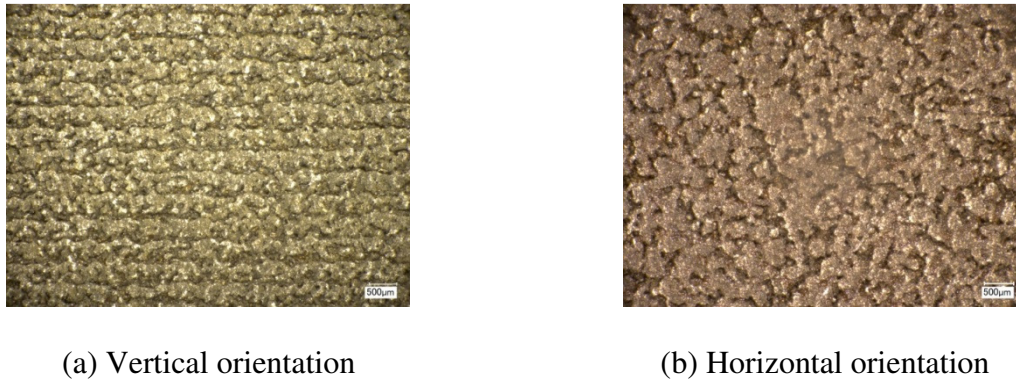


Fig. 6.23 Specimen surface produced using different orientation strategy at  $P=300$  W and  $V=4000$  mm/s

6.3.3.3 Influence of Thickness on Permeability

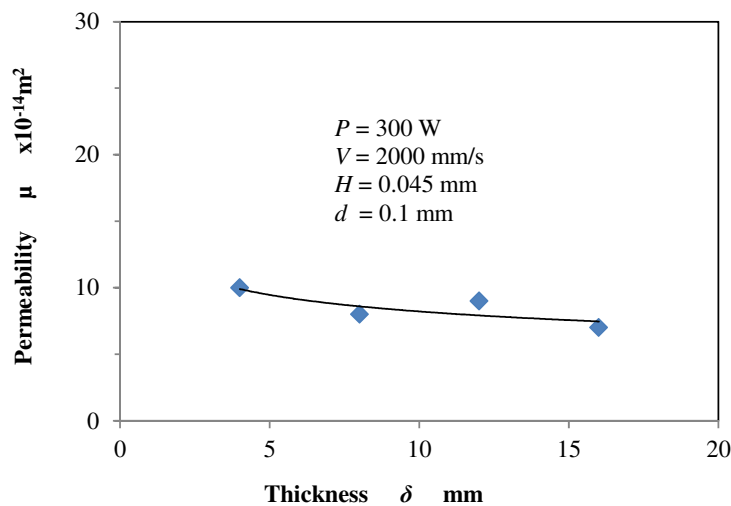


Fig. 6.24 Influence of specimen thickness on permeability

Since the additional weight on the upper layer affected the permeability of the consolidated material, it is essential to investigate the effect of different specimen thickness on the permeability. The specimens were prepared at the thickness of 4 mm, 8 mm, 12 mm and 16 mm. The result is depicted in Fig. 6.24. The graph shows the permeability value is decreasing with the increasing thickness. Nevertheless, the effect was not significant and very small.

### 6.3.4 Hardness

Investigation on the hardness of the material showed that the value varies approximately from 140 HV to 220 HV for the tested conditions. During the hardness test, the consolidated material was prepared with setting condition of 300 W, scan speed range from 1000 mm/s to 4000 mm/s, hatching size 0.045 mm and spot size of 0.1 mm. The result is depicted in Fig. 6.25. It is shown that the porosity of the consolidated material is affecting the overall material hardness. The hardness of the material is decreasing with the increase of porosity.

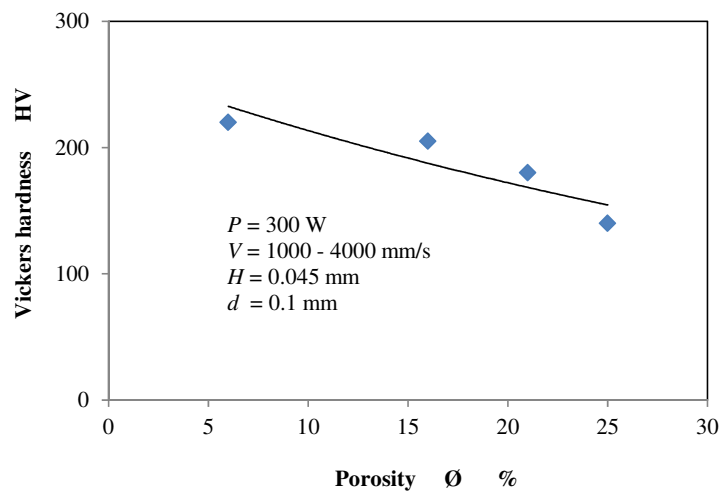


Fig. 6.25 Hardness of consolidated material

6.3.5 Strength

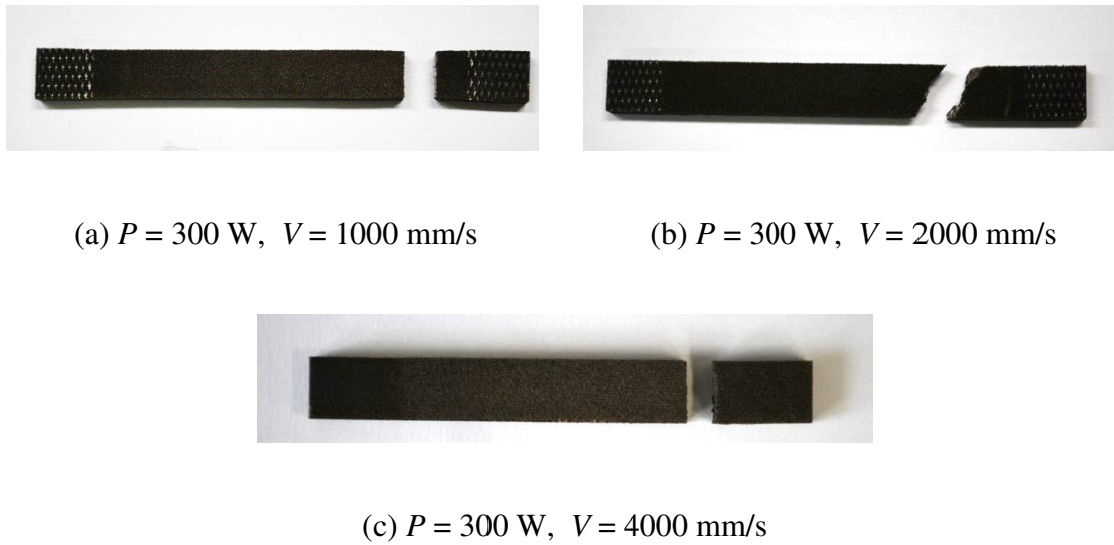


Fig. 6.26 Fractured specimens during tensile test

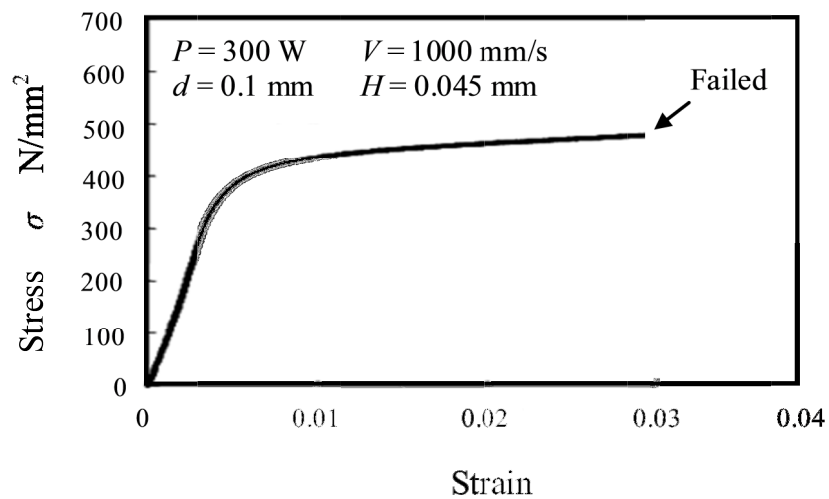


Fig. 6.27 Typical stress-strain test result

Investigation on the strength shows that the tensile stress of the material range from 200 to 580 N/mm<sup>2</sup>. Samples of the fractured specimens during the test are shown in Fig. 6.26. The position and modes of the failure differ from one specimen to another. The pores within the structure are the main caused that contributed to the lower strength of consolidated material and accelerated material failure.

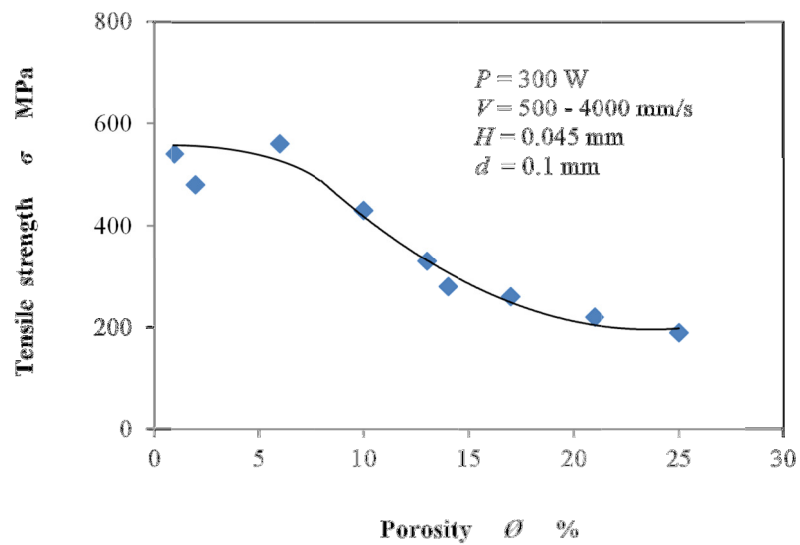


Fig. 6.28 Influence of porosity on tensile strength

Typical stress-strain graph of strength test is shown Fig. 6.27. The consolidated material specimens were prepared under the setting conditions of 300 W, 1000 mm/s, 0.1 mm spot size and hatching space of 0.045 mm. The graph indicates the amount of stress increases with the applied load and fails at approximately 500 N/mm<sup>2</sup>. Different specimens of the material were prepared, and the relation between porosity and the tensile strength was plotted. The result is presented in the Fig. 6.28. The graph depicts the decreasing value of the material strength with the increasing porosity. As generally accepted, the porosity within the material is the weakest point. Therefore, the increase of porosity value significantly affects the strength of the consolidated material.

### 6.3.6 Characteristics of Consolidated Structures

After successfully determining the properties of the consolidated material, comparison was made to other bulk materials that are commonly used in injection mold manufacturing

and the commercialized permeable insert. The evaluation was made to determine the ability of the material to have comparable properties to the other materials. The comparison was determined based on the permeability, porosity, surface roughness, hardness, tensile strength and thermal conductivity. The comparison is tabulated in Table 6.8. The table shows the comparison of other mold materials to the consolidated material manufactured in the study using the SLS/SLM.

Generally, the properties of the permeable SLS/SLM consolidated structure had comparable properties to other the bulk materials that are produced through other manufacturing techniques. There are many materials used as mold materials. These materials range low hardness materials such as aluminum to high hardness materials such as hardened steel. Selection of the materials is based on the complexity, cost, and production quantity. Therefore, by comparing the properties to other materials, the performance of the consolidated material is known.

Investigation on the properties of the consolidated structure enables development of the process map for the material used in the study. The quality of the structure with respect to the process parameter is illustrated in Fig. 6.29. The laser power and the scan speed were varied in the process map development. Whilst, the hatching size and the laser spot size were set at 0.045 mm and 0.1 mm respectively. Generally, the quality of the consolidated structure can be divided into two namely, high porosity and low porosity structure.

Table 6.8 Comparison of other bulk materials to consolidated material

Properties		Other bulk materials		Consolidated material
Physical properties	Permeability (m <sup>2</sup> )	1 x 10 <sup>-10</sup> to 1 x 10 <sup>-14</sup>	[13]	3 x 10 <sup>-11</sup> to 25 x 10 <sup>-14</sup>
	Porosity (%)	20 to 25	[13]	5 to 30
	Pore Size (µm)	3 to 20	[13]	0.5 to 120
		0.1 to 100	[14]	
		25	[15]	
Surface Roughness (µm)	0.05 to 1.6	[23]	0.5 to 10	
Mechanical Properties	Hardness (HV)	Porcerax - 330 to 360	[13]	140 to 250
		Aluminum 6061 - 107	[24]	
		Steel - 290 to 420	[25]	
		SCM 440 - 340 to 430	[26]	
	Tensile Strength (MPa)	Porcerax - 450 to 500	[13]	200 to 600
		Aluminum 6061 - 310	[24]	
		Steel - 415 to 1750	[25]	
		SCM 440 - 980	[26]	
Thermophysical properties	Thermal Conductivity (W/m·K)	Porcerax - 30 to 33	[13]	8.3
		Aluminum 6061 - 167	[24]	
		Steel - 15 to 52	[25]	
		SCM 440 - 42.6	[26]	

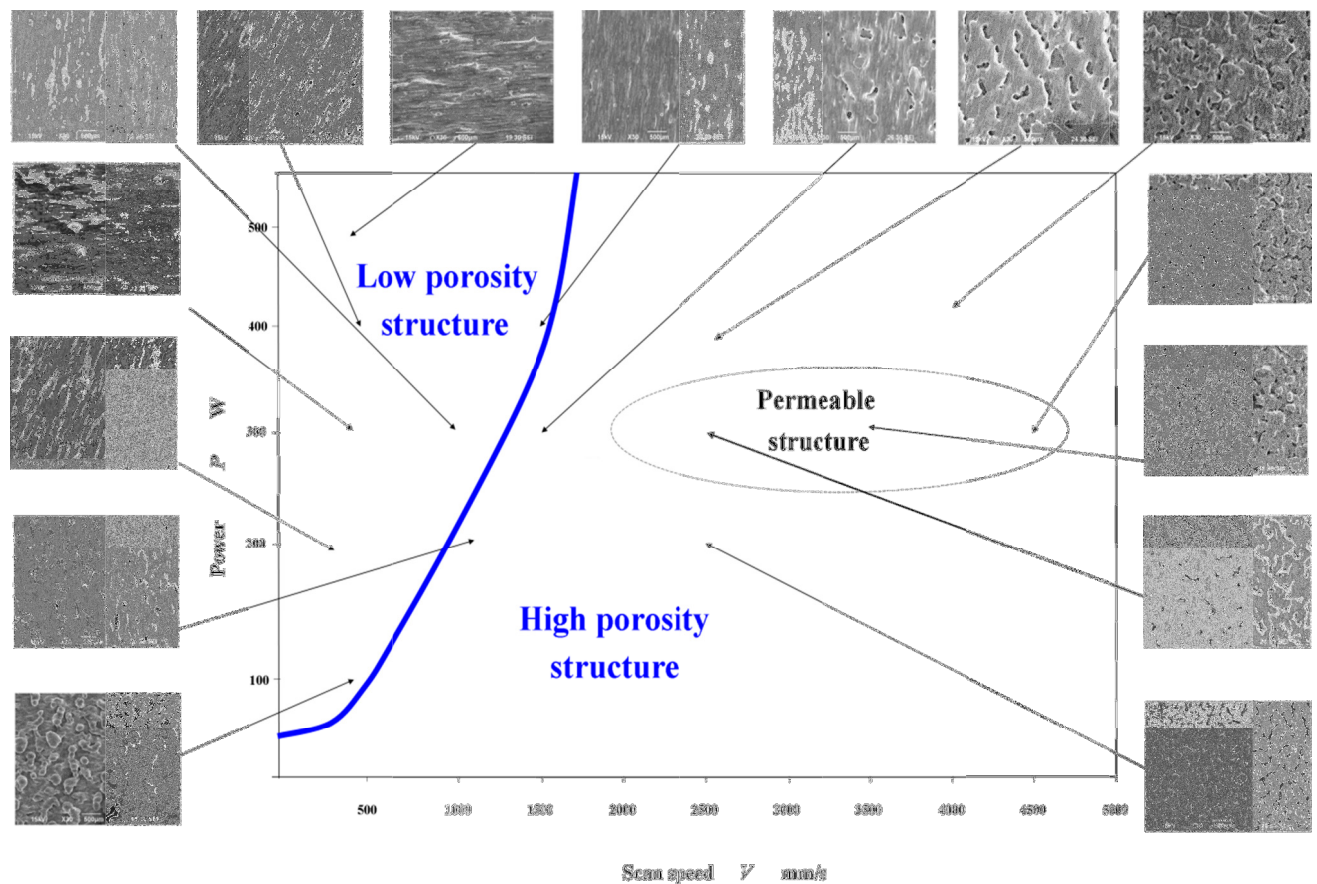


Fig. 6.29 Process map of consolidated structure

The low porosity structure is characterized by less than 10% porous area on the consolidated surface. In contrast, high porosity structure is characterized by randomly scattered void area, which is more than 10%. The region is relatively large on the process map. Examination of the permeability has successfully determined the range of the process parameters, where the permeable structure could be produced.

Higher temperature due to increase in energy density permitted the formation of denser structures. Generally, this was achieved at low scan speed and high laser power. Greater porous area was formed with the increase of scan speed. At temperatures above the melting temperature, the metal powder was fully changed to a liquid state. The flowability and

wettability were increased at the higher temperatures. Hence, the liquid melt flowed towards filling the porosity within the consolidated material. Nevertheless, too high temperature resulted in higher ball surface. The balls were scattered randomly on the material surface. When the temperature was below the melting point, only sintering of metal powder occurred. Consequently, high porosity on the structure was obtained. This is reflected in the process map.

### 6.4 CONCLUSIONS

Based on the experiment conducted, the following conclusion can be made.

1. Porosity is an important property of the consolidated material fabricated via the SLS/SLM process. The porosity of the consolidated structure is a function of laser power, scan speed, hatching size, spot size and its orientation direction during manufacturing.
2. Porosity significantly affects other properties of the consolidated material such as surface roughness, permeability, hardness and strength.
3. Permeable consolidated structure is feasible to be manufactured through the SLS/SLM process. Comparison of its properties to the commercialized permeable insert indicates that the permeable structure manufactured through the SLS/SLM has acceptable property.
4. The temperature during consolidation is very important as it affects the flowability and wettability of the molten powder. Higher temperatures melt the metal powder and enhance the liquid flow. As a result, relatively denser consolidated structure with superior property could be obtained.

**REFERENCES**

- [1] E. N. Hopkinson and P. M. Dickens, *An Industrial Revolution for the Digital Age*. John Wiley & Sons, Inc, 2006.
- [2] J. P. Kruth, L. Froyen, M. Rombouts, J. Van Vaerenbergh, and P. Mercelis, “New Ferro Powder for Selective Laser Sintering of Dense Parts,” *CIRP Ann. - Manuf. Technol.*, vol. 52, no. 1, pp. 139–142, 2003.
- [3] J. P. Kruth, P. Mercelis, J. Van Vaerenbergh, L. Froyen, and M. Rombouts, “Binding mechanisms in selective laser sintering and selective laser melting,” *Rapid Prototyp. J.*, vol. 11, no. 1, pp. 26–36, 2005.
- [4] K. Abd-Elghany and D. L. Bourell, “Property evaluation of 304L stainless steel fabricated by selective laser melting,” *Rapid Prototyp. J.*, vol. 18, no. 5, pp. 420–428, 2012.
- [5] I. Yadroitsev, M. Pavlov, P. Bertrand, and I. Smurov, “Mechanical properties of samples fabricated by selective laser melting,” in *4th European Meeting Prototyping & Rapid Manufacturing*, 2009, vol. 625, pp. 24–25.
- [6] K. N. Amato, S. M. Gaytan, L. E. Murr, E. Martinez, P. W. Shindo, J. Hernandez, S. Collins, and F. Medina, “Microstructures and mechanical behavior of Inconel 718 fabricated by selective laser melting,” *Acta Mater.*, vol. 60, no. 5, pp. 2229–2239, Mar. 2012.
- [7] C. C. Ng, M. Savalani, and H. C. Man, “Fabrication of magnesium using selective laser melting technique,” *Rapid Prototyp. J.*, vol. 17, no. 6, pp. 479–490, 2011.
- [8] S. Abe, Y. Higashi, I. Fuwa, N. Yoshida, and T. Yoneyama, “Milling-Combined Laser Metal Sintering System and Production of Injection Molds with Sophisticated Functions,” in *11th International Conference of Precision and Engineering (ICPE)*, 2006, pp. 288–293.
- [9] T. Yoneyama and H. Kagawa, “Fabrication of Cooling Channels in the Injection Molding by Laser Metal Sintering,” *Int. J. Autom.*, vol. 2, no. 3, 2008.
- [10] J. Liu, Z. Lu, Y. Shi, W. Xu, and J. Zhang, “Investigation into manufacturing injection mold via indirect selective laser sintering,” *Int. J. Adv. Manuf. Technol.*, vol. 48, no. 1–4, pp. 155–163, Sep. 2009.
- [11] I. Ilyas, C. Taylor, K. Dalgarno, and J. Gosden, “Design and manufacture of injection mould tool inserts produced using indirect SLS and machining processes,” *Rapid Prototyp. J.*, vol. 16, no. 6, pp. 429–440, 2010.

- [12] T. Yoneyama, S. Abe, and M. Miyamaru, "Reducing Weld Line by Heating Mold Surface with Heater Embedded by Laser Metal Sintering," *Int. J. Autom.*, vol. 6, no. 5, pp. 591–596, 2012.
- [13] "Introducing Procerax II," *International Mold Steel Inc*, 2013. [Online]. Available: <http://www.imsteel.com/pdf/porcerax.pdf>. [Accessed: 21-Nov-2013].
- [14] "Porous Metal Vents for Injection Molding," *Mott Corp*, 2013. [Online]. Available: <http://www.mottcorp.com/resource/pdf/ventplugs.pdf>. [Accessed: 20-Nov-2013].
- [15] "Porous Metallic Tooling May Improve the Productivity and Quality of Injection Molded Plastic Parts," *Carpentry Technology Corp*, 2013. [Online]. Available: <http://www.carttech.com/techarticles.aspx?id=1478>. [Accessed: 20-Nov-2013].
- [16] M. Kojima, H. Narahara, H. Suzuki, H. Koresawa, and S. Abe, "Injection mould with permeability utilised Metal Laser Sintering Combined with High Speed Milling," *Int. J. Precis. Technol.*, vol. 1, no. 1, p. 55, 2007.
- [17] M. Kojima, H. Narahara, Y. Nakao, H. Fukumaru, H. Koresawa, H. Suzuki, and S. Abe, "Permeability Characteristics and Applications of Plastic Injection Molding Fabricated by Metal Laser Sintering Combined with High Speed Milling," *Int. J. Autom.*, vol. 2, no. 3, pp. 175–181, 2008.
- [18] H. Narahara and N. Fujiwara, "Fundamental study on improvement in air permeable performance of metal laser sintering mold," in *Proceedings of International Symposium on Flexible Automation*, 2010, vol. 2010.
- [19] H. A. Stoffregen, J. Fischer, C. Siedelhofer, and E. Abele, "Selective Laser Melting of Porous Structures," in *Proceedings of the Solid Freeform Fabrication Symposium*, 2011, pp. 680–695.
- [20] C. Klahn, F. Bechmann, S. Hofmann, M. Dinkel, and C. Emmelmann, "Laser Additive Manufacturing of Gas Permeable Structures," in *Physics Procedia*, 2013, vol. 41, pp. 866–873.
- [21] L. Pal, M. K. Joyce, P. D. Fleming, and D. S. Law, "A Simple Method for Calculation of the Permeability Coefficient of Porous Media," *TAPPI J.*, vol. 5, no. 9, pp. 10–16, 2006.
- [22] A. Yassin, T. Ueda, T. Furumoto, A. Hosokawa, R. Tanaka, and S. Abe, "Experimental investigation on cutting mechanism of laser sintered material using small ball end mill," *J. Mater. Process. Technol.*, vol. 209, no. 15–16, pp. 5680–5689, Aug. 2009.
- [23] D. V. Rosato, D. V. Rosato, and M. G. Rosato, *Injection Molding Handbook*. Kluwer Academic Publishers, 2000.
- [24] "Aluminum 6061," *ASM Aerospace Specification Metals, Inc.*, 2013. [Online]. Available: <http://asm.matweb.com/search/SpecificMaterial.asp?bassnum=MA6061t6>. [Accessed: 23-Nov-2013].

- [25] S. Kalpakjian and S. R. Schmid, *Manufacturing Engineering and Technology*. Pearson Prentice Hall, 2010.
- [26] “MISUMI Press 2010,” *MISUMI Press*, 2013. [Online]. Available: [http://in.misumi-ec.com/pdf/press/09\\_pr0659.pdf](http://in.misumi-ec.com/pdf/press/09_pr0659.pdf). [Accessed: 18-Dec-2013].

## **CHAPTER 7 : CONCLUSIONS AND FUTURE WORKS**

### **7.1 CONCLUSIONS**

AM is the future of manufacturing industry due to its ability to revolutionize the industry by improving the product development time. One of the most promising AM processes is SLS/SLM. In the SLS/SLM processing, the powder metals are sintered/melted and then solidified to form a consolidated metals part based on the CAD data. SLS/SLM is a generation of 3D part product that is accomplished through the layer-by-layer manufacturing technique. In the SLS/SLM process, usually metal powder within the range of 20 to 100 micron thickness is deposited on each layer. Then, the laser is irradiated line by line to the metal powder successively until the final part is produced. This has improved the lead-time from design to manufacture in comparison to the classical method. However, currently, the 3D product fabricated the SLS/SLM system still does not meet some of the stringent quality issues and technical requirement. The consolidated material manufactured via the SLS/SLM is characterized by porosity, low strength, high residual stresses, poor surface roughness and others. These problems are some of the common technical barriers that limit the wide expansion of the process in various applications.

Since SLS/SLM involves the consolidation of the metal powder to the porous solid structure under the influence of high-energy density from the laser source, it is paramount to

investigate how the consolidation process occurs. As the metal powder consolidates at high temperatures, the thermo physical of the metal powder and the consolidated material is essential. Hence, the property was discussed in Chapter 3. In Chapter 4, temperature during the laser irradiation on the metal powder in the SLS/SLM was analyzed. In order to understand the transformation process of the metal powder to the consolidated structure and the mechanism involved, high speed imaging technique was used and examined in Chapter 5. After the structures had been successfully fabricated, the properties were analyzed in Chapter 6. The relation of the properties with respect to the porosity was discussed in detail. Based on the research, the following conclusion can be made on the respective chapter.

As previously mentioned, in Chapter 3, the physical properties and the thermal conductivity of the metal powder and the consolidated material were studied. Thermal conductivity is crucial in SLS/SLM processing since heat is transferred continuously to the metal powder, substrate material and consolidated material. Based on the result, it can be concluded

1. The existence of the air gap between randomly distributed metal powder particles caused low thermal conductivity of the metal powder. Nevertheless, the value was found to be increasing with the increment of the metal powder bulk density and the powder particle diameter. When the metal powder was mixed with a different particle diameter, the metal powder with the larger particle diameter has more influence on the value of overall effective thermal conductivity.
2. The thermal conductivity of the consolidated material is a function of the pores inside the material. The value was decreasing significantly with the increase of

porosity. This was attributed to convective heat transfer mechanism experienced by the pores in the consolidated material.

3. Porosity and air gap of material at the different state affects its thermal conductivity. There is very high difference between the same material when it is in powder, consolidated and solid state.

In Chapter 4, temperature measurement during metal powder consolidation using the two-color pyrometer was performed. Despite the very high temperatures during SLS/SLM within the localized region, the temperature was successfully determined. Therefore, the temperature measurement technique used in the study could be applied for temperature monitoring in additive manufacturing. The recorded temperature was relatively high at the maximum temperature approximately 2200 °C. The main findings are

1. The temperature profile of area consolidation indicates repetitive line consolidation that occurred on the surface. This was obtained due to laser beam scanning as it approached and moved away from the center of the target area.
2. The temperature during consolidation is highly dependent on laser power and scan speed. The temperature during consolidation was increasing with the increase of laser power. In contrast, the temperature was decreasing with the increase of scan speed.

In Chapter 5, consolidation characteristics during SLM/SLS were successfully monitored despite challenges due to high temperature, limited space and accessibility constraint. This is demonstrated through proper equipment design and experimental setup. SLS/SLM visualization revealed the consolidation mechanism that occurred during laser irradiation, and

the subsequent solidification after the laser moved away from the consolidated area. Based on the study, it can be concluded that

1. Within the FZ, all microstructure, changes and transformation of the metal powder to the consolidated structure occurred. Therefore, the area is one of the important characteristics in the SLS/SLM process, which affect overall part quality.
2. Line consolidation width, the FZ and splattering are affected by the selection of parameters used in the SLS/SLM. This is because the parameter influences the wettability of the molten powder and heat transfer process that occurred during interaction of the laser beam, metal powder and underneath/substrate surface. The surface condition affected the quality of the consolidated structure. This is because the movement of the metal powder and the wettability of the molten powder are dependent on the surface condition. Other than that, with the increase of layer thickness, splattering occurs more prominent. Furthermore, the movement of the metal powder during the laser irradiation was more chaotic without proper wetting with the substrate surface.
3. The melt pool, which is located inside the FZ, is the most important behavior observed since the flow and spread of the molten metal occurred within this region. The melt pool formed during the laser irradiation was relatively larger than the size of the spot size of the laser beam. The size was increasing with the energy density.
4. High temperature is required to melt the metal powder to form a good and continuous structure. However, too high temperature caused overheating of the laser irradiation area. At too high temperature, the heat was transferred radially at the rate where it affected the surrounding metal powder. As a result, a poor

consolidated structure was produced.

5. During area consolidation, overlapping of single track occurred. Proper selection of the processing parameters leads to a better surface finish when the overlapping of the molten metal flow and spread on the consolidated structure. As a result, the porosity within the consolidated structure is closed.

In Chapter 6, the properties of the consolidated material were evaluated and discussed with respect to the porosity, microstructure, surface roughness, permeability and strength. Instead of the drawback of the material for its well-known porous characteristic, optimization of processing parameter was performed. This was studied in order to reveal its potential for the development of permeable structure. Therefore, based on the investigation of the properties of the consolidated material, it can be concluded

1. Porosity is an important property of the consolidated material. The porosity is highly dependent on the parameter used during the SLS/SLM. This finally affects other properties of the consolidated material such as surface roughness, permeability, hardness and strength. Among the most important processing parameters that influence the properties are laser power, scan speed, hatching size, spot size and part manufacturing forming strategy.
2. Properties of the consolidated structure are relatively good for the development of permeable structure for injection mold application. Comparison to the properties of commercialized insert, other mold material and common practices in injection mold manufacturing was also made. It indicates that the permeable structure fabricated through SLS/SLM has approximately comparable quality.

Based on the research, it can be concluded that consolidation process of the metal powder is a very complex process. The process involves changes of the metal powder to the consolidated structure at a very high and localized maximum temperature of approximately 2200°C. Laser parameters such as laser power, scan speed, layer thickness, surface condition, hatching size, and others significantly affect the final properties. Nevertheless, the quality of the material manufactured via the process is relatively good. This is reflected in the properties of the part. Therefore, SLS/SLM is a potential process as the product could be manufactured relatively fast. Furthermore, its properties could be controlled through optimization of the processing parameter. This reveals the consolidated material potential as an alternative material in a wide variety of engineering applications. It also highlights the SLS/SLM as a credible technique that able to revolutionize the manufacturing industry in the near future.

### **7.2 RECOMMENDATION AND FUTURE WORKS**

The study has revealed other opportunities that might be explored to enhance deeper understanding of the consolidation process of the metal powder during the SLS/SLM. Recommended future works are as follows.

1. The research concentrates in understanding the consolidation behavior of metal powder through process monitoring. By successfully monitoring the process, it is essential to improve the quality when the process is still on-going. Therefore, it is recommended that future works integrate online monitoring and control system so that correction on the process parameter can be made before the process completed. Hence, the consolidated structure quality could be controlled directly.

2. Properties and permeability investigated in the study only cover the hatching size of 45  $\mu\text{m}$ , which are the most common practices in the SLS/SLM. The porosity of the consolidated material increases with the increase of hatching size. However, the roughness and strength will be affected. Nevertheless, it is recommended permeability to be tested at the bigger hatching size so that its potential in the other applications might be revealed.
3. Temperature measurement assumes the temperature within the target spot is constant. However, in practical, temperature at the laser irradiation spot involves temperature distribution. Furthermore, laser beam used in the study is a gaussian shape. Therefore, temperature at spatial and higher resolution is recommended for future study.
4. The melt pool was successfully observed, and the size was measured. However, the depth of the melt pool also important but was not measured in the study. Future study might incorporate this.

## **ACKNOWLEDGEMENT**

I would like to express my sincere gratitude to my main advisor, Professor Takashi Ueda for his advice, supervision and guidance throughout my research. I also would like to express my gratitude to my co-advisors, Associate Professor Tatsuaki Furumoto and Professor Akira Hosokawa. They have been deeply involved during the research. I would also like to thank the advisory committee members, Professor Takeshi Yoneyama and Professor Ryoichi Monzen for their guidance, help and insightful comments.

Special thanks to Panasonic Corporation Eco Solutions Company for providing financial grant, additive manufacturing facilities and support. I would like to thank to the members of Manufacturing System Laboratory for their immense help and fruitful discussion.

It is an honour for me to acknowledge scholarships from Malaysian Government through Ministry of Education Malaysia and Universiti Teknikal Malaysia Melaka (UTeM) for their financial support during my studies at Kanazawa University. I also would like to express my gratitude to all Malaysian students in Kanazawa and all my friends for their friendship and hospitality.

Last and the most important of all, my deepest appreciation and love to my mother, Hajjah Siti Fatimah Ahmad, my dearest wife, Noor Fauziah Seman, my sons, and to all my family for their understanding, unconditional love, advice, patience and support throughout this work.

## LIST OF PUBLICATIONS

1. Mohd Rizal Alkahari, Tatsuaki Furumoto, Takashi Ueda, Akira Hosokawa, Ryutaro Tanaka, Mohd Sanusi Abdul Aziz, "Thermal Conductivity of Metal Powder and Consolidated Material Fabricated via Selective Laser Melting", *Key Engineering Materials*, 523-524, 2012, Pages 244-249.
2. Tatsuaki Furumoto, Mohd Rizal Alkahari, Takashi Ueda, Mohd Sanusi Abdul Aziz, Akira Hosokawa, Monitoring of Laser Consolidation Process of Metal Powder with High Speed Video Camera, *Physics Procedia*, Volume 39, 2012, Pages 760-766.
3. Tatsuaki Furumoto, Takashi Ueda, Mohd Rizal Alkahari, Akira Hosokawa, "Investigation of laser consolidation process for metal powder by two-color pyrometer and high-speed video camera", *CIRP Annals - Manufacturing Technology*, Volume 62, Issue 1, 2013, Pages 223-226.
4. Mohd Rizal Alkahari, Tatsuaki Furumoto, Takashi Ueda, Akira Hosokawa, "Consolidation Characteristics of Ferrous based Metal Powder in Additive Manufacturing", *Journal of Advanced Design, System and Manufacturing. JSME*, Accepted Jan 2014.
5. Mohd Rizal Alkahari, Tatsuaki Furumoto, Takashi Ueda, Akira Hosokawa, "Temperature Measurement in Additive Manufacturing", *International Journal of Heat and Mass Transfer*, Submitted.
6. Mohd Rizal Alkahari, Tatsuaki Furumoto, Takashi Ueda, Akira Hosokawa, "Line Consolidation Characteristics of SCM based Metal Powder", *International Conference on Manufacturing, Machine Design and Tribology (ICMDT 2013)*, KSME/JSME, Busan, Korea, Page 114.  
\* Note - Best Paper Award from Korean Society of Mechanical Engineer (KSME) and Japan Society of Mechanical Engineer (JSME)
7. Mohd Rizal Alkahari, Tatsuaki Furumoto, Takashi Ueda, Akira Hosokawa, Ryutaro Tanaka, Mohd Sanusi Abdul Aziz, "Study on Sintering Characteristic of Metal Powder - Influence of Laser Scan Speed", Proceedings of Academic Conference, Japan Society for Precision Engineering (JSPE), Hokuriku Shin-Etsu, 2012, pp. 77-78.
8. Mohd Rizal Alkahari, Tatsuaki Furumoto, Takashi Ueda, Akira Hosokawa, "Process Visualization of Metal Powder Transformation to Consolidated Structure in Layered Manufacturing-Effect of Laser Parameter", Japan Society of Mechanical Engineer (JSME) 51<sup>st</sup> General Assembly and Conference, Hokuriku Shin-Etsu, Accepted Jan 2014.